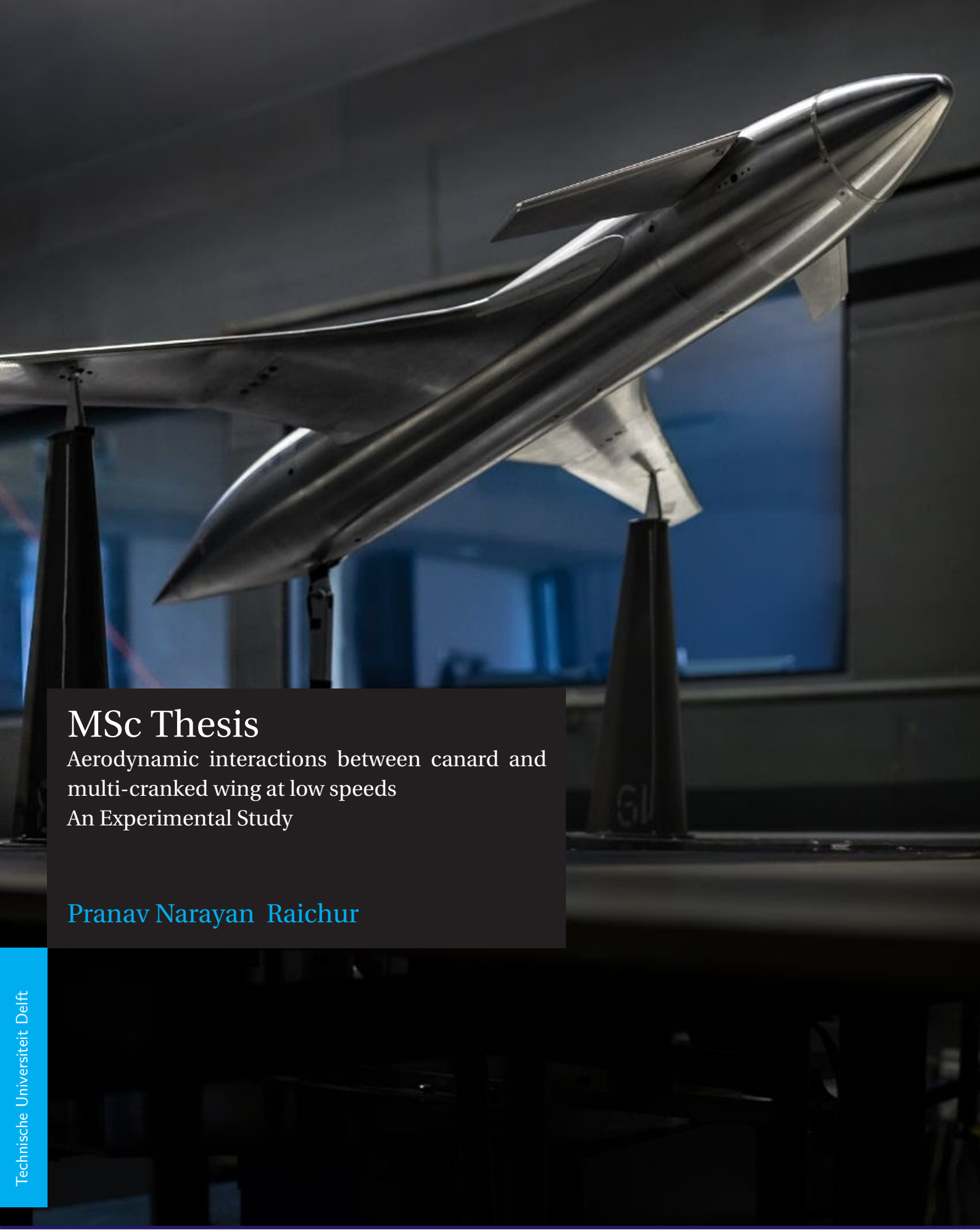

MSc Thesis

Aerodynamic interactions between canard and multi-cranked wing at low speeds
An Experimental Study

Pranav Narayan Raichur

Technische Universiteit Delft

TU Delft Delft University of Technology

Challenge the future

MSc Thesis

Aerodynamic interactions between canard and multi-cranked wing at low speeds
An Experimental Study

by

Pranav Narayan Raichur

in partial fulfillment of the requirements for the degree of

Master of Science
in Aerospace Engineering

at the Delft University of Technology,
to be defended publicly on Thursday June 13, 2019 at 10.00

Student number: 4519280

Supervisor:	Dr. A. Gangoli Rao,	
Thesis committee:	Dr. A. Gangoli Rao,	TU Delft
	Ir. W.A. Timmer	TU Delft
	Prof Dr. Ing Georg Eitelberg (Chairman)	TU Delft
	Mr. Biagio Della Corte (PhD)	TU Delft

This thesis is confidential and cannot be made public until September 1, 2022.

TU Delft Delft University of Technology

ACKNOWLEDGEMENTS

Dedicated to my mom and sister

The section is only available on the hard copy.

Pranav Narayan Raichur
Delft, June 2019.

SUMMARY

The longitudinal characteristics of a multi cranked wing in tandem with a canard were investigated on a 2% scaled generic modular wind tunnel model in the 2.85m x 2.85m Open Jet Facility (OJF) at Delft University of Technology. The experimental campaign yielded force, moment and surface oil flow data for a moderate angle of attack range of −5 to +22 °, at a freestream velocity of 30 m/s, and at a Reynolds number of 0.5 million based on the wing mean aerodynamic chord.

An experimental approach was followed to understand the complex aerodynamic characteristics of the multi cranked wing. Interactions between the canard and multi-cranked wing planform were studied for optimizing the location of the canard (both longitudinal and vertical positions). Thereby, general trends were identified to improve aerodynamic performance of such a novel configuration. A modular generic test bed was developed to allow further modifications of the planform characteristics of both the canard and wing at this early stage of design. The modularity in the wind tunnel model design can accommodate various fixes for future design studies, in order to alleviate or inhibit the pitch up tendencies at moderate lift coefficients on the wing body and improve the overall aerodynamic performance of the configuration. The aerodynamic data set obtained from the experimental study can be used to validate future numerical simulations. Oil flow measurement techniques, and limited cases of qualitative wake rake analysis were applied to understand effects of canard on the wing flow field.

The results presented in this thesis provide the low speed trends for a canard and multi cranked wing configuration, with emphasis on canard and wing interactions. It provides insights on optimal longitudinal and vertical placement of the canard with respect to the multi-cranked wing for maximizing improvements with respect to lift, drag and longitudinal stability characteristics of the configuration. Close coupled canard benefits and the mutually beneficial vortex interactions are discussed in detail. Other than this the importance of vertical locations of the canard and its influence on flow trajectories affecting the wing body aerodynamics and its performance are quantized. Thereby, allowing designers to make a weighted decision on placement of the canard. In addition to the canard-wing interaction, influence of canard deflection on steady state aerodynamics of wing body combination is also discussed. High fidelity aerodynamic database developed as part of this thesis can be used in the design of future fuel-efficient unconventional canard aircraft configuration(s).

Important findings from the experimental campaign include:

- 'Pitch up' tendencies of the mutli-cranked wing are observed at moderate lift coefficient of 0.6.
- High close coupled canard configurations provide the best trimmed lift to drag ratio for low to moderate lift coefficient. (0.3 - 0.6)
- Mid close coupled canard has the best mutual interference effects at moderate angles of attack (10° - 22°), with highest maximum lift coefficient.
- Low close coupled canard has the least mutual interference effects at moderate angles of attack, with least maximum lift coefficient.
- Far coupled canard configurations result in loss of mutual interference effects at all the angles of attack range tested, as expected. However, the trimmable range for low and moderate lift coefficient increases.

CONTENTS

List of Figures

List of Tables

List of Symbols

Variables		Unit
a	Speed of sound	$[m/s]$
AR	b^2/S, aspect ratio	$[-]$
b	$2s$, span	$[m]$
c	chord length	$[m]$
$c(y)$	Local chord of canard or wing	$[m]$
c_r	Root chord of canard or wing	$[m]$
c_t	Tip chord of canard or wing	$[m]$
$\overline{c}$	Mean Aerodynamic Chord	$[m]$
c_d	$d/q_\infty c$, sectional drag coefficient	$[-]$
c_l	$l/q_\infty c$, sectional lift coefficient	$[-]$
c_m	$m/q_\infty c^2$, sectional pitching moment coefficient	$[-]$
C_D	D/q_∞, Drag coefficient	$[-]$
C_{Dmin}	Minimum Drag coefficient	$[-]$
C_L	L/q_∞, Lift coefficient	$[-]$
C_M	$M/q_\infty c$, Pitching moment coefficient	$[-]$
C_N	N/q_∞, Normal force coefficient	$[-]$
C_A	A/q_∞, Axial force coefficient	$[-]$
C_p	$(\frac{p-p_\infty}{q_\infty})$, static-pressure coefficient	$[-]$
C_{pt}	$(\frac{p_t-p_\infty}{q_\infty})$, total-pressure coefficient	$[-]$
q_∞	Dynamic Pressure	$[Pa]$
d	drag force per unit span	$[N-m]$
D	drag force	$[N]$
L	Lift force	$[N]$
N	Normal force	$[N]$
A	Axial force	$[N]$
$\dot{m}$	mass flow	$[kg/s]$
M	$V/a, Machnumber$	$[-]$
M	Pitching Moment	$[N-m]$
p	static pressure	$[Pa]$
r_f	radius of circular section of the fuselage	$[m]$
Re	$U_\infty \overline{c}/\nu$, Reynolds number	$[-]$
s	wing semispan	$[m]$
S	wing reference area	$[m^2]$
$u,\ v,\ w$	x, y, z velocity components	$[m/s]$
x	axial direction	$[m]$
U	velocity	$[m/s]$
u'	velocity fluctuation	$[m/s]$
Δu	Longitudinal interference factor	$[-]$
Δw	Vertical interference factor	$[-]$
y^+	dimensionless wall distance	$[-]$
z_{CT}/c_{iw}	Vertical position of the canard's trailing edge over the wing, plane z=0	$[-]$

Greek		Unit
α	angle of attack	$[deg]$
δ	canard setting angle	$[deg]$
λ	Leading edge sweep angle of canard or wing	$[deg]$
ν	Kinematic viscosity	$[m^2/s]$
ρ	density	$[kg/m^3]$
τ	shear stress	$[N/m^2]$

Subscripts	
c	canard
w	Wing
f	Fuselage
wb	Wing Body
∞	Free stream conditions
H, M, L	High,Mid,Low
d	drag
l	lift

1

INTRODUCTION

Aircraft designers, over decades, have overcome a myriad of design challenges to meet specific requirements of different end users, be it the development of efficient commercial transport aircrafts, supersonic combat aircrafts or endurance aircrafts for flights across the globe.

Currently, reduction in fuel consumption, noise, and emissions are the stiff challenges faced by aircraft designers. As per targets laid out by the Advisory Council for Aviation Research and Innovation in Europe (ACARE) [9], quantitatively, it is required by year 2050 to reduce emissions especially of CO_2 by 75%, NOx by 90%, and with perceived noise level reduction by 65% relative to the year 2000. Achieving these stiff targets, and maintaining industrial growth in aviation, calls for a paradigm shift in design philosophy rather than mere evolutionary development. Novel propulsion systems, with alternative fuels requiring large volumetric storage capability, and their integration to the airframe are expected to alleviate the environmental problems, and help reach the required targets.

To achieve these performance targets, in the past couple of years, a European Union (EU) consortium with the Faculty Aerospace at TU Delft are currently studying such novel configurations. One such wing configuration proposed to be studied is a muti-cranked wing layout to meet specifications of high subsonic cruise speed, good volumetric storage of alternative fuels, improved load carrying capability and low-speed performance.

For a conventional transport wing layout to achieve high cruise speed at high altitude,a moderately swept wing with high aspect ratio was a logical choice. The design philosophy has been largely to minimize tip stall, and have attached flow over the complete flight regime. To achieve these objectives, the aerodynamic tip loading has to be minimized and this is achieved either by giving a negative washout or negative twist as compared to the inboard wing. This modification, however, leads to higher induced drag as a result of deviation from elliptical spanwise lift distribution. Other than this wing leading-edge modifications such as slats are utilized to prevent tip stall by decreasing the effective angle of attack outboard and there by reducing tip stall of wings at high-angle-of-attack. Incorporation of these leading edge modifications, even though well designed would lead to increase in drag at cruise conditions [10].

Deviating from convention, Küchemann proposed the idea of designing transport wings which can combine attached flow wings with classical attached flow cases. To overcome the high cost of maintaining attached flow over the entire flight regime, with conflicting design choices and aerodynamic tailoring, Küchemann believed that combined vortical and attached flow would alleviate some problems of the conventional aft swept wings [11, 12]. He favored attached flows for cruise conditions and for superior field performance, utilization of vortical flows at high angles to maximize efficiency across the envelope of the flight. The combined effect of vortical and attached flows have been largely used by highly swept low aspect ratio wings on peacekeeping aircraft. However, the low aspect ratio thin profiled with large wing area had volumetric constraints and reduced field performance with lower C_{Lmax}.

Thus, to achieve the unique requirements of the combined vortex and attached flow, improved low-speed performance with good volumetric carrying capability, high cruise speed for a long range, a trade-off between wing layouts of low aspect ratio with high sweep and moderate sweep with high aspect ratio was required. This led to the utilization of a multi-cranked wing configuration which is characterized by highly swept root or inboard section, in comparison to the outboard panels of the wing. To attain the design objective of having a constant critical Mach number along the span, the wing sweep and thickness to chord ratio was reduced along the span. This aerodynamic requirement led to the design of thick wing root, convenient for large volumetric storage and decreased bending moment at the root owing to increase in moment of inertia and placement of thicker spar at the root.

An experimental investigation done by Handley, 1946 suggested that three-stage sweep configuration, which leads to multi crank would result in better behavior at low speeds [13]. The outboard wing had the lowest sweep leading to a moderate aspect ratio as compared to having a constant high sweep low aspect ratio delta wings. The outboard sweep reduction was limited by the loss of aileron power at low speeds. The aeroelastic advantage of such a wing layout was minimizing the wing induced bending, thereby, reducing the negative washout at the tip. This could be achieved by reduction of sweep over the wing with optimum spar and torsion box placement to prevent twisting. One other prospective advantage of the stepped reduction of the outboard sweep is an increased aspect ratio to moderate levels with combined vortical and attached flows, which allowed for better low-speed performance with an acceptable lift to drag ratio. This consequently is expected to reduce engine thrust and thereby take off noise as compared to low aspect ratio slender wings. Currently such wing layouts are studied on Blended Wing Body (BWB) configurations and Unmanned Combat Aerial Vehicles (UCAV), for the aforementioned advantages.

Based on all the promising characteristics listed of the cranked wing layout, the major disadvantage of such a layout as compared to the were that the conventional wing configurations, the highly swept root of the cranked wing, which did not stall easily resulted in tip-stalling problems and non-linear pitch up tendencies. These effects are increased either due to formation of leading-edge vortex inboard or a vortex breakdown at low incidences of $4-8°$. Nonlinear aerodynamic effects of such nature are difficult to model with linear aerodynamic methods and numerical simulations find it difficult to capture this complex flow field, with lack of proper calibration data from the experimental databases. From an experimental campaign, it would be critical to understand the causes leading to pitch-up and to determine the effective strategies in reducing pitch-up and increasing the usable low-speed lift.

Canard configurations for such cranked wing configurations from initial assessment seems a promising control device. As highlighted in previous paragraphs, the wing layout is expected to form a leading edge vortex, and when a well-designed canard is placed in such a flow field, it is known to cause mutual positive vortex interaction. This interference effects result in higher C_{Lmax} values for an improved low-speed field performance. It would be interesting to study how the canard influences the parent wing with its own field, whether with its own vortical flow field would alleviate or increase pitch up is to be understood. Other than this, canard would allow the deployment of trailing edge flaps as it could be used to trim the excessive nose down moment caused. The pitch control effectiveness of the canard must be further investigated to understand its impact on performance. All of these effects are specific to the given wing layout or configuration and need to be studied in detail.

This work describes an experimental investigation on multi-cranked wing layout in the presence of a canard. The objective of this thesis is to understand the pitch-up problem at low incidences as observed from previous studies on such wing layouts. Other than this it was proposed to understand the complex flow phenomena involved, focusing on understanding vortex flow interactions based on canard placement, considering only a few such configurations have been previously studied. From these studies it was observed that the pitch up occurred at low incidences of 4-6° and was largely due to an outboard separation, with a region of re-circulation. With respect to the aerodynamic interaction between the canard and the wing it was observed that the close coupled canard configurations had higher positive interference as compared to the far coupled configurations. Pitch up was not totally eliminated with the canard on cases, however, was able to decrease the pitch up magnitude.

1.0.1. THESIS APPROACH

To understand the aerodynamic interactions for the unconventional configuration introduced in the chapter 1, an experimental approach was selected. This was done for the following reasons:

- Unconventional configurations with lack of reference data are tested at such preliminary stages in a tunnel to establish its aerodynamic characteristics.
- A generic modular wind tunnel experimental setup would allow for modifying various components, understanding aerodynamic contributions of different components of the aircraft via component build up method. This provides data on sensitivity of variables on the interaction phenomenon between the canard and the wing.
- Data set obtained from such studies can be used for validating numerical simulations and provide designers insight to make further modifications to the configuration.

1.0.2. THESIS LIMITATIONS

It is important to be critical of the approach followed and the conditions in which the experimental campaign was carried out. Some of the thesis limitations emerging from the experimental conditions are listed below:

- As the experiments were carried out in a low-speed wind tunnel, for a 2% scaled model the Mach and Reynolds numbers of 0.1 and 0.5 million respectively were low when compared to those of full-scale take-off, landing conditions, where Reynolds number can vary in the range of 20-30 million. The results obtained from the experiment will have been affected by relatively larger boundary-layer thickness, and absence of compressibility effects. The vortex interactions between the lifting surfaces are a direct result of viscous effects, the low Reynolds number may have led to offsets in a quantitative sense. However, the interactions are as a result of communication between the velocity and pressure fields in the vortical regions. Further, for the viscous interactions, the low Reynolds number condition is alleviated by the low Mach number condition, since the ratio of pressure and viscous forces scales with Re/M^2 as described by Sinnige et.al, [14].
- Aircraft scaled model testing in open test sections are avoided due to large streamline curvature effect as compared to testing free air, and corrections are difficult to be applied with lack of precise definition of wall boundary conditions, [15]. Thereby, it is difficult to validate the results in a quantitative manner for performance and flight mechanics study. However, this was mitigated to some extent,by using a floorboard, thus, creating a $3/4^{th}$ tunnel. Also, as a baseline study to understand the trends and interference effects, open jet facility for the scale chosen was deemed suitable.

1.1. THESIS STRUCTURE

Prior work on aerodynamic interactions between the canard and similar highly swept wing configurations are detailed in chapter 2, highlighting key knowledge gaps, in turn leading to the formulation of the research objectives. Research questions and the experimental methodology followed, in conjunction with model design choices for the experimental setup are discussed in detail in the chapter 3. In chapter 4, the results of the wind tunnel experiments with analysis are presented. In this chapter first the results of the balance measurements are discussed and then the corresponding flow field is explained with aid of flow visualization and previous numerical studies conducted. Effect of canard and its deflection on the parent wing with trimmed flight characteristics of different canard configurations are discussed. The thesis research report is concluded in chapter 5, in which the findings from the studies are summarized. Finally recommendations for future research work and bettering the experimental setup are documented.

2

STATE OF THE ART/LITERATURE REVIEW

Based on the understanding of the design intent of the proposed model elaborated in the previous section, prior work done for cranked and canard wing configurations in the literature are presented in this section.

2.1. CRANKED WING DESIGN CONCEPT

To achieve the targets of fuel efficiency, reduced emissions and noise levels, superior aerodynamic performance, propulsive and structural efficiency are required. By way of explanation, design drivers at this moment in the commercial aircraft are to travel faster over a long distance and carry more payload. That is to achieve a combination of, higher cruise speed, range and high payload carrying capability

In order to achieve a higher cruise speed, the primary aerodynamic requirement is to minimize wave drag. Generally, a low aspect ratio with a high angle of sweep-back is applied to the wing to the wing planform to give it a high critical Mach number. However, these wings are known to suffer in the low-speed regime with reduced lift curve slope and lower the lift to drag ratio owing to reduction of leading-edge suction and formation of leading-edge vortex .

The other suitable candidate to achieve these targets were to use a thin wing of high aspect ratio with a moderate sweep. Although they are able to achieve good aerodynamic characteristics both at the high-speed design and low-speed off-design points, they suffer from space constraints. These constraints largely manifest especially, as volumetric constraints at the root of the wing. This volumetric constraint, leads to a large structural weight penalty, considering the utilization of a thicker spar to reduce the root bending moment.

To overcome these performance issues and to reach an aerodynamic and structural compromise, Cranked or compound sweep configurations were envisaged as a design concept.

Cranked wing planforms are characterized by highly swept inboard and moderately swept outboard wing [16]. The high swept wings enhance the high-speed transonic regime performance by delaying the wave drag [17]. The moderately swept outboard wing increases the effective aspect ratio of the wing, in combination with the highly swept inboard provide vortex lift which increases the ground effect with the runway and reducing landing speeds. These characteristics help in providing good field performance (high Lift to drag ratio) and thereby reducing the need for high thrust, fuel consumption, and noise associated with take-off and landing [18].

By gradually reducing both sweep and thickness/ chord ratio, a constant critical Mach number along the span is obtained; This aerodynamic tailoring allows for better cruise performance and improved high-speed stall characteristics. These wings with larger and thick root chord allow for easy structural integration to the main body and aid in providing adequate volume to store and carry alternative as well as conventional fuel systems.

Although, cranked wings provide good high-speed design performance, and improved low speed off design performance, they tend to have pitch up tendency at low incidence (for a range of 4-8°) [16, 19]. In comparison, the low aspect ratio, highly swept wings where the pitch up tendencies are delayed up to high angles of attack. Configuration characteristics of stability and control are unknown parameters with cranked wings and have to be studied and optimized for specific configurations. [17, 19–21]

2.1.1. CONCEPT OF PITCH UP AND LEADING-EDGE VORTEX

Pitch up is an aerodynamic phenomenon marked with a sudden increase in the pitching moment. This sudden change in the pitching behavior for the cranked wing is associated with a host of nonlinear aerodynamic characteristics, mainly the formation of a leading-edge vortex, boundary layer separation on the moderately swept outboard wing and occurrence of vortex breakdown at these nominal angles of attack [16].

It thus becomes critical to understand the concept of the leading-edge vortex, especially its development and movement across a wing planform. Leading edge vortex formation as the name suggests arises at the leading edge as a result of separation and this is carried on by the spanwise pressure gradient associated with swept wings. This separated leading-edge flow is converted into stable helical vortex structures characterized by low static pressure and high dynamic pressure on the wing leeward surface. This pressure drop and increase in velocity leads to increased maximum lift of the planform. However, as it is a result of leading-edge separation and loss of attached suction, it adds a drag penalty and diminishes the overall L/D of the configuration. Stable leading-edge vortices formation is determined by a variety of factors mainly the leading-edge sweep, airfoil leading curvature (i.e. a function of leading-edge bluntness and thickness or the contrary), Reynolds number and attitude of the configuration [22].

For a highly swept low aspect ratio wing, a primary leading-edge vortex is formed and the vortex core moves inboard of the wing forming a strong and stable vortex at high incidences [23]. Typical leading-edge vortex is seen in fig. 2.1. In relation to the cranked wing, due to the compound sweep involved leading to multiple kinks, generally two or more vortex systems emerge from the leading edge. They can be broadly classified into inboard and outboard wing vortex.

The inboard wing vortex carried by the spanwise outboard flow tends to move to the aft of the outboard wing, thereby inducing a flow field of a higher angle of attack or upwash on the outboard portion of the wing. Initially, at lower angles of attack, the strengthened outboard vortex increases the lift, resulting in moving the center of pressure behind the center of the gravity, thereby increasing the stability of the configuration (i.e. increase nosed down pitching moment). However, on a further increase of attitude of the configuration, post a critical angle of incidence, plausibly a vortex breakdown [23] occurs on the outboard wing with boundary layer separation and reversed flow. Conversely, on the inboard wing, due to its high sweep, the vortex system tends to become coherent and stronger as the angle of attack increases. This results in movement of the center of pressure to move further inboard and closer to the center of gravity, leading to instability associated with the pitch up [16, 24–26].

Thus, it would be interesting to study if pitch up tendency is triggered by the inboard vortex, or the outboard separation or a combination of both on the proposed wing configuration.

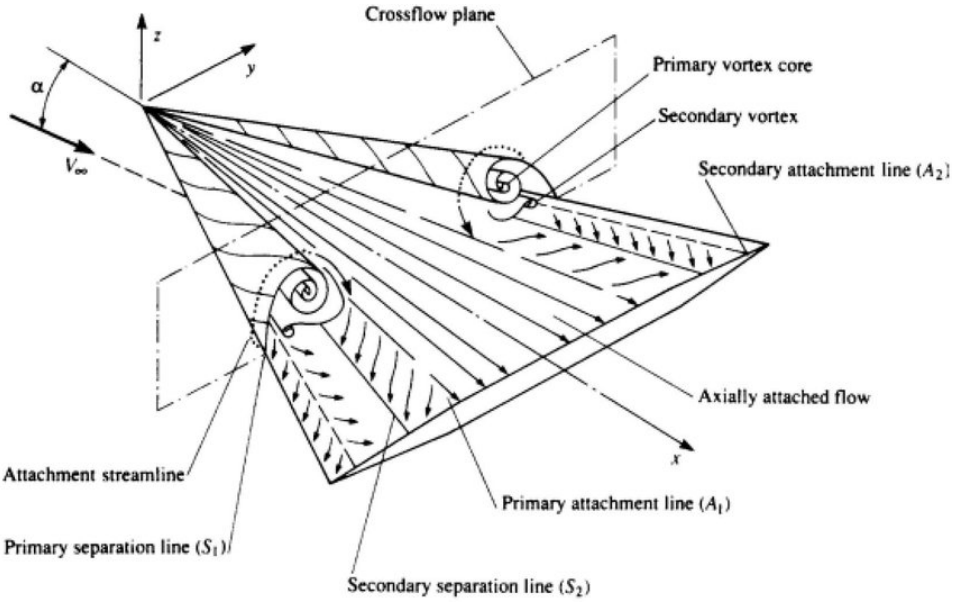

Figure 2.1: Typical Leading edge vortex formation on a low aspect ratio delta wing , [1]

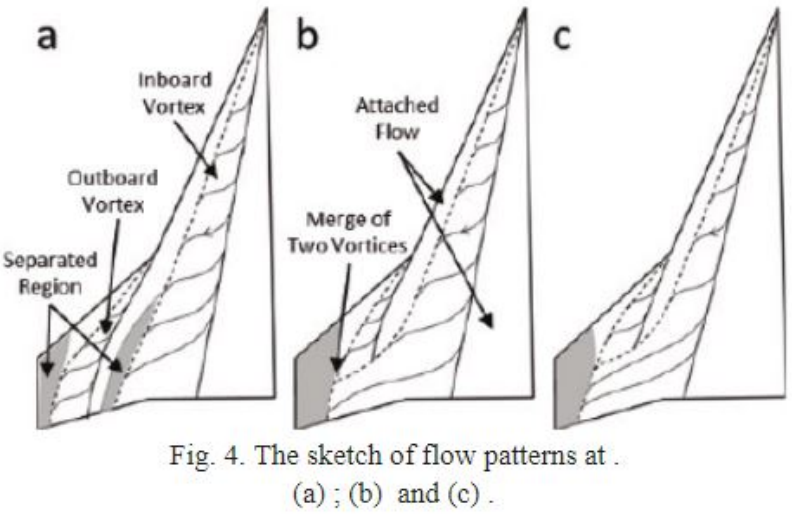

Fig. 4. The sketch of flow patterns at .
(a) ; (b) and (c) .

Figure 2.2: Oil flow topology of cranked wing, indicating inboard and outboard vortex systems, [2]

2.1.2. EXISTING CRANKED WING CONFIGURATIONS

Vast literature cannot be found on existing cranked wing configurations. Cranked wings have been mainly tested on configuration designs for high-speed civilian aircraft (HSCTs), to attain acceptable supersonic, transonic and subsonic performance. One of the major driving factors for improved low-speed/subsonic performance with such configurations is to reduce the impact of noise on society by increasing low-speed field performance, which would allow for lower thrust settings corresponding to reduced fuel consumption and engine noise.

F-16XL as seen in fig. 2.3a, the enhanced tactical fighter, an evolution of the original F-16 aircraft, utilized the cranked wing design with the goal to achieve low wave drag in the supersonic flow regime and to have better handling and maneuverability at low subsonic speeds.

Several geometry changes on the original cranked wing were done to alleviate the pitch up effects both at moderate to high angles of attack: At low to moderate angles of attack, it was observed many factors affect the pitch up, geometrical characteristic of kinked trailing edge was identified as one of the critical factors affecting the pitch up. The rationale behind this finding is that the leading-edge vortex moving inboard with increasing incidence has lesser wing area to effect with the trailing edge kink or notch. The vortex effect is concentrated inboard and at the leading edge, placing the aerodynamic center ahead of the center of gravity leading to large instability and pitch up. To overcome the severity of pitch up at these moderate angles, trailing edge extensions were studied and promising results were obtained. This modification is on the lines of a pure delta wing configuration, which has no kink at the trailing edge and has a straight trailing edge.

At high angles of attack range, inboard wing leading edge was modified to blend with the fuselage. A so-called, "S-blend curve" was placed in the leading edge to reduce pitch instability that was found to occur at high angles of attack in wind-tunnel tests [27].The modification is shown in fig. 2.3a [1] and fig. 2.3b.

(a) F16 XL

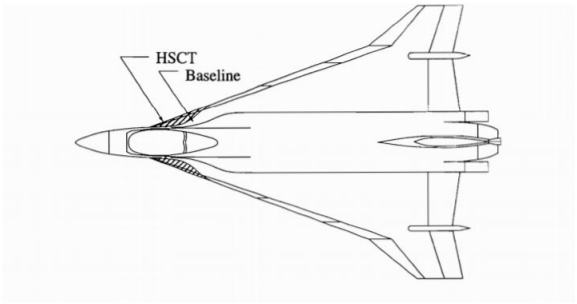

(b) F16 s curve blending [16]

C.P. Nelson's extensive experimental work on Boeing 2700-300 conceptual planforms discusses the off-design performance of cranked wings with varying strake (highly swept inboard wing, blending with the fuselage or lifting body) sizes, leading edge radius and aspect ratios [19, 20]. From these experimental studies, it was inferred that the strake size had a significant impact on the low-speed performance especially the pitching moment behavior. As part of the strake generated lift, it shifts the aerodynamic center ahead of the moment center or reference point. Sharper leading edge resulted in steeper lift curve due to the increase in the vortex lift as compared to the lower and more linear lift curve achieved by a blunt leading-edge planform at the low-speed regime. Thus, blunter leading strake resulting in reduced pitch up tendencies.

From these studies, it was also concluded that the combination of thick strakes and blunt leading edges provide for increased volume carrying capability, and allows for housing leading edge flaps and systems. The moderate outboard sweep, in conjunction with the blunt leading-edge, helps in providing the necessary performance at subsonic and transonic flow regimes, which holds good even at higher angles of attack.

This literature study critically compares the performance parameters of high-sweep, low aspect ratio planforms, moderately swept thin high aspect ratio and the hybrid cranked wing configurations. From literature, it is understood that these planforms suffer from the pitch-up problem at moderate lift coefficient and incidences.

[1] https://www.militaryfactory.com/aircraft/detail.asp?aircraft_id=259

Determining the lift coefficients and incidences at which this tendency would occur, especially the cause for such a pitch up on the baseline configuration, would further aid in making detailed design choices at the conceptual level.

2.2. CANARD CONFIGURATIONS

It is well known that utilizing wing high lift devices, especially the trailing edge flap deflections increase the lift of a given aircraft configuration considerably. Consequently, beneficiary effects such as lower operating costs and higher payload carrying capability are achievable [18, 27]. However, these high lift trailing edge devices create a nose down pitching moment which needs to be trimmed. Thereby, a control surface needs to be added to trim the airplane configuration. Other than this basic requirement, the choice for control surfaces is configuration specific. Based on the layout and design choices of unconvention configurations such as BWB and UCAV, placing the wing quite aft foreseeing a large center of gravity (CG) shift with use of unconventional fuels, a canard configuration seems an attractive solution.

Canards are fore-planes, secondary wings of smaller planform area placed ahead of the wing which is used as a horizontal stabilizer. Despite the fact that first human-powered flight was controlled with a canard configuration, the aft tail configuration has been predominantly been used for control, trim and stability in the civilian aircraft domain [28]. Aft tails have been used in approximately 70% of conventional aircraft because they provide longevity, lightweight construction and the necessary stability and control over a larger center of gravity range.

However, a range of canard configurations has taken to flight with varying degree of success. Canard configured aircraft have seen a rise in popularity especially in the military, experimental and high-speed civil transport configurations (HSCT). Interest in canard configurations has risen due to the potential benefits both in high and low speed operating conditions which are listed below:

Low-speed performance benefits

- Providing positive lift, unlike the conventional tail configurations, thereby possible to achieve a higher C_{Lmax}. Conventional aft tail configurations in order to trim the plane about the center of gravity have to provide a negative lift. This loss in lift has to be augmented by the main wing. On the contrary, canard configured aircraft designs have to provide positive lift about the center of gravity to trim the moment from the main wing.
- Passive stall: If designed well, canard configurations stall earlier than the wing, providing natural stall limit with a pitch down or nose down moment and thus prevent a deep stall.
- Close coupled canard configurations when placed at a relatively short distance from the wing tend to suppress wing vortex bursting, postponing this phenomenon to higher AOA by vortex mutual interference [29, 30]. Low aspect ratio highly swept wings offer to provide lesser wave drag over a wide range of Mach number and utilization of canard higher resulting in higher L/D [17]. This increases usable lift during takeoff and landing.

Transonic performance benefits

- Mach tuck phenomenon alleviation – Considering the ability of canard to provide positive pitch control, this capability could lead to alleviate the effect of nose down moment an aircraft encounters in the transonic regime, a phenomenon referred to as Mach tuck.
- Reduced fuselage length as compared to the conventional aft tail layout [17].
- Reduced wave drag by better cross sectional area (CSA) distribution- Close coupled canard configuration reduces the longitudinal variation of cross-section area distribution thereby reducing the wave drag as the cross-sectional variation is closer to a sear hack's body [17].

Canard configurations inherent of their location results in an aerodynamically clean fuselage aft section, thereby providing aerodynamically clean aft fuselage section and allowing placement of an aft propulsion system, especially for experimental BLI systems integration.

Better spin recovery - unlike the conventional tail configuration, canards don't blanket the vertical tail or the rudder[29].

The success of canard configurations is dictated by the sensitivity of the center of gravity (CG) location and its ability to provide stability and control in stall and post- stall regions. The challenges of canard layouts are highlighted below:

- As canards are placed ahead of the center of gravity (CG), they tend to be destabilizing in nature, and hence have to be designed in a small and compact manner to reduce this effect. The trade-off with such a design choice is a decrease in pitch control effectiveness.
- Effect of induced drag - In order to increase the center of gravity (CG) range of the aircraft, and to achieve the Center of gravity ahead of the wing leading edge the canard area has to be increased, thus making the canard carrying a greater load than the wing, increasing the loading on the canard surface, thereby increasing the induced drag. To reduce its destabilizing effect and reduce its loading, canards have to be designed with a low lift curve slope. As a consequence, the ability of canard aircraft to trim the moment created by the wing flaps is greatly reduced. With reduced wing flap effect, higher approach speeds and flatter approach angles are common. This design tradeoff has to be carefully considered [31].
- Effect on lateral aerodynamics – Canard affects the lateral and directional stability owing to its interaction with the main wing. Wind tunnel studies carried on VariEze aircraft showed that the aileron effectiveness diminished at moderate to high angles of attack as a result of a combination of outboard boundary layer separated flow near the trailing edge, associated with highly swept wings, and influence of canard to increase the effective angle of attack at the outboard span. Flight tests at low speeds also revealed wing rocking for the conceptual models [28, 32].

From these studies, it is therefore required to understand the canard and wing interaction to maximize the benefits and minimize the drawbacks

2.2.1. CLASSIFICATION OF CANARD CONFIGURATIONS

As explained in Section 2.1.1, the wing flow is governed by vortex flow even at low angles of attack. It would be therefore critical to maximizing the coherent vortex lift effect on the wing in the vicinity of the canard. Thus, optimal placement of the canard in relation to the wing is key from an aerodynamic performance perspective while not compromising stability and control.

Canard configurations are categorized into close and far coupled canard based on their proximity to the main wing. As defined by Roskam et.al. [29, 33] "if the ratio of the distance between the canard aerodynamic center and wing aerodynamic center normalized to the mean aerodynamic chord of the wing is less than three", they are termed as a close-coupled canard. However, if this ratio exceeds three, they would be termed as far coupled canard.

Far coupled canard configurations are designed with the sole objective of reduction in cruise drag. Owing to the lack of proximity, the interference effects between the lifting surfaces are largely reduced and resulting in lesser loading of the canard to trim the plane. These above effects largely reduce the trim drag at cruise.

However, in order to achieve stability for such configurations, Toernebeek suggests that the canard should be sized such that its area is 10% of the wing area [31]. This design constraint results in canard acting as a pitch control surface than as lifting canard to improve field performance. The reduced sizing of the canard also leads to large deflection angles to achieve pitch control and trim requirements.
[2] X-31, Tu-144 are examples of far coupled canard configurations. X-31 required canards to deflect between +20 and −70 degree deflection to achieve pitch control requirements. TU-144 canards were fitted with double slotted LE slats and retractable double slotted flaps to increase the lifting capability of the canard and in turn, improve the field performance at low speeds.

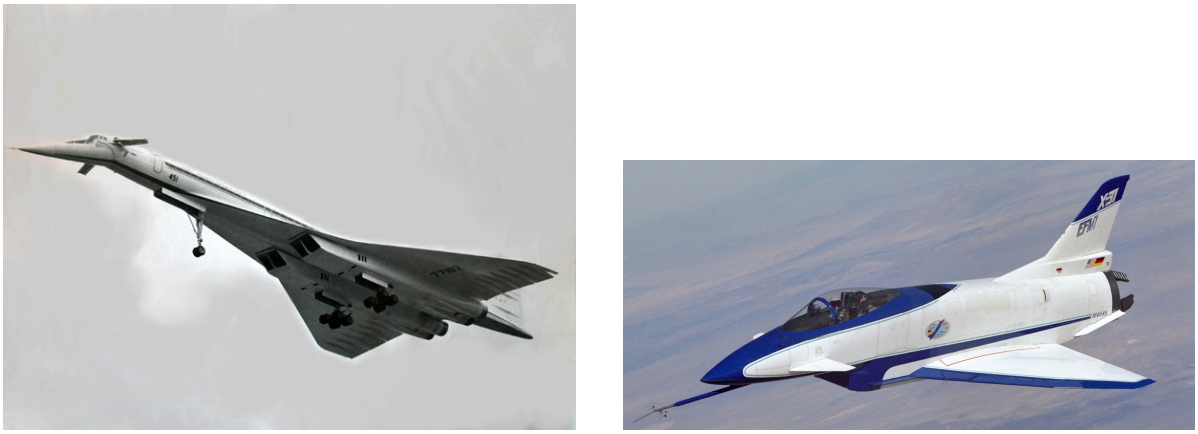

(a) TU-144[r] (b) Rockwell MB X31 [⊕]

Figure 2.4: Examples of far coupled canard configurations

Close coupled canard configurations are known to increase the maximum lift as a result of the wing and canard interaction. Basically, these are larger than a far coupled canard and act as lifting surfaces as well as control surfaces. The behavior of close coupled canard configuration is best described as function of the angle of attack (AOA) of configuration. At low angles of attack, the canard in close proximity of the wing creates a downwash field on the inboard part of the main wing and an upwash on the outboard wing as a result of the flow field induced by tip vortex from the canard.The resulting flow field results in a non-elliptical lift distribution over the main wing causing with the attached flow over the inboard wing and outboard separated flow. Consequently, canard on configuration results in a loss of lift and increase in drag over the main wing. However, the loss in the lift is augmented by the lift of the canard alone.

2.2.2. FLOW FIELD OF CLOSE COUPLED CANARD CONFIGURATIONS

Vortex lift contribution and vortex structure are rapidly altered when a vortex breakdown occurs. Vortex breakdown (VBD) is said to occur when the vortex stagnation point crosses the trailing edge and moves upstream with the wing apex as the angle of attack is increased. There is an adverse pressure gradient or increased pressure associated VBD, which leads to separation, further resulting in loss of lift, reduction in lift curve slope and increase in drag and inboard movement of the center of pressure [34].The phenomenon of VBD can be mitigated by utilizing straked wing/double delta wing planforms in tandem with close coupled canard configurations.

Highly swept strake acts as a supplementary wing which aids in the formation of a stable vortex and also creates a flow field which induces a strong lateral velocity field which re-energizes the turbulent boundary layer on the main wing. This beneficial effect persists up to the critical angle of attack where the VBD of the strake occurs ahead of the wing trailing edge.

Close coupled canard configurations are found to be an attractive option to delay the process of VBD on main wings.

[2] https://www.wikimedia.org/

Berhbohm hypothesized that the main wing vortex separation is suppressed from the apex of the wing to further downstream due to the downwash trajectory created by the canard flow on the main wing vortex system [30]. This leads to a delay in VBD over the main wing. Gloss and Mckinney showed that with an increase in canard leading edge sweep the VBD over the main wing was further delayed indicating mutual positive interaction between the two leading edge vortex systems [35].

(a) SAAB VIGGEN [r]

(b) SAAB GRIPEN [⊕]

(c) DASSAULT RAFALE [v]

(d) NASA X29 [π]

Figure 2.5: Examples of close coupled canard configurations

[3] Viggen was one of the earliest configurations that utilized fixed canard configuration for superior aerodynamic performance. Viggen was designed as an interceptor and was required to have superior high-speed performance combined with high lift low speed ability to achieve good field performance to use short run ways or gravel paths during a wartime scenario. The layout of this aircraft includes a low aspect ratio delta wing for reduction of wave drag and includes elevon. Elevons, other than providing pitch and roll control, also are deflected for low speed operations. The fixed canard configuration with flaps are used only for trimming purposes. Unlike previously discussed, providing passive stall characteristics was not its key function. However, remaining stall resistant for a large range of angle of attack and maximizing the lift utilizing the favorable interference from the close coupled layout is an added benefit. This was done to achieve an acceptable field performance. This goal was realized by intensive wind tunnel testing [30] for placement of the canard to maximize the interference effects. It was determined that placing the canard above and in a close-coupled configuration resulted in an increase 40% in maximum lift value of the canard, meeting the required field performance targets [28, 30].

These vortex interactions and the complex flow field of the canard on the wing and vice versa are described based on comprehensive force, pressure and flow visualization studies carried out at TU Braunschweig [36–39].

[3] https://www.wikipedia.org/

The favorable interactions basically entail prevention of vortex breakdown both on the canard and wing vortex system. The canard vortices are governed by vortex breakdown at their trailing edge, however, this is prevented by the strong leading-edge suction from the wing. The canard vortex system creates a downwash on the inboard wing especially, thereby alleviating the wing vortex breakdown to higher angles of attack [40].

Eugene describes how the flow structure on the wing is altered in presence of close coupled canard configuration and how the wing vortex communicates with the canard vortex system [1]. The primary canard vortex is transported downstream and modifies the wing flow structure.The wing within the canard-tip span is in the downwash field created by the canard and thereby decreases the effective angle of attack of the inboard wing. Beyond the canard tip, upwash from the canard increases the wing's effective angle of attack. Canard and wing trajectories in presence of each other are described as follows: "The wing vortex flow field induces a relative downward and inward motion of the canard vortex while the canard vortex induces an upward and outward movement of the wing vortex" [1]. In case of far coupled configuration without any mutual favorable interference, Eugene anticipates that the canard and wing vortex trajectories would follow an upward and outward path. This statement however, is dependent on the angle of attack range and the leading-edge sweep of both the canard and wing.

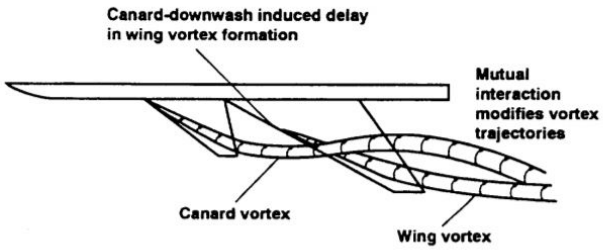

Figure 2.6: Typical canard and wing flow field interaction at moderate to high angles of attack [1]

Other than the criticality of axial location for maximizing constructive interference of close coupled canard configuration, the vertical placement of the canard with respect to the wing is important. In particular, the studies by Gloss et al.[21, 35, 41] indicated that canards which are in the plane or above the wing plane are identified as ideal candidates to maximize the beneficial interactions. Low-canard configurations at high angles of attack showed substantial loss of lift due to the interaction between the low-canard wake and the pressure side of the wing was experimentally measured.

From the extensive studies of Lacey and O'Leary, it was inferred that the canards with leading edge sweep greater than the main wing had the highest favorable interference [42]. This was possible by the formation of stronger canard vortex system. At low angles of attack, it was observed the canard vortex system delayed the formation of wing vortex system further downstream and delayed its formation. At moderate to high angles of attack and helped in increasing the maximum lift by preventing separation on the main wing and helping to maintain vortex flow over the wing without breakdown.

2.2.3. EFFECT OF CANARD DEFLECTIONS

For far-coupled canard configurations, the effect of canard deflections on the aerodynamic performance is restricted to the performance of the canard alone, as the interference effects are minimal [1]. However, in the close-coupled configuration, canard deflections have a notable effect on the wing flow field and in turn its performance. It is observed the canard part of the lift increased with deflection, whereas, the wing contribution to the total lift saw a decrease. This can be associated with canard being loaded and the wing being unloaded due to the downwash created by the canard wake on the inboard part of the wing. As a consequence, the vortex system on the wing moves downstream and leads to the center of pressure to move aft and outboard, alleviating the pitch up tendencies to a higher angle of attack.

Experiments from Lacey [43, 44] indicated that δC_L for low canard deflection was lesser as compared to the high canard deflection configuration. These low-speed force and moment trend have to be understood with aid of extensive flow field measurements on the wing. The aerodynamic behavior can be critically understood, by varying the vertical location of the canard trailing-edge relative to the wing chord line, and consequently analyzing how the canard vortex trajectory influences the main wing vortex system.

As established from the previous paragraphs the vortex flow field and interactions between the canard and wing are complex and configuration specific. Many computational studies both utilizing relatively lower fidelity Euler solutions [45–48] to high fidelity viscous Navier-Stokes simulations have been carried out. A reasonable degree of success has been achieved with respect to computational data matching the experimental data at low angles of attack.

However, at high angles of attack, there is a large deviation between computational and experimental data [48]. Recently conducted computational study over a canard-aided transonic cruise ranger configuration studies indicated lower values than the experimental data [29]. This under prediction of the numerical data versus the experimental data has been associated with the global truncation error and the inability to capture canard and wing vortex systems merging over the wing. This inconsistency at higher angles is also attributed to the inability of computational simulations to capture vortex breakdown[38, 39].

The above studies indicate the numerical analysis techniques need to still evolve and proper calibration is needed to make accurate predictions with respect to the flow field. Thus, wind tunnel and experimental simulations were chosen as the primary option to realize the aerodynamic characteristics of such unique wing planforms and its interaction with a canard [48].

Literature for close coupled canard effects and interactions were largely limited to low aspect ratio delta wing configurations. Flow structure and effect on a multi-cranked wing system with the canard on and off cases are still open to be understood. To maximize these performance benefits offered by canard to delay the VBD process on the wing, the aerodynamic interactions between the canard and the multi cranked wing need to be understood in detail.

The literature study provides a perspective on the background work, clarity on the design challenges and nuances to keep in mind while formulating the research questions. These research questions and thesis objective will be elaborated in the next section.

3

Testing Methodology and Experimental setup

3.1. Research Question, Aims and Objectives

3.1.1. Research Objective

In this section, the research goals are outlined. Based on what exists in literature, the contribution of this thesis project is to add the knowledge base of aerodynamic interactions between a canard and a wing, particularly a multi-cranked wing. This experimental research will provide useful high fidelity aerodynamic database for novel configurations desired to meet requirements of superior load carrying capability, long range and high cruising speed without compromise on low speed performance.

The primary research goal is to understand the flow field and aerodynamic interaction about a canard and multi-cranked wing body, low-speed trends for such configurations.

From chapters 1 and 2 one can realize that canard and wing design is quite a complex and sensitive design, with each specific configuration bringing its own challenge.

Though many studies are conducted on the canard configurations and its interaction with the wing. However, the aerodynamic interaction, stability studies are quite limited to low aspect ratio delta wings and research questions regarding canard influence over a mid aspect ratio hybrid mulit-cranked wings are still a knowledge gap open to be resolved.

Therefore, the main research questions of this proposed thesis project would be described as:

How to design and optimally locate a canard in a flow field ahead of the multi-cranked wing, such that maximizing vortex interactions, thereby increasing the aerodynamic efficiency of the configuration and also a configuration that would provide adequate longitudinal stability and control ?

In order to achieve this main objective, multiple sub questions in the domain of canard and wing aerodynamic design, stability and control have to be formulated and answered. Other than this the bounds for the research have to be established to maximize the focus on the knowledge gap identified from section 2.

The sub-questions and research framework are discussed further.

3.1.2. RESEARCH FRAMEWORK

The bounds established on the research for a canard and wing configuration are as follows:

- The research will be limited to characterizing canard and multi-cranked wing at low speeds via experimental simulations. The relevant characteristics of low speed will be databased and will be compared to a numerical study done at low incidences to see if the trends are comparable and scalable.
- The second bound domain in this research that tests will be done to understand longitudinal aerodynamics and stability of the said configuration. Lateral and directional stability will not be investigated as a part of this experimental campaign.
- As these tests are done at the open jet facility, which are associated with large wind tunnel corrections for airplane models.The main aim was to understand the interaction effect and understand the force and moment trends for this novel configuration.

RESEARCH QUESTIONS

From the set objectives of section 3.1 and bounds from section 3.1.2, research questions were formulated as follows:

Questions related to low-speed wing planform characteristics
What is the principle of vortex flow over high and moderately swept leading edge planforms?

1. What are the aerodynamic advantages of a multi-cranked wing and their drawbacks?
2. At what incidence is there an onset of vortex formation on the wing? In turn, understand the nature (full span leading edge vortex or part span vortex) and the location of initial vortex formation.
3. What is the effect of strake or leading edge extension on the mid-high aspect ratio outboard wing?
4. To determine the aerodynamic pitch up angle an inherent drawback associated at low speeds over such wing planforms?
5. To determine the range of usable lift at low speeds.

Questions related to aerodynamic canard and wing interaction
Utilization of canard configuration to improve the aerodynamics of these wings and to check if it alleviates pitch up tendencies Canard and wing vortex interactions, its impact on steady-state aerodynamics and stability of the configuration.

1. What are the planform characteristics and design parameters to be considered for the design of canard configuration to maximize beneficial interference between the canard and wing?
2. Canard planform characteristics to provide an airplane stall
3. What is the effect of the canard proximity with respect to the wing?
4. What is the effect of the canard vertical position with respect to the wing?
5. What is the effect of canard deflection on the parent wing?

Questions related to experimental setup
What is the scale of the experimental model?

1. What is the kind of set up to go ahead with (half scaled model or full scale model)?
2. What are the modular components required to achieve the design objectives?
3. What is the kind of mounting system to utilize in order to simulate various angle of attacks?
4. Which fabrication technique would meet the wind tunnel model system design criterion in terms of surface finish, strength, stiffness, cost and time estimate as bounds ?

3.2. WIND TUNNEL MODEL GEOMETRY PARAMETERS AND DESIGN CHOICES

To further answer the specific research questions formulated in 3.1, it is important to understand the modular nature of the wind tunnel model and how the design of the setup aids in achieving the objectives.

Quantity	Value	Unit
Wing span, b_w	1.28	m
Wing reference area,S_w	0.2512	m^2
Aspect Ratio, AR_w	6.52	-
Canard span, b_c	0.54	m
S_c/S_w (exposed)	20%	-
Aspect Ratio, AR_c	6	-
Λ_{LEc}	45	°
Wing Airfoil	n0011sc-il-naca-langley-symmetrical-airfoil	-
Canard Airfoil	NACA 64A010	-
Fuselage cylinder diameter (D_f)	0.16	m
L_f/D_f	8.75 -close coupled configuration 10 - far coupled configuration	-

Table 3.1: Wind tunnel model parameters

The experiments conducted on the canard wing body configuration are as shown in fig. 3.2 and fig. 3.3 for close and far coupled canard configurations. Wing design is derived from the previous work for the AHEAD project [4], with langley symmetrical 11% thick supercritical airfoil, with a blunt leading edge. Thickness distribution and twist distribution of the wing are varied to obtain an elliptical lift distribution on the wing at cruise conditions for 2° incidence. The wing has compound three stage sweep with leading edge extension or strake swept at 76°, followed by 52° outboard wing sweep blending to highly swept extension and the moderately swept outboard wing of 36°. Canard had a leading edge sweep of 45°, which is greater than outboard wing sweep to increase mutual interactions between the canard and wing [21]. The ratio of canard exposed area to the wing exposed area is 20% for both the close and far coupled canard configuration, which is shown to be practical for such configurations [29]. A high aspect ratio canard of canard was chosen to make the airplane stall proof, i.e to make canard stall before the main wing. Also, the sweep back adds to this effect, due to tip loading resulting in lower stall angle for the canard. Stall of the canard would result in nose drop, acting as stall indication to the pilot. On the contrary the wing stall would result in pitch up and increase the tendency of deep stall. Both the longitudnal/axial and vertical positions of the canard can be varied with respect to the wing. Different canard positions evaluated with respect to parent wing is illustrated in the fig. 3.1. Canard and its deflection mechanism is explained in the subsequent section.

The fuselage is an axis-symmetric body of revolution. It consists of cylindrical section of 0.16m diameter, with 0.43 L_f portion of length for the close coupled canard configuration. The cylindrical section is increased to simulate the long close coupled canard configuration with 0.5L_f portion of length for the far coupled canard configuration. The nose block and the aft cone are designed as a function of a cubic polynomial function, such that it meets cylindrical constant diameter section of the fuselage with constant slope and curvature. The nose fineness ratio (L_n/D) of 2, was chosen to achieve divergence mach number of 0.85, based on empirical data from[49]. The aft cone finess ratio of 2.5 was chosen and shape of ending with a sharp tip was done with the intent to minimize pressure /base drag [50]. A myring cubic profile with a 25° was followed which had the least velocity perturbations along its external contour [51], there by reducing adverse pressure gradient and hence reducing pressure drag from the aft cone.

The geometric data of the wing body and canard are tabulated in the section 3.2. A mid wing configuration was chosen to minimize the fairing design , and the wing trailing edge is within the cylindrical section of the main fuselage, to avoid velocity perturbations associated with the aft cone. The setting

angle between the wing exposed root chord and fuselage reference was designed to have 2°. To integrate the canard with the fuselage for various vertical positions, small fairings were designed to blending with nose block contour.

Floor mounted half scaled model was explored, and wasn't favored due to the so called "peniche" effect and formation of horse shoe vortex formed at the leading edge of the wing combination. Following disadvantages of the half scaled model testing are listed below:

- The wall boundary layer modifies the free stream velocity approaching the model close to the wall, and its displacement thickness reduces the model's effective aspect ratio. Especially, at the Open Jet Facility, where it doesn't have an active boundary layer removal system to reduce boundary layer thickness.
- Lack of degree of freedom in terms of model attitude change, with the floor model is limited only to angle of attack simulation, and no side slip simulation is feasible.
- There is a detached stagnation point established upstream of the model along with a horseshoe vortex influencing the flow around the model. Especially canard being mounted close to the symmetry plane, its aerodynamic interactions with the wing which is one of the main objectives of the project seems to be highly influenced.

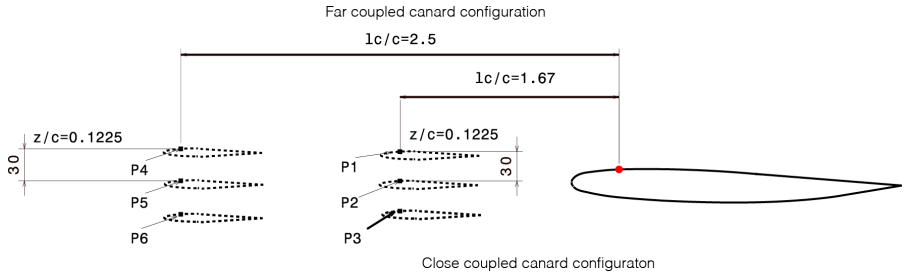

Figure 3.1: Different canard configuratons tested

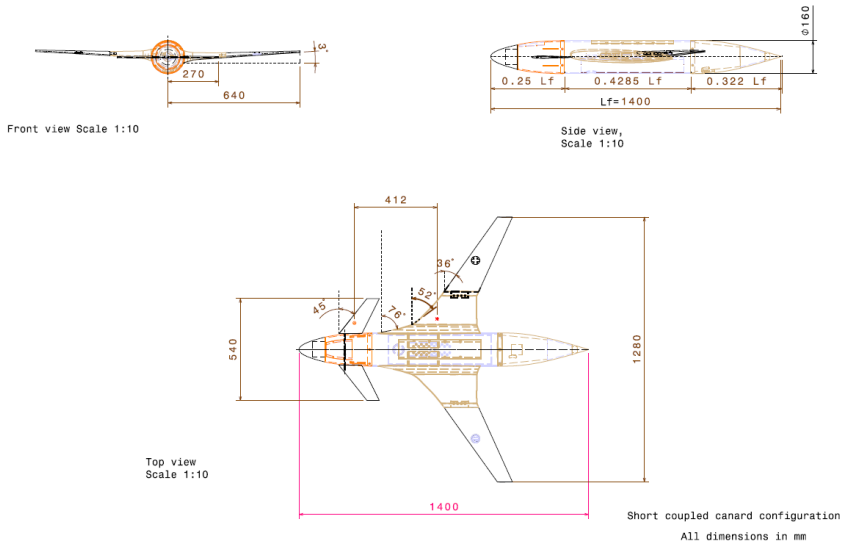

Figure 3.2: Canard wing body geometry for close coupled canard configuration

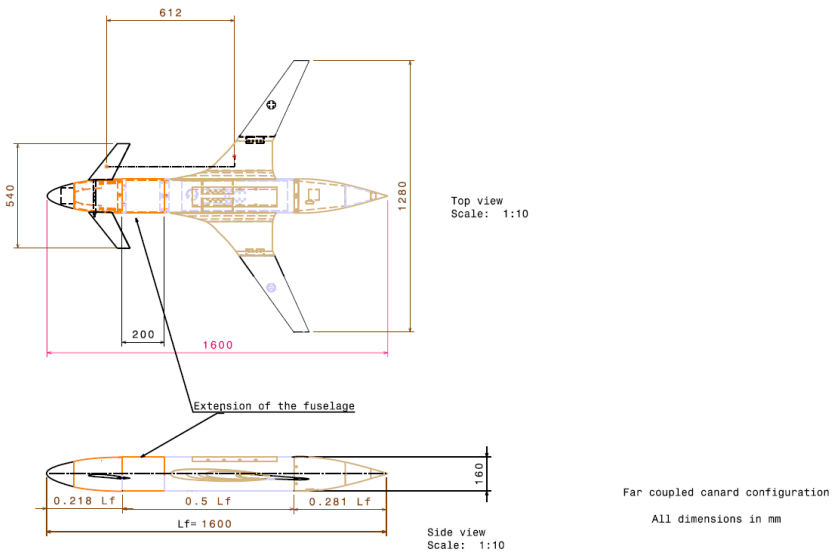

Figure 3.3: Canard wing body geometry for far coupled canard configuration

3.3. EXPERIMENTAL APPARATUS AND SETUP

3.3.1. WIND TUNNEL FACILITY DESCRIPTION

The experiment investigation for this MSc Thesis Project was carried out at the Open Jet Facility (OJF), high-speed lab, at Delft University of Technology. In this wind tunnel, the (theoretical) maximum speed is limited to 35 m/s, although in practice the maximum free stream velocity reached during the test campaigns was U_∞ =30m/s

The wind tunnel test section has an octagonal nozzle with an equivalent diameter of 2.85m. The facility is of closed circuit, and single return type.

The flow path in the tunnel is as follows:

The flow in the OJF is driven by a fan that is propelled by a 500kW electric motor. After the fan section, the flow passes through a long diffusor and it is guided by two rows of corner vanes for rotating the flow by 180°. The flow then enters a second, shorter diffusor, in which a wire mesh prevents any flow separation. Post the diffusor, in the settling chamber, the flow passes through several dense wired meshes reducing velocity perturbations and turbulence in the flow. The turbulence intensity of the flow in the OJF is in the order of 1% [52]. After the settling chamber, the flow is accelerated through a contraction section (contraction ratio of 3:1) and is then blown to the open test section at the set free stream speed. Considering the recirculation of the flow, heat is added to the flow and to compensate and maintain the optimal operating conditions, the flow is cooled by a 350kW radiator at the end of the test section. Finally, before the flow re-enters the fan, it is redirected 180° again by two rows of corner vanes. Thus, completing the closed circuit.

To measure and monitor the operating conditions of the tunnel, the following sensors are in place:

- A thermocouple placed in the settling chamber, which measures freestream temperature, T_∞.
- A pitot-static tube placed in the settling chamber, which measures freestream dynamic pressure as the difference between total and static pressure, the reading from this pitot tube is connected to a Mensor digital pressure gauge.

$$q_\infty = p_t + p_\infty \tag{3.1}$$

With the measurements from this set of sensors, a LabVIEW script in the WindTunnel data acquisition system, enables monitoring of all these variables and computation of p_∞ and U_∞. The freestream velocity of the wind tunnel can be varied, by altering the fan rotational speed.

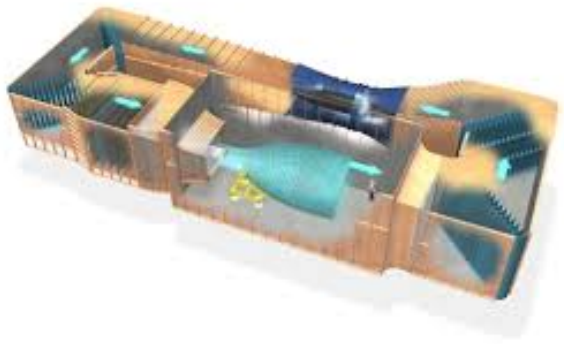

Figure 3.4: Circuit layout of the open jet circuit facility
[1]

No active floor boundary layer removal/control system is available to reduce the floor boundary layer height. Utilization of a boundary layer splitter plate, serves to reduce the floor boundary layer developed from the tunnel section, with a fresh boundary layer formed on the splitter plate. The splitter plate is placed≈ 12 cm above the test section floor, which is the measured thickness of the boundary layer formed at the test section. The splitter plate in conjunction with the floor board creates a $3/4^{th}$ tunnel minimizing the open test section corrections, which is elaborated in section 3.7.

3.3.2. MODULAR WIND TUNNEL MODEL AND EXPERIMENTAL SETUP DESCRIPTION

The wind tunnel model used for the experimental campaign was 2% scaled hybrid wing body configuration made of Aluminum Al 6061 alloy. The generic three view sketch is presented in the fig. The model in the close coupled configuration is 1.6 m and in the far coupled configuration is 1.8 m long with a wing span of 1.28m. The fuselage is made of modular pieces consisting a total of 8 pieces, with most modular parts at the aft section to further allow mounting of proof of concept BLI engine systems. The wing is mounted as mid wing configuration which is modular in nature as well, consisting of the inboard wing with a straked leading extension and the outboard wing. The wing is mounted at the constant cylindrical section of the fuselage, this is done to minimize the fuselage effect on the wing [53]. The wing is modular, with ability to traverse 125mm back and forward axially along the fuselage reference line.

Considering the high inertial loads and aerodynamic loads on the external balance, a new model support system was designed and fabricated for this campaign.

A three-point support system with a mounting plate on the balance was designed with wing support beams, trunnions and a pitch strut.

The wing support beams were designed to provide strength and stiffness to the model under high aerodynamic loading and unsteadiness expected at moderate to high angles of attack. The trunnion and the wing pivot were housed at approximately 60% of the semi span and 30% along the local chord of the wing. The wing pivot utilized a bearing mechanism to provide smooth rotation about the wing pivot axis. The wing support struts were elliptical in cross section and tapered to minimize the interference effects. They were further faired by housing them in symmetrical profiled fairings available at the Low speed Lab, TU Delft. Fairing itself were not connected to the external balance and was mounted on the floor board. The clearance between the fairings and the wing struts were approximately 2 mm on all sides at the highest loading case, ensuing no transfer of load transfer between the model and the fairing.

The pitch strut was mounted on to the bottom of the aft section at 68.75% of fuselage length aft of the model nose. It was located to minimize the interference and near field interactions with the fuselage [53]. An elliptical cross section of 10mm X 10mm aluminum was utilized with bearing assembly at the bottom attaching itself to the bell crank mechanism used to modify the attitude of the model. It did not have any significant loading bearing requirement; however, it was designed to be stiff enough for holding is position at different model attitudes. The angle of attack sensor wire was routed through the hollow fuselage center fuselage and was attached to the pitch strut as a support and prevent any fluttering during the wind on condition. The drag increase with attachment of the sensor wire was also considered in the application of the support interference corrections.

In addition to the modular wing and fuselage design, another modular geometry feature of the model is the three longitudinal and vertical position of the canards, simulating the close and far coupled configurations at high, mid and low vertical positions. The variation in the vertical positions especially the high and low canard configuration is brought about by rotating the symmetrical part of the nose block by 180°. The longitudinal variation of close and far coupled configurations is achieved by extending the constant cross section of the center fuselage. The aerodynamic implications are critically discussed in the result section etc.

The final variable geometrical aspect of the wind tunnel model is the all moving canard. The canard deflects symmetrically connected by a single shaft running spanwise through the nose block and pivots bout 25% of the root chord of the starboard and port canards. Canard can be set in the range of −40 to +40 °(postive(+) deflection is trailing edge down), with the required stiffness.

The schematic drawing of the experimental setup and the model configuration has been included in fig. 3.5 and fig. 3.6. The Model mounting and the dimensions with respect to the tunnel are shown in fig. 3.7.

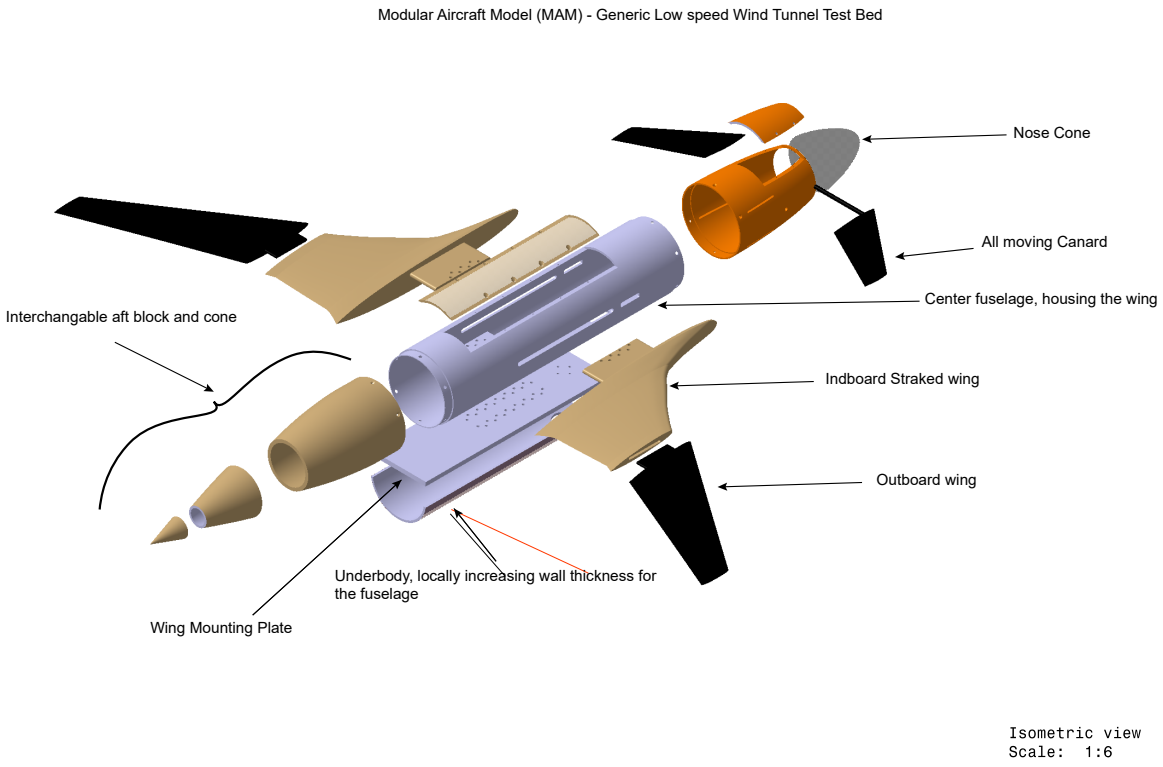

Figure 3.5: Modular aircraft wind tunnel model

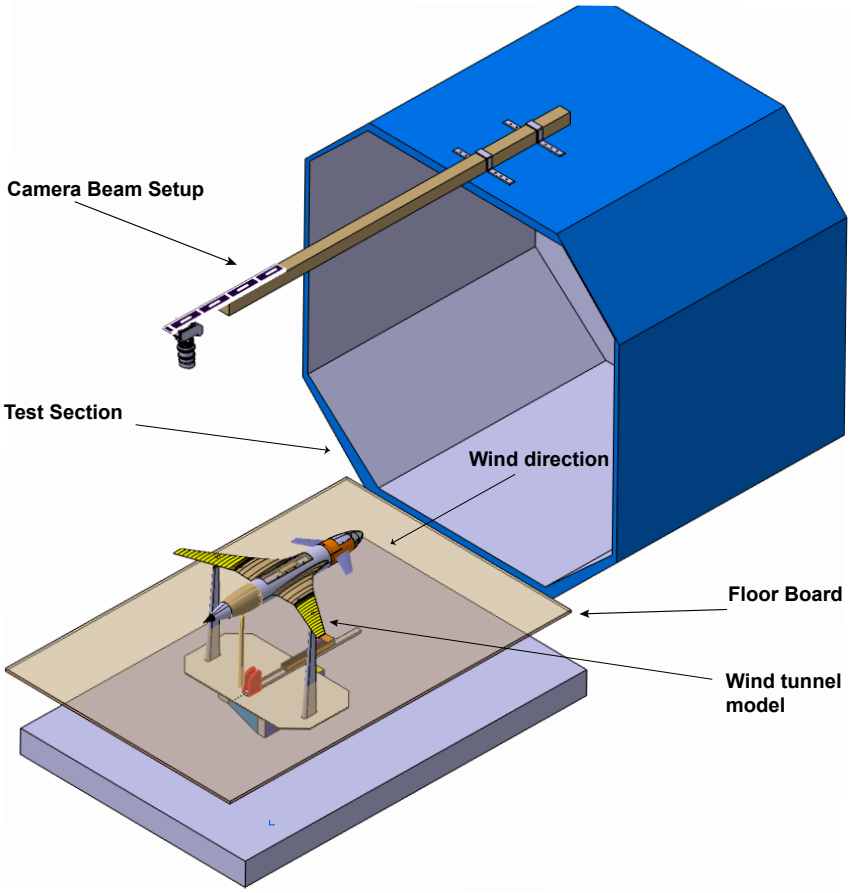

Figure 3.6: Generic Experimental Setup

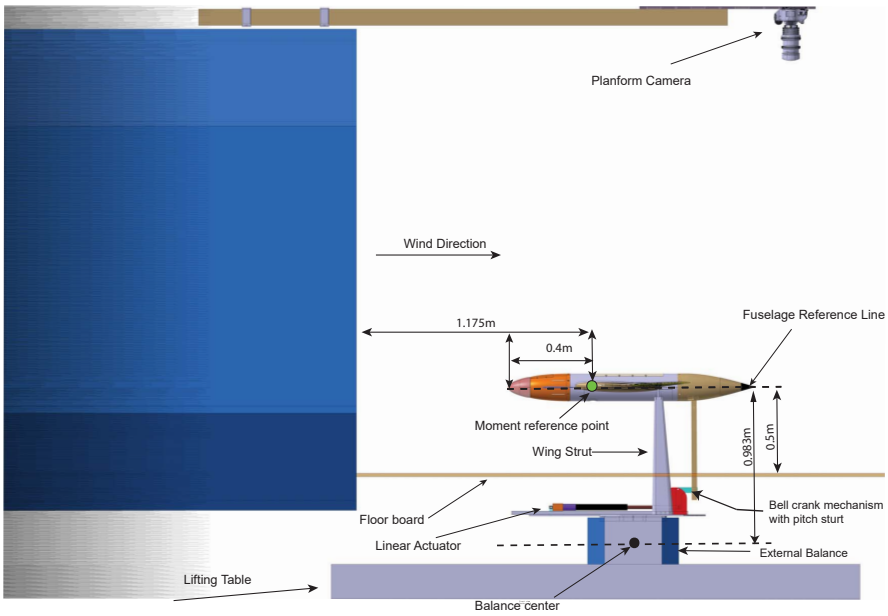

Figure 3.7: Experimental setup, individual components

3.4. INSTRUMENTATION

3.4.1. EXTERNAL BALANCE

NLR designed and manufactured 6 component external balance was used for force and moment measurements for the experimental campaign. The axis system followed is shown in the fig. and load range of the load cells when loaded individually and simultaneously loaded are tabulated in tables section 3.4.1

The balance consists of a metric (painted yellow) and a non-metric (painted blue) frame connected by six (6) load cells. The loads cells are sensitive in one direction only and are decoupled from the other directions by means of elastic hinges. The test model is connected to the metric side by means of an aluminum plate which has several holes in a pattern for mounting various setups. The non-metric side of the balance is attached to the lifting table or rigid ground by means of three M10 bolts for a torque of 40 N-m. Other than this the load cells are temperature compensated for a temperature range of -10°C to +40°C, as the calibration of the balance is done at room temperature.

Other than the tabulated load range, the load envelope is limited by the Load Rhombi Equations, which is obtained from the calibration matrix of the load cells. These equations can also be used as load monitoring equations in real time. Any inertial or aerodynamic load combination, should satisfy all the equations to avoid overloading of the balance load cells.

The load envelope check was carried out to decide on the scale of the model and extent of support system. Ideally, models are mounted to the tunnel center axis to alleviate any ground effects from the floor board. However, specific to our experimental setup this was not feasible, owing to the long moment arm (in z direction) between the balance center and the wing body aerodynamic center (assuming the lift resultant acting at this point). This led to a possibility of exceeding the limits for the pitching moment component especially at negative angles of attack, considering the addition of negative lift component to the weight component elevating the load on the pitching moment load cell. As a trade-off, the support system height was reduced and the model was below the tunnel center line by 'x' distance. The height was reduced such that the fuselage is well clear of the boundary layer developed on the floorboard at moderate to high incidences (20-25°). The negative angle of attack testing range was also limited to −5°. The load rhombi equations were programmed into the data acquistion software for live monitoring of the load ranges. Also, a warning display was incorporated into the data acquisition program to prevent exceeding of the load cell range beyond 90% of its rated load capability under simultaneous loading.

Component	Load Range	Unit
Axial Force	± 250	N
Side Force	± 500	N
Vertical Force	± 500	N
Rolling Moment	± 500	N-m
Pitching Moment	± 250	N-m
Yawing Moment	± 50	N-m

Table 3.2: Maximum nominal load range for all components loaded simultaneously

Component	Load Range	Unit
Axial Force	± 250	N
Side Force	± 600	N
Vertical Force	± 3500	N
Rolling Moment	± 550	N-m
Pitching Moment	± 500	N-m
Yawing Moment	± 125	N-m

Table 3.3: Maximum single loads

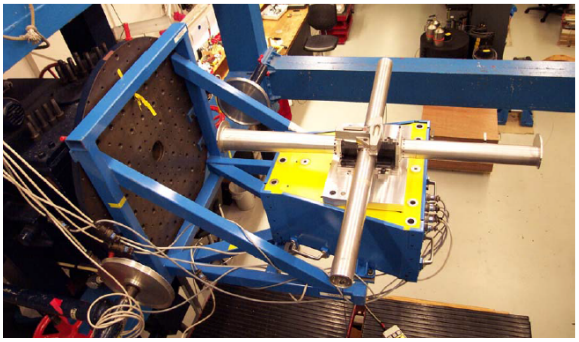

(a) External Balance with universal calibration model

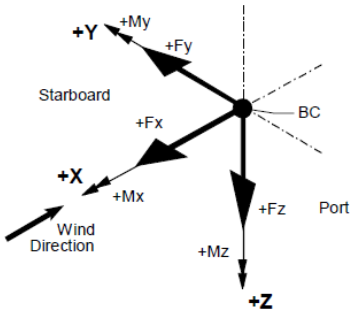

(b) Axis system and balance sign conventions

3.4.2. ANGLE OF ATTACK MEASUREMENT SENSOR

JDI 100 MEMS ±30 ° is a single axis inclinometer was used as the sensor is used to find the geometric inclination of the WT model for both wind on and wind off conditions.. It has an integrated temperature sensor and is temperature compensated for best possible absolute accuracy.

The geometric angle of attack error and resolution is a function of the tilt sensor instrumentation error housed in the model. The tilt sensor was mounted on a three triangle finished steel plate with a 100-micron finish to avoid any undulations for mounting of the sensor. The sensor was fastened on to the steel plate with help of two M3 screws along with double sided tape, for uniform surface adhesion.

The sensor completed a closed loop for angle of attack measurements, with each linear actuator movement, the exact geometric attitude irrespective of the stiffness of the support system is measured and recorded. In other words, the actual true value of the model attitude is recorded as a function of resolution and absolute accuracy of the sensor. Normally, angle of attack measurements is done at the actuator level (i.e. sector with sun and planetary gear mechanism) with aid of an encoder. This value is assumed to be the model angle. However, this uncertainty is reduced/eliminated with angle of attack sensor housed within the model.

Closed loop of measurement is achieved by manual intervention (by means of digital readout, available from the sensor) than the conventional electronic feedback to fix a desired geometric angle of attack. However, each recorded value is a true value. (Though it is not an exact integer, as desired in the test matrix or followed as a standard practice by control and performance engineers). The data set was measured in steps of 1°, providing enough data points for trend analysis and to capture any nonlinear aerodynamic effects which may be characteristic of such an unconventional configuration.

Performance parameter	Value	Units
Absolute Accuracy	0.015	°
Relative Accuracy	0.004	°
Digital Resolution	0.0001	°
Repeatability	0.01	°
Non-Linearity[FS ± 30]	± 1	-
Accuracy-Temperature	0.5	°C

Table 3.4: Angle of Attack sensor equipment uncertainity parameters

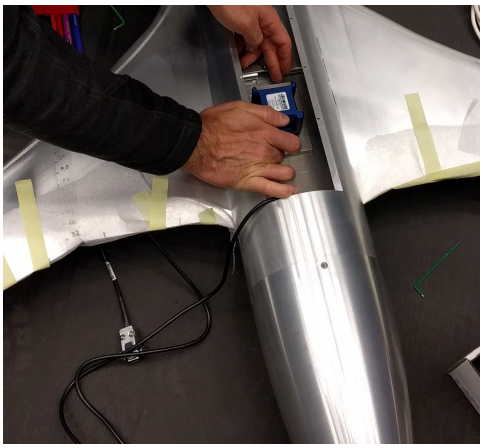

Figure 3.9: Angle of attack sensor mounting in the scaled model

3.4.3. LINEAR ACTUATOR-INCIDENCE CHANGING MECHANISM

In order to change the incidence of the model and automate it, a bell crank mechanism with friction less bearings in conjunction with a linear actuator was incorporated. The linear movement of the actuator was converted into the angular movement about the wing pivot point, by causing a piston movement of the pitch or the aft strut. Varying the stroke length resulted in a change of attitude of the model. The stroke length for the desired angle of attack over the incidence range was first calibrated, with feedback from the tilt sensor housed in the model. This stroke length was fed each time to achieve the desired angle of attack. At higher incidences the stroke length had to be fine-tuned depending on the configuration, considering the various unsteadiness for different configurations.

The primary criteria in the choice of the linear actuator was to provide a stiff setup i.e to hold position under aerodynamic loading. The other criteria was to provide the required stroke length to achieve the required angle of attack range and easy coupling with the bell crank bearing mechanism.

To meet the first criteria a linear actuator was chosen which could handle a dynamic axial force of up to 90 kgf without any significant bending was to be chosen. A factor of safety of 2 was considered. Under static loading conditions, the linear actuator could handle up to 200kgf. From the free body diagram of the bell crank mechanism, considering the distance to the wing pivot and pitch strut pivot a stroke length of 200 mm was required to achieve an angle of attack range of -5 to +25°. Considering further feasibility of high angle testing for other configurations, a linear actuator with 300mm stroke length was chosen. Other than this the linear actuator had a least count of 3mm allowing for a change in incidence of 0.1°. This least count could be further reduced with the utilization of PWM micro-controller to drive the servo motor, which was used in our case to achieve greater repeatability.

Based on these requirements heavy duty servocity linear thrust actuator which could handle 90kg dynamic thrust or axial force and stroke length capability of 300 mm was chosen. The servo was made of metal gear and had ACME steel lead screw to create a linear movement.

This was housed in a zinc aluminum alloy casing with the piston end and clevis end compatible to be machined with bearing mechanism of the bell crank. The specifications of this actuator are tabulated in section 3.4.3 and the engineering drawing is seen in the fig. 3.11

Voltage Range (Recommended)	6V - 14V
Voltage (Nominal)	12V
Product Weight	1.41kg
PWM Signal (Fully Retracted)	2000µs
PWM Signal (Fully Extended)	1000µs
Operating Temperature	-20°C to +60°C
Speed (No Load)*	0.30” per second
Speed (Max Load)*	0.20” per second
Current Drain (Idle)*	140mA
Current Drain (No-Load)*	1A
Current Drain (Max Load)*	4.5A
Deadband Width	8µs
Dynamic Thrust*	180 lbs
Static Load	500 lbs

Table 3.5: Specifications of the linear actuator

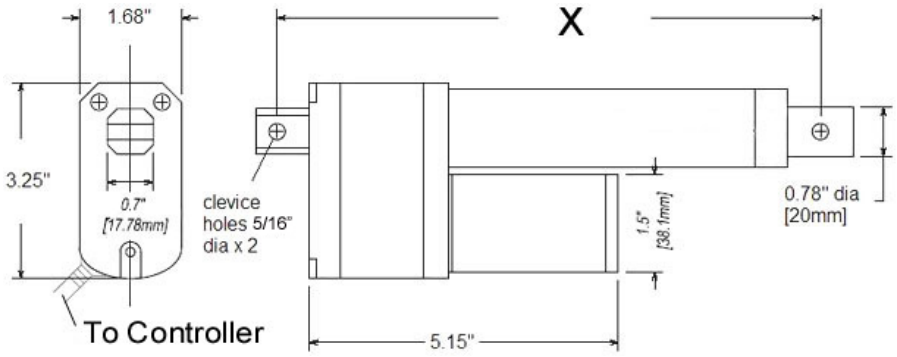

Figure 3.10: CAD specifications of linear actuator

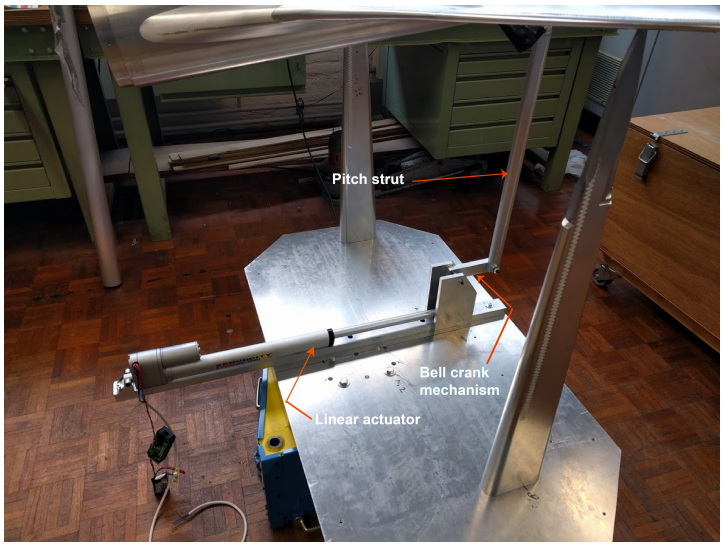

Figure 3.11: Linear actuator and bell crank mechanism setup

3.5. FLOW MEASUREMENT TECHNIQUES

3.5.1. OIL FLOW VISUALIZATION SETUP

Oil flow surface visualization technique was used to capture the surface streamlines or the shear stress footprint. An aromatic-free paraffinic white mineral oil of medium viscosity was mixed with fluorescent dye and applied on the upward surface of the wing with the aid of soft paint brush. The fluorescent dye has a characteristic glow when brightened with Ultra Violet (UV) light in a dark test section. The paint would be re-applied for each configuration change or for every 5 runs whichever was earlier. The re-application involved cleaning of the upper surface with ethanol and tissue paper, rather than cloth to prevent cloth fibres from sticking to the surface.

On application of the oil mixture, the tunnel was run for approximately 3 minutes to obtain a consistent surface oil flow pattern. Photographs were taken at intervals of 15 seconds to see how the surface streamlines develop over the wings and to further analyze the topology of the flow field. The photographs were taken from a Nikon D7500 camera at 24mm focal length capturing both the starboard and port wings. The camera was mounted on a cantilever wooden beam designed and on a aluminium traverse plate just above the test section. The camera was remotely controlled to capture the photos. Due to availability of only one UV light source, the light source was placed closer to the port wing, just out of bounds from the test section. This resulted in emphasized images on the port side as compared to the starboard side which was in the shadow of the fuselage.

(a) UV light source setup

(b) Camera beam mounted on top of the OJF test setion

(a) Camera mounted on aluminium traverse mount

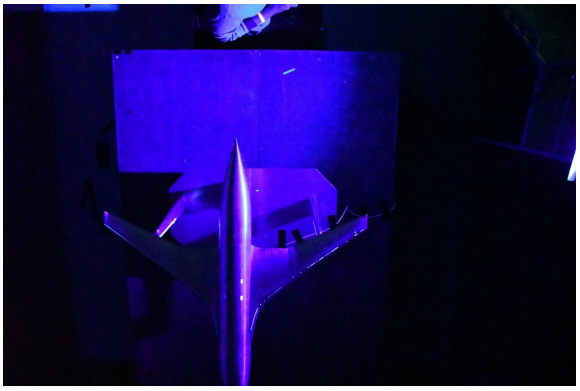

(b) Preliminary UV light setup check on illumination

Figure 3.13: Oil flow visualization setup and checks

3.5.2. WAKE RAKE - TOTAL PRESSURE MEASUREMENTS SETUP

The wake rake system was placed 1.2 times $\bar{c}$ from the wing trailing edge to survey the wake and quantize the total pressure as see in fig. 3.15a. The wake survey plane measured was 400 mm (spanwise/y direction) x 450mm (z direction). It was mounted on a manual traverse system, 8 spanwise stations were measured in steps of 50 mm. The wake rake along the z axis was traversed in steps of 20 mm to capture the wake structure developed behind the wing.The reference or the origin for the wake rake setup from the z axis was from the surface of the floor board and the reference for the y axis was the point corresponding to the fuselage reference line. At α=0° incidence the tip of the fuselage reference line was at 500mm from the floor board and at α=6° was 430 mm from the floor board as shown in fig. 3.15b

Prior to data acquisition, a functional test was performed to check each probe in the pressure rake. This was done by creating a small pressure difference in each channel, using a regulator valve to blow air from the wind tunnel secondary air supply. This test also served to associate each pressure probe with its corresponding plastic tube and to assign a number them for easier post processing.

Then, the plastic tubes were connected to the pressure scanning system electronic modules. For the test cases at U_∞ =15 m/s, the 160 Pa modules were sufficient. The 16 pressure tubes were connected to a 160 Pa module (channels 1-8 in side A and channels 9-16 in side B) and the 2 static pressure tubes to a different 160 Pa module. For the test cases at U_∞ = 25 m/s, total pressure measurements required the 600 Pa module.

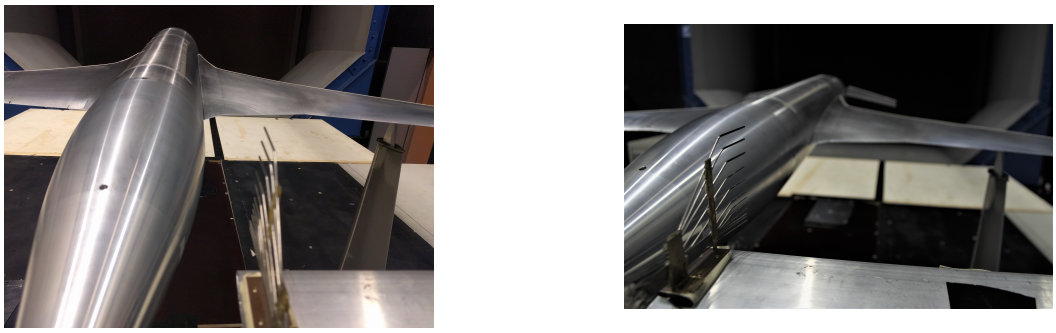

Figure 3.14: Wake rake setup with manual traverse

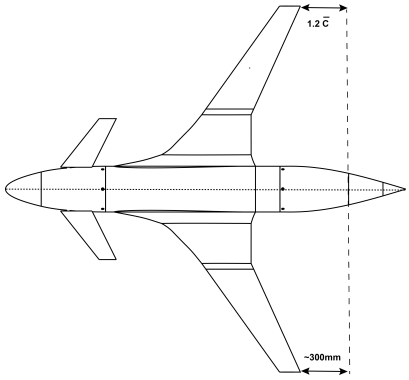

(a) Wake rake plane position along the x axis

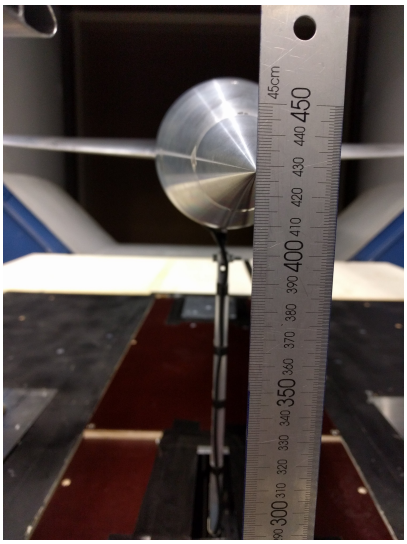

(b) Wake rake position z axis with respect to the floor board at α=6°

Figure 3.15: Wake rake setup positioning

3.6. EXPERIMENTAL TEST MATRIX

To answer the research questions formulated in section 3.1, an experimental campaign is proposed. Modular component build-up method is planned to be utilized, spanning over two experimental campaigns. Considering the novelty of the configuration and to understand the aerodynamic effect of each component, component build-up method is proposed.

To evaluate and understand the aerodynamic interaction of the canard and the wing, and for initial evaluation of static stability, the test matrix for the experimental campaign was designed around the following configurations, thus, highlighting the aerodynamic build-up, as follows:

- Wing body configuration - henceforth referred to as baseline configuration.
- Effect of axial proximity of the canard to the wing. (viz. Close coupled and Far coupled configurations). Based on the axial location of the canard three vertical locations (viz. High, Mid/coplanar and Low position) of the canard are varied.
- Effect of canard deflections for both close and far coupled configurations at three vertical locations.

A total of 9 combinations, consisting a total of 70 runs was planned for understanding the effect of canard on the wing is proposed capturing the important design points for future studies. To understand the flow field, especially the regions of separation and vortex footprint, detailed oil flow visualization studies are planned at critical angles of attack, where non-linearities and breaks in the longitudinal parameters are to be observed during the force and moment characteristics measurement. Along with oil and tuft flow, qualitative wake rake measurements was planned to understand the off-surface phenomenon typical of vortical flows. Several repeat runs were planned to understand the data repeatability of the experiment both in short and long-near term time frames.

Configuration	$H = z/\overline{c}$	$lc/\overline{c}$	δ=10°	δ=0°	δ=-10°
Wing body	0	0	-	X	-
High close coupled Canard	0.1225	1.67	X	X	X
Mid close coupled canard	0	1.67	X	X	X
Low close coupled canard	-0.1225	1.67	X	X	X
High Far coupled canard	0.1225	2.5	X	X	X
Mid Far coupled canard	0	2.5	X	X	X
Low far coupled canard	-0.1225	2.5	-	-	-

Table 3.6: Experimental Test Matrix

3.7. OPEN TEST SECTION CORRECTIONS

Though wind tunnel tests and data from them aid in understanding aerodynamic characteristics and validating numerical predictions of complex unconventional configurations. There are still certain errors which need to be corrected for the data to be comparable to free air conditions. These inaccuracies are associated with the support structure interference and the wind tunnel boundary corrections. For the close test section, corrections are applied for the bounding walls, as compared to the open test section where corrections are limited due to free jet boundaries and deflection of the jet altering the streamline curvature on the model, there by largely changing the lift curve slope as seen in figs. 3.16a and 3.16b respectively. Though, closed test section corrections are larger in magnitude, they are much accurate as the wall boundary conditions are well established. Barlow et.al [5] states that when using a floor board to shield the balance from the airflow is, the open wind tunnel is not completely open and one solid boundary tunnel exists. This tunnel configuration was referred to as $3/4^{th}$ tunnel and correction method was detailed by Heyson et.al [3] and Ewald et.al [15].

From section 3.3.2 and fig. 3.7 it can be seen that setup used for this study can be classified as a $3/4^{th}$ tunnel and corresponding corrections needs to be applied. In the $3/4^{th}$ tunnel case the floor board

primarily used to shield the external balance from the tunnel airflow and minimize its interference with aerodynamic characteristics. For the application of corrections, floor board acts as a reflection plane and is used to minimize the correction factors as compared to free jet boundaries of complete open test section. Figures 3.17a and 3.17b shows the large deviation in correction parameters for the open test section to close test section as compared to the open test section with floor and the closed test section. Please, note the complete wind tunnel in these figures refers to the closed test section.

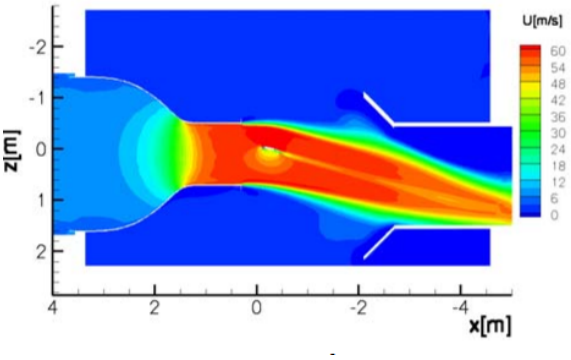

(a) Deflected jet from the open test section,[54]

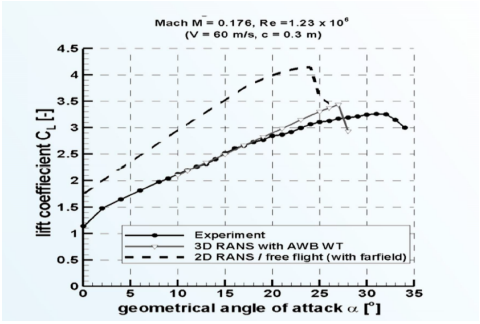

(b) Change in lift curve slope as compared to experiment with CFD,[54]

Figure 3.16: Open test section limitations for corrections

3.7.1. HEYSON'S METHOD OF CORRECTIONS FOR THE $3/4^{th}$ TUNNEL

In the classical wall corrections formulated by Glauert for lifting surfaces, it is assumed that the lift is due to circulation alone and the trailing wake is straight aft of the plane. Thus, the free stream provides a vertical interference to the model. Heyson et.al[3] on the other hand considered the wake as point of doublets with axis tilted relative to the model wind axis system. This modeled wake for a $3/4^{th}$ tunnel proceeds linearly to the floorboard and as it coincides with the floor, it moves aft along the floor. The floorboard acts as a closed wall boundary, leading to the boundary condition of velocity components normal to the wall to be zero. From the image and superposition of these doublets, the interference at the model is calculated. Heyson's method results in correction for both vertical and horizontal components. From fig. 3.18a it can be seen that the wake passes downward intersecting the floorboard and moves backward along the floor. The floorboard acts as a reflection plane and by applying the boundary condition of the vertical doublets cancel each other out, which are acting normal to the wall. The longitudinal or the horizontal doublets acting along the wall add, rather than subtract.

Heyson's corrections methodology described in the report will follow the references of [3, 55, 56] for calculating the various interference and correction factors. The interference factors are calculated as a function of the wake skew angle χ as shown in fig. 3.18b. The wake skew angle is angle formed between the vertical and wake, and is complement to the downwash angle. The downwash angle θ is computed utilizing the definition of an elliptically loaded wing and average downwash angle over the wing. This downwash angle is used in calculation of the wake skew angle following the procedure laid out in reference [3]. The effective downwash and the effective wake skew are calculated from eq. (3.3) and [56]. Interference factors are determined from the effective angles, where as the induced velocities are determined from the wake skew and the downwash angle.

$$tan\theta_i = \frac{4 \cdot tan\theta}{\Pi^2} \tag{3.2}$$

$$tan\chi_i = \frac{\Pi^2 \cdot tan\chi}{4} \tag{3.3}$$

The interference velocities at quarter chord mean aerodynamic chord as reference point are determined from the interference factors computed. Equations eqs. (3.4) to (3.7) for the same are listed

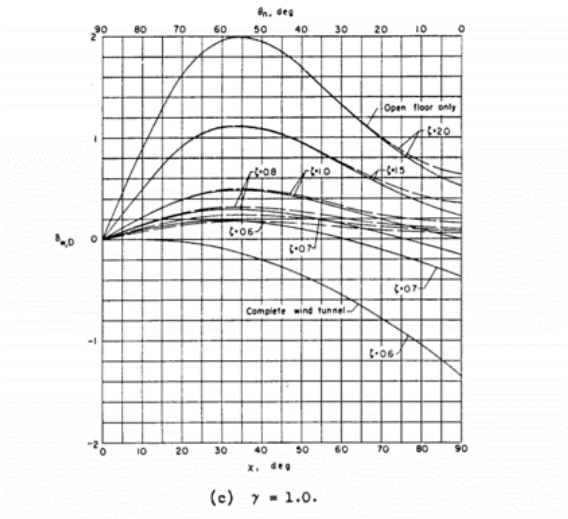

(a) Comparision of boundary layer corrections for open test and closed test section,[3]

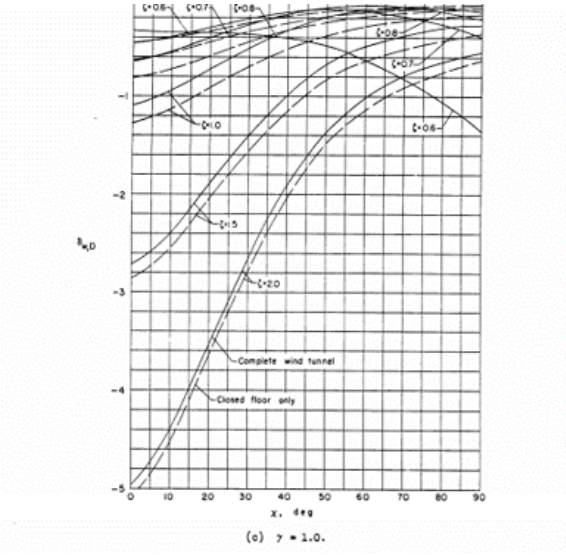

(b) Comparision of boundary layer corrections for open test section with floor only and closed test section,[3]

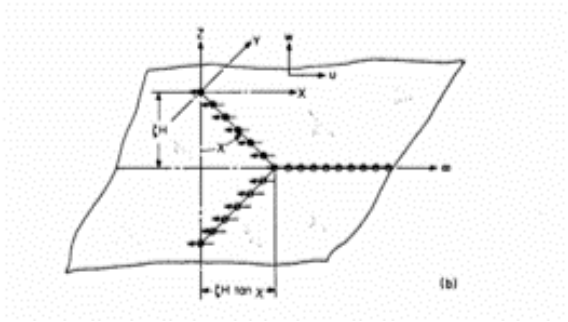

(a) Wake and image system for closed floor only. [3]

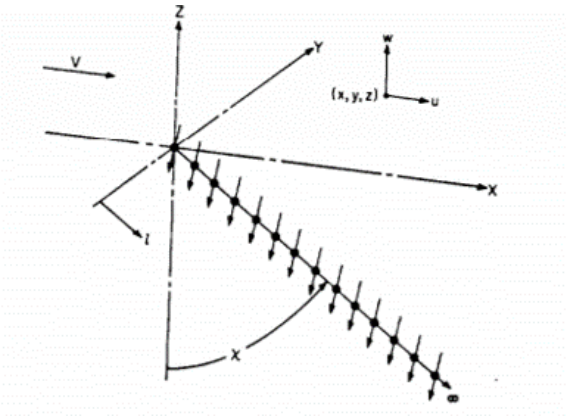

(b) Wake skew angle and reference system,[3]

below, where w_0 and u_0 are mean value of vertical induced velocity and mean value of longitudinal induced velocity. A_m and A_t are momentum area of the wing and tunnel cross sectional area respectively. The δ factors are similar to the wall correction factor and are dependent on the tunnel dimensions, span loading, height of the model from the tunnel center.

$$\Delta w_l = \frac{\delta_{wl} \cdot A_m \cdot w_0}{A_t} \tag{3.4}$$

$$\Delta u_l = \frac{\delta_{ul} \cdot A_m \cdot w_0}{A_t} \tag{3.5}$$

$$\Delta w_d = \frac{\delta_{wd} \cdot A_m \cdot u_0}{A_t} \tag{3.6}$$

$$\Delta u_d = \frac{\delta_{ud} \cdot A_m \cdot u_0}{A_t} \tag{3.7}$$

The interference velocities obtained are combined used to calculate the total interference at the reference point on the model.

$$\Delta w_l = \Delta_{wl} + \Delta_{wd} \tag{3.8}$$

$$\Delta u_l = \Delta_{ul} + \Delta_{ud} \tag{3.9}$$

The corrections for the angle of attack and dynamic pressure are computed from the total interference velocities as follows :

$$\Delta\alpha = tan^{-1} \cdot \frac{\Delta w}{V + \Delta u} \tag{3.10}$$

$$\frac{q_c}{q} = (1 + \frac{\Delta u}{V})^2 + (\frac{\Delta w}{V})^2 \tag{3.11}$$

From the corrections to the dynamic pressure and change in angle of attack due to interference velocities, the change in lift coefficient and drag coefficient are computed. Figure 3.20 illustrates the change in angle of attack acting on the lifting surface.

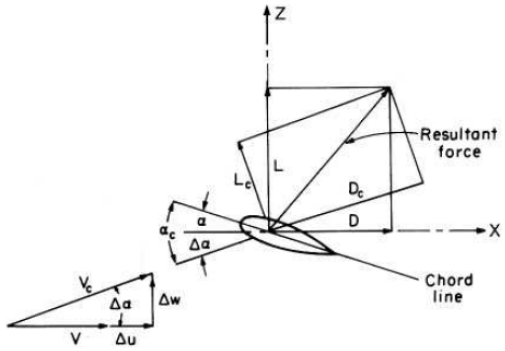

FIGURE 10.43 Nomenclature for Heyson's wall corrections.

Figure 3.19: Change in angle of attack due to induced velocities, [3]

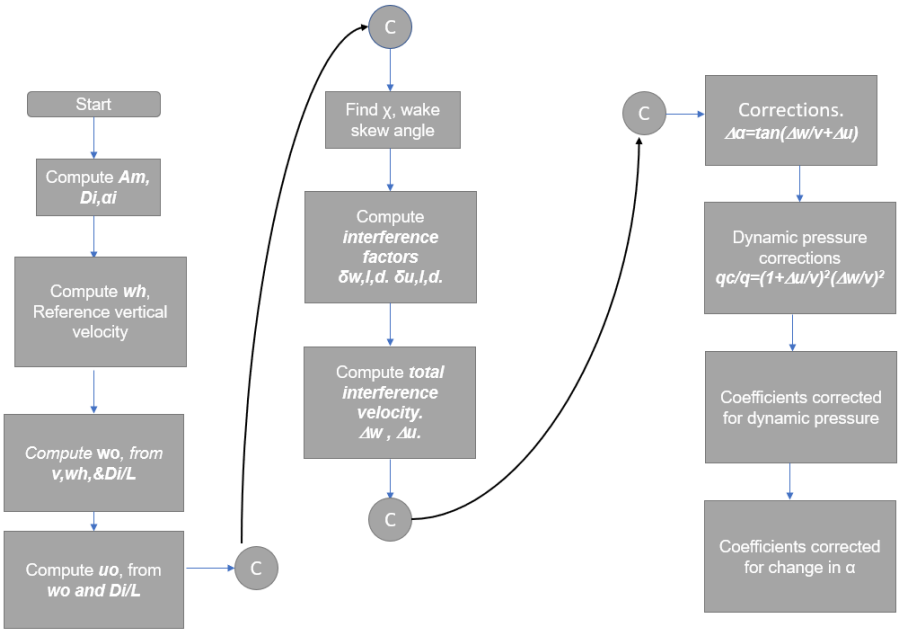

Figure 3.20: Flow chart for steps involved in open test section corrections as formulated by Heyson

Corrections led to an increase of 14.2% increase in lift curve slope in the linear region for the baseline configuration with $\Delta\alpha$ change of 3°. Dynamic pressure variation of up to to 0.5-1% were observed, especially at high angles of attack.

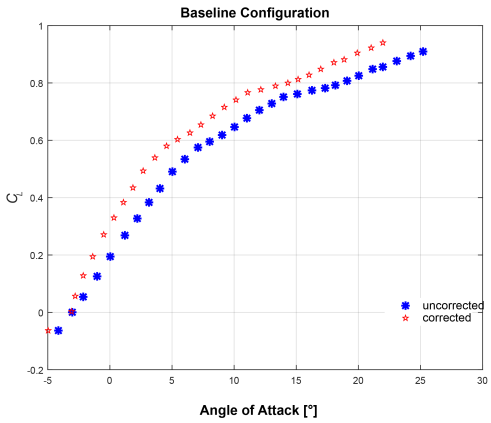

(a) Comparison of corrected and uncorrected lift coefficient curve

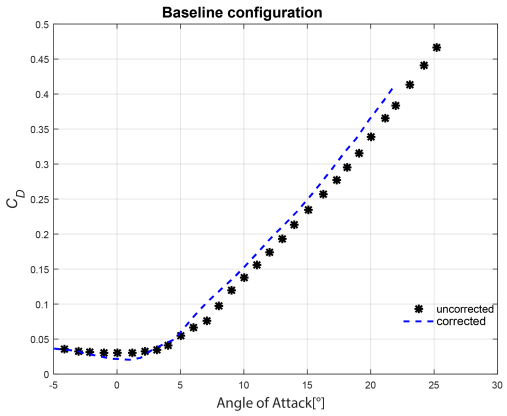

(b) Comparison of corrected and uncorrected drag coefficient curve

Figure 3.21: Comparison of corrected and uncorrected longitudinal coefficient data for a open test section

3.7.2. TARE AND INTERFERENCE EFFECTS

To sustain a scaled model in a wind tunnel and provide stiffness to get accurate aerodynamic force measurements support structures are utilized. These support structures attached to the model alter the model aerodynamics in the near field leading to interference drag and add their own profile drag. As discussed in section 3.3.2 a three point support mechanism was utilized for supporting the wind tunnel model. The wing supports were shielded by fairings to reduce the tare drag of the supports. However, this increase in size of the fairings shielding the structure results in an increased interference drag. So, these effects need to be cautiously corrected for.

In order to evaluate the tare and interference effects in combination usually the image or mirror system is utilized as discussed in [5], where the model mounted on 3 point support system is first tested in a normal manner and them the model is suspended from the tunnel roof with similar supports. The bottom supports remain in their original position, however, certain clearance is provided such that the balance measures drag of the support system in presence of the model. This provides the interference and the tare drag combined which can be used for correcting the influence of support structure on the force and moment data.

Such methodology was hard to follow in the open jet facility as the inversion of model and suspending model would be impractical. Tare drag were obtained without the model and the pitch strut height was varied simulating various incidence conditions of the support system. Also, care was taken the data acquisition cable was attached to the pitch strut while measuring the tare drag, to account for any profile drag changes that might emerge. These tare drag measurements for different incidences were subtracted from the measured drag curve. As expected the drag values reduced the highest at zero lift conditions, with variation of around 10 drag counts. On application of overall dynamic pressure correction and streamline curvature corrections, drag variation of 5 drag counts was computed for the baseline configuration, as seen in fig. 3.21b. To understand the effect of interference of the fairing on the model, as an exploratory study tests with and without fairings were conducted, which showed that C_L values decreased by a factor of 0.5-1%,especially at higher angle of attack indicating the fairings created an extra suction on the lower side of wing. C_{Dmin} with and without fairing varied by a factor of 40 drag counts, indicating the large amount of profile drag created by the elliptical profiled (bluff body) struts.

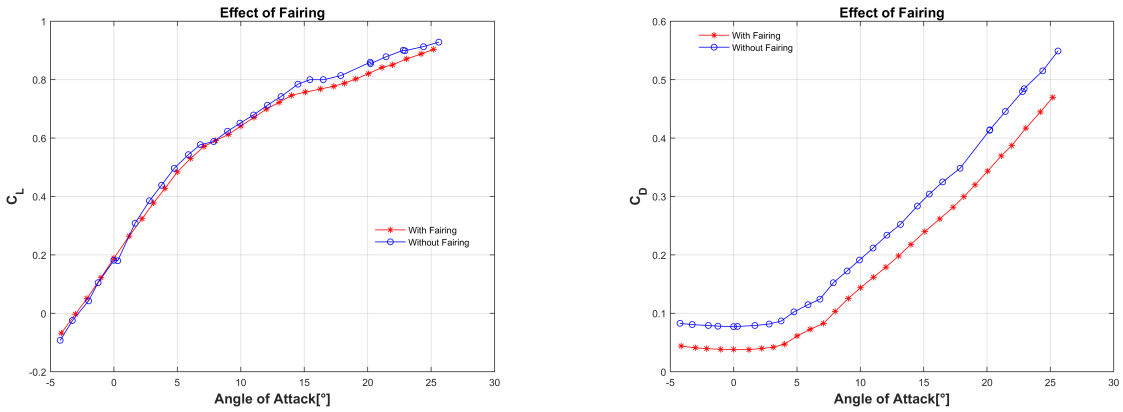

(a) Comparison of with and without fairing over the uncorrected lift coefficient curve

(b) Comparison of with and without fairing over the uncorrected drag coefficient curve

Figure 3.22: Comparison of fairing and without fairing longitudinal coefficient data

3.8. NUMERICAL SETUP

The hybrid wing body canard geometry optimized for elliptical lift distribution at cruise is imported into SALOME mesh generator to create a fluid domain and boundary layer mesh. The flow field grid formed is imported into the SU2 solver for carrying out RANS simulations. Symmetrical flight conditions were studied on a half model to reduce computational time with a hemispherical fluid domain as illustrated in fig. 3.23. An unstructured mesh was generated on the symmetry, farfield and the hybrid wing body configuration. Considering viscous simulations were conducted, a boundary layer mesh was generated with y+ value < 1. Mesh sensitivity studies were conducted from 0.2 to 10million elements, with 6.5 million elements to find a converged solution for drag coefficient variation. Simulation conditions are listed below in the table table 3.7.

The variation in the geometry of the numerical simulations to the wind tunnel model, were that no body of revolution was used. However, during the component build up method used in the wind tunnel, the effect of body alone was calculated in the potential region and wing alone effects were isolated. The interference effect from the fuselage would still exist from this isolation exercise. Yet, the main objective was to compare the trends from the wind tunnel data to free air numerical simulations and to utilize flow field data trends to validate the force and moment data. Such studies of comparison of low speed data with high speed data in the potential region was done by Hall et.al [57] on compound sweep winged aircraft. The surface pressure distributions for the inboard wing sections and the canard sections are illustrated in the fig. 3.24. Other than this also the fairings on the canard of the wind tunnel model to blend with the nose cone was absent in the numerical simulations, however, equivalent exposed span remained the same.

Parameter	Value	Unit
Mach number	0.8	[-]
Reynolds number	$10e^6$	[-]
Altitude	11000	m
Speed	296	m/s

Table 3.7: Simulation operating conditions

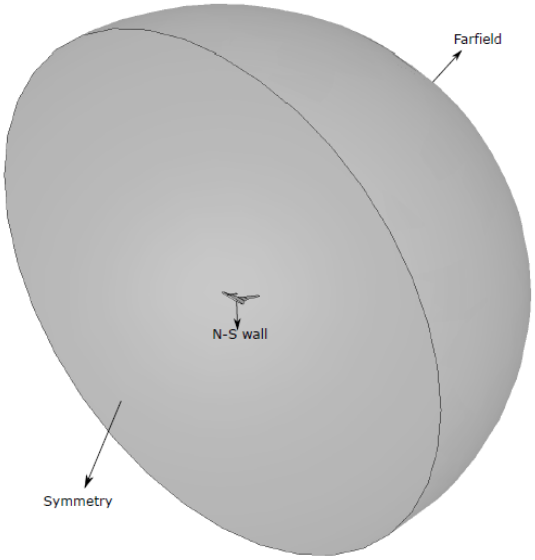

Figure 3.23: Fluid domain and boundary conditions applied to the numerical simulations,[4]

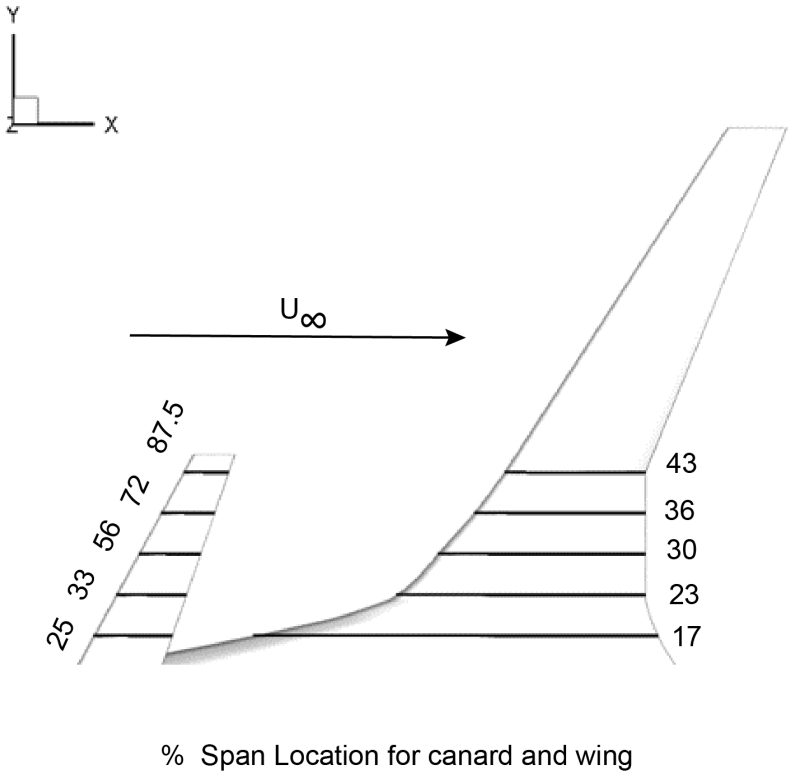

Figure 3.24: Wing and canard sections studied for pressure distribution,[4]

3.9. DEFINITIONS

- Pitch up -Pitch-up is defined as sudden change in slope of the C_M-α curve, consequently the slope of the C_M-α increases rapidly, thereby increasing the instability of the configuration. The magnitude of the change in slope of the C_M-α curve defining the pitch-up varies depending on the configuration [16]

- Reference axis system - Data from the wind tunnel is measured in the wind axis system considering an external balance is used, i.e the lift is perpendicular to the free stream velocity vector and the drag parallel to free stream velocity vector. To understand better the aerodynamic characteristics, body axis data is also plotted. Body axis system refers to the forces which are aligned with the model/body than the free stream vector. The normal force acts normal to the body and the axial force acts along the body. This difference in the axis system is shown in fig. 3.25

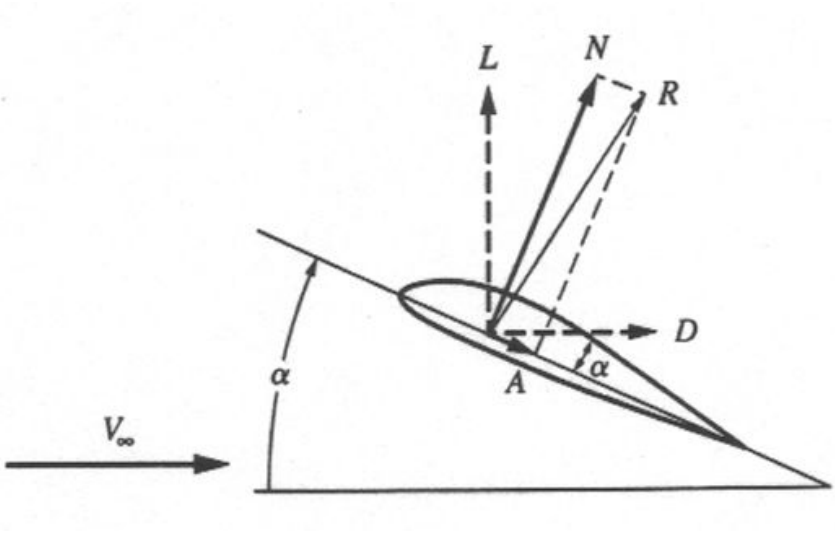

Figure 3.25: Free body diagram representing wind and body axis system,[5]

- Wing reference area was computed as per the shaded region in the figure fig. 3.26, the leading extension or strake area was not projected to the fuselage reference line.

- Re-circulation zone-Re circulation is a specific condition where the flow separates from the body of the obstacle. This creates a low pressure area immediately downstream which creates a suction and causes the fluid to recirculate in a direction opposite from the main flow, resulting of creating a circulating vortex or pair of vortices. This condition creates marked increase in drag compared to situations where the flow remains attached to the surface due to lower leading edge suction thrust.

- Usable lift- For highly swept wings with combined vortical and attached flows, unlike the attached flow wings C_{Lmax} may not be the range of usable lift for a safe flight. Highly swept cranked wing configurations and their tendency to pitch up, wing rock etc, determine the maximum lift that can be used to safely fly the configuration. C_{Lmax} for such wing layouts are higher due to vortex lift at higher angles, however usable range is limited due to non linearity in the configuration as explained above.

- Error bar - Error bar represents the uncertainty of measurement. The error bar computed and represented in this document is from the standard deviation of the data set.

3.9.1. SURFACE FLOW TOPOLOGY DEFINITIONS

- Skin friction line - Skin friction line refers to the tangent to the point of the local skin friction vector.

  To identify the vortex flow trajectories and flow in 3 dimension on the surface of the object, some critical points are defined from[6] as follows:

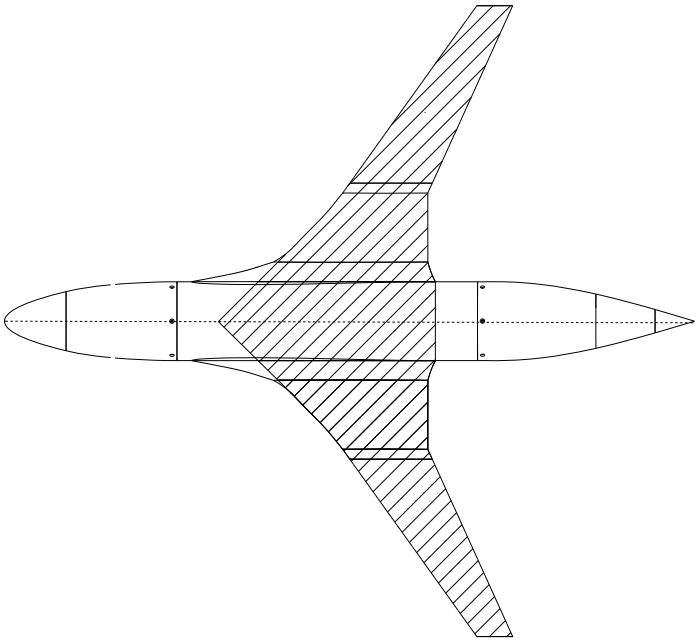

Figure 3.26: Schematic of wing reference area

- Node-All the trajectories are distinct, except one, which has a common tangent as seen in **??**
- Saddle -Flow trajectories go through a singular point, with other trajectories flow around in hyperbolic shape.
- Focus-Flow trajectories end up in the singular point with flow spiraling around it.

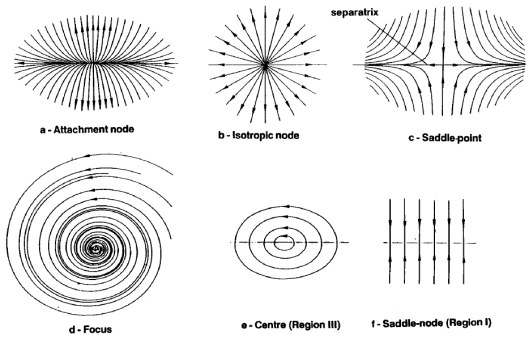

Figure 3.27: Flow trajectories around a critical point for flow in 3 dimensions,[6]

- Leading edge vortex - Leading edge vortex refers to the vortex formed at the leading edge of slender moderate to highly swept wings. The flow separates from the leading edge and re-attaches along the chord, creating an increased suction or low pressure on the upper side of the wing surface. Thus, leading to increased lift, known as vortex lift. However, also increases lift induced drag or vortex drag, due to loss in leading edge suction.
- Separation line - Separation line refers to the point where the vortex separates from the surface of the wing. These emerge from a saddle point.
- Attachment line -Attachment line refers to the point where the vortex system re-attaches on the surface of the wing. These emerge from an attachment node.

- Concept of vortex breakdown -To identify the vortex breakdown using surface oil flow measurement, lambourne et.al, [7] from his experiment on swept plate of 60° sweep, showed that the secondary separation line is straight except when there is a breakdown, resulting in an inward bend of the separation line at the tip, when VBD happens post the trailing edge of the surface as shown in fig. 3.28. This breakdown corresponds to an adverse pressure gradient faced by the vortex, which it cannot overcome, resulting in a breakdown. The point of vortex breakdown moves inboard on the wing with increasing incidence.

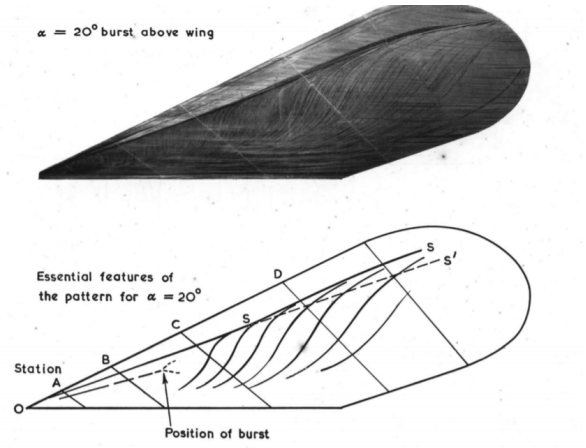

Figure 3.28: Oil flow visualization of vortex breakdown for a 60° flat plate,[7]

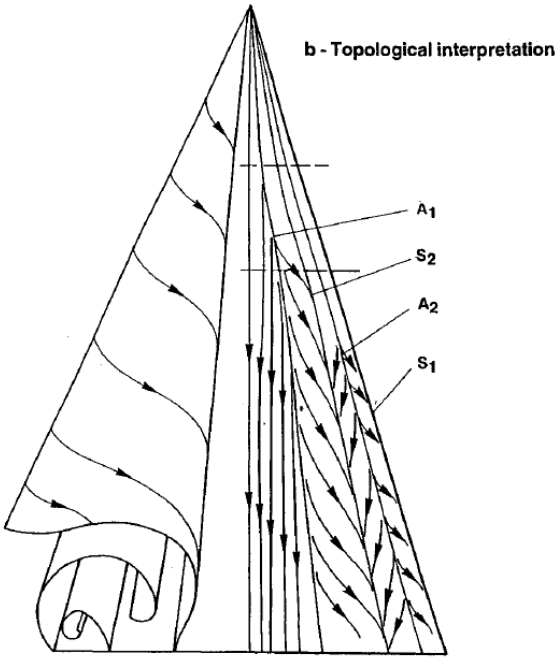

Figure 3.29: Oil flow topology on the upper surface of the delta wing at α=7.5°,[6]

A typical topological interpretation of oil flow visualization on a delta wing is show in fig. 3.29. S1 an S2 refer to the separation line, where S1 is the primary separation line which coincides with the leading edge and S2 corresponds to the secondary separation line. A1 and A2 refer to the attachment line indicating the re-attachment of the vortex along the chord. A1 is the primary attachment line along the plane of symmetry of the wing. Attachment lines are hard to detect and exist between the separation lines.

4

RESULTS

This chapter presents the relevant results from the experimental campaign and compares results from numerical investigations at low incidences to understand better the flow phenomenon and interpret the balance force measurements . The results chapter contains a detailed discussion of the aerodynamic characteristics of the multi cranked wing (i.e the canard off case), canard on case, and the effects of canard vertical and axial positions with its deflections.

Coefficients are normalized, based on the gross wing area of the basic design throughout this report, as shown in fig. 3.26. All the pitching moments and Reynolds number are standardized with the mean aerodynamic chord of the wing planform. The moment reference point is at 0.10 $\overline{c}$(400mm from nose tip). This point coincides with wing body aerodynamic center and was chosen to understand the canard sensitivity to the pitching moment curve, and in-turn try to understand the canard aerodynamics. Incidences are in relation to the fuselage reference line as the datum.

The measured data from the experiment corresponds to the wind axis system and to understand better the flow phenomenon they are resolved to body axis system using trigonometric relations. Difference in lift and normal force, as well as drag and axial forces are shown in fig. 3.25

4.1. EXPERIMENTAL TEST CONDITIONS

The experimental investigation, consisted of multi day testing, split over 2 campaigns. The first campaign was to test the baseline wing body configuration setup and identify the challenges in testing. The model support system was modified, with a semi-automated closed loop attitude changing mechanism as a result was developed to minimize the run time. The campaigns resulted in providing force and moment database in conjunction with the surface flow visualization data. Force and moment data were obtained for an angle of attack range from -5 to +22 °. All data presented and the database is for a free stream velocity U_∞ of 30m/s until and unless otherwise mentioned. Tests were conducted for a Reynolds number of 0.5million based on the wing mean aerodynamic chord as a reference.

4.2. PRELIMINARY RUNS

Preliminary runs included understanding the effectiveness of the trip on the wing body baseline configuration initially by acoustic studies, i.e noise increase in a turbulent flow as compared to the laminar flow. A microphone setup, also commonly known as stethoscope was traversed across the wingspan at different chord stations. At first, trip off runs were evaluated at the lowest Reynolds number to observe the location of the natural transition. The natural transition occurred in the region of 55-60% of the chord location on the suction side of the wing. Later, for trip on runs, with trips enforced at x/c =5% were conducted and it was found that the transition occurred at 10% of the chord, confirming the effectiveness of the trip strips. The aerodynamic effect of transition trip strip is further discussed in section 4.3.5

Short term repeatability checks were performed at the highest Reynolds number, especially at high angles of attack (20-22 °) representative of the pre-stall conditions to realize the interval of data acquisition time. The criterion for this decision on time interval was such that minimum time in which standard deviation variation of the coefficients measured didn't exceed 2 sigma limits. 20 seconds of data acquisition interval was found to be apt for this setup.

Other than this, preliminary runs were conducted to find out the compatibility of the model and setup on the external force balance. These tests were carried out, as a new mounting mechanism was designed for the open jet facility to allow mounting of a full scaled model. Thereby, it was deemed logical to ascertain the stiffness of the scaled model and assess the functionality of the attitude varying mechanism during the wind on conditions. The major bottlenecks that were observed from the preliminary runs were that the stiffness of the balance mounting plate wasn't found to be satisfactory and had to be reinforced, the attitude changing mechanism which was done manually initially with a sector concept had to be automated utilizing a bell crank mechanism with a linear actuator as described in section 3.4.3. This resulted in lesser run times and increased stiffness. Preliminary runs provided the overview of challenges to incorporate a full-scale airplane wind tunnel model in the OJF, these bottlenecks were eliminated in the subsequent wind tunnel campaign.

4.2.1. EFFECT OF REYNOLDS NUMBER ON THE BASELINE CONFIGURATION

To understand the effect of Reynolds Number on lift and drag characteristics, wing body configuration was tested for three different velocities, U_∞ = 10 m/s, 21m/s and 28m/s on the clean model (i.e no transition zig zag strips). The corresponding Reynolds number are tabulated in the section 4.2.1

	U_∞=0.16	U_∞=21m/s	U_∞=28m/s
Reynolds number	$0.16X10^6$	$0.342X10^6$	$0.46X10^6$

Table 4.1: Variation of Reynolds number for $\bar{c}$ of 0.242m

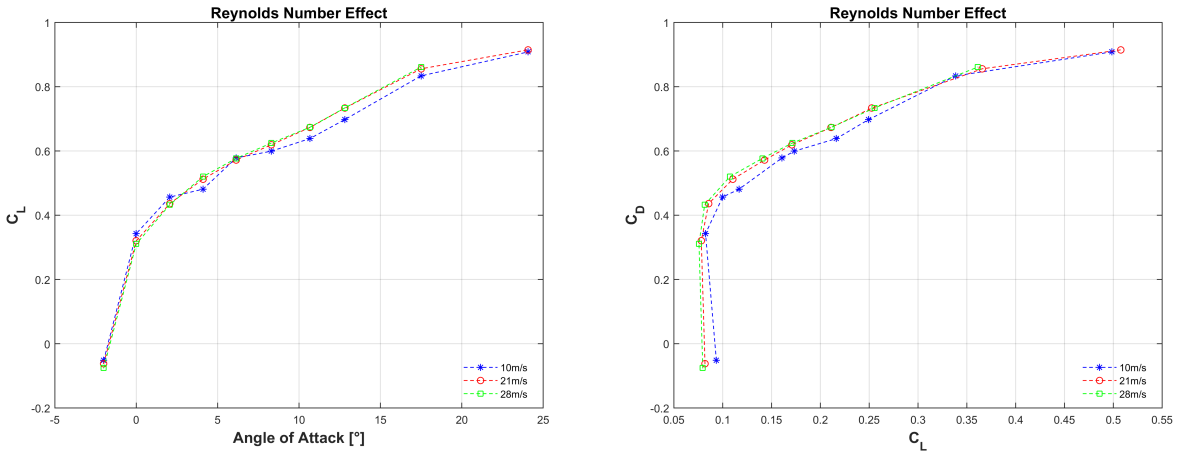

(a) Lift curve for different Reynolds number

(b) Drag polar for different Reynolds number

Figure 4.1: Effect of reynolds number on lift and drag characterisitics on baseline wing body configuration

The effect of Reynolds number on the lift coefficient is illustrated in the fig. 4.1a. Lift increases with increasing Reynolds number, especially in the moderate angle attack range of 5-18°. This may be associated with a reduction in turbulent boundary layer thickness with an increase in Reynolds number. However, at low incidences for Reynolds number of 0.16 million the lift curve is marginally higher than the Reynolds number of 0.342 million and 0.46 million, due to laminar flow at low Reynolds number of 0.16 million. This followed by a sudden fall in the lift at α= 4° and 6° can be due to laminar separation. Post the laminar separation, a turbulent reattachment takes place followed by an increase in lift curve slope.

Therefore, lift curve slope increase with Reynolds number is primarily due to a decrease in thickness of the turbulent boundary layer and the secondary cause is due to the decrease in laminar separation region with an increase in Reynolds number. From fig. 4.1b it can be seen that drag reduces with increase in Reynolds number, with turbulent boundary layer more resistant to separation for such swept wing configurations. Also, at lower Reynolds number on transition from laminar to turbulent, the turbulent skin friction coefficient is higher as it scales by the 1/7th power law.

This phenomenon of laminar separation can be further validated with the body axis coefficient plot in fig. 4.2. From the axial coefficient plot, an increase in axial force coefficient can be associated with reduced leading edge suction or thrust, decrease in attached flow and increased chances of separation. However, one has to carefully examine the results as there are two kinks observed one at α = 4° and other at 6°, as seen in the lift curve, one has to repeat these runs with smaller incidence steps of 0.5-1°, and understand the flow physics with flow visualization studies. Post 6°, until 18° there is a decrease in the slope of axial force, indicating turbulent reattachment flow with higher leading edge suction, corresponding to reducing axial force. At high angles from 18-24°, there is an increase in axial force coefficient and an increase in slope of the normal force coefficient.

From these runs, testing at 0.16 million Reynolds number is not practical with larger laminar flow and localized aerodynamic phenomenon occurring at low incidences. It would be difficult to scale up these results. From the data, it can be seen that testing at 0.342 and 0.46 million Reynolds number would be preferred for better scalability.

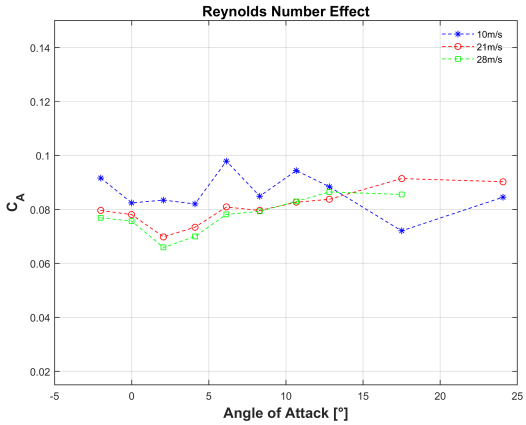

Figure 4.2: Axial force coefficient for different Reynolds number

4.3. DATA REPEATABILITY

This section documents a study of data repeatability in the Open Jet Facility (OJF), performed during as a part of this low Reynolds number experimental campaign. The aim of this investigation was to understand the repeatability of the longitudinal axis coefficients of lift, drag and pitching moment. The repeatability goals for these coefficients were set for 2 sigmas or 95% confidence level. According to Simon, Leslie E, et al. this corresponds to extremely probable repeatable values for an experiment.

Measurement accuracies were quantized during the experimental campaign by the acquisition of several repeated data sets. Two timescales for repeatability were chosen long to near term repeatability and short term repeatability. Long to near term repeat data were obtained at multiple different times throughout the experimental campaign with a gap of 5-7 days, were multiple changes were made on the model. Certain repeat data were obtained on a short term basis by following repeats in a random manner for various incidences over multiple runs during the same day. Specifically, force and moment data were obtained within a typical pitch polar for the high canard deflection case, δ= 30 °. These runs were all conducted at U_∞ of 30m/s, and comparision plots are as shown in fig. 4.12

Delta coefficient data, as well as standard coefficient data, are presented versus angle of attack. The collected delta coefficient data represent the difference between the coefficient value measured and the average value of the coefficient at that particular angle of attack. These delta coefficients, or residual data, show the level of variation in the repeat runs. The dashed lines shown on each plot indicate the 2-sigma limits based on all the measured data across the angle-of-attack range. Data repeatability then tends to degrade as separated flow behavior begins to dominate the flow field at moderate angles of attack (i.e 4 and 6 °). It is observed that, other than the region of separated flow or where nonlinear aerodynamic behavior is observed for a given configuration, all data are within the 2-sigma limits.

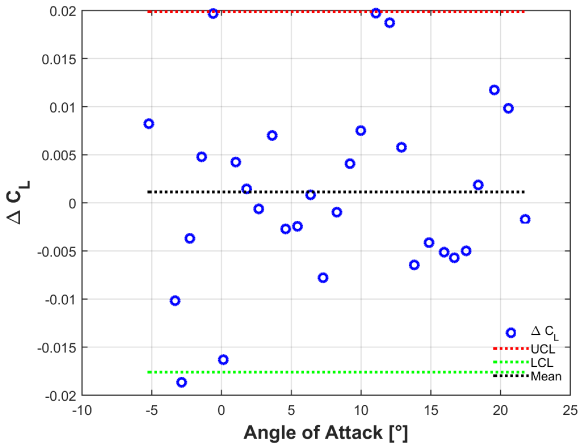

Figure 4.3: Undeflected Canard Repeat Runs

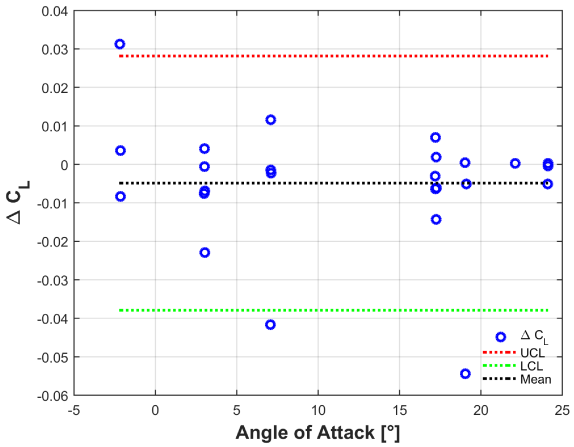

Figure 4.4: Deflected Canard Repeat Runs

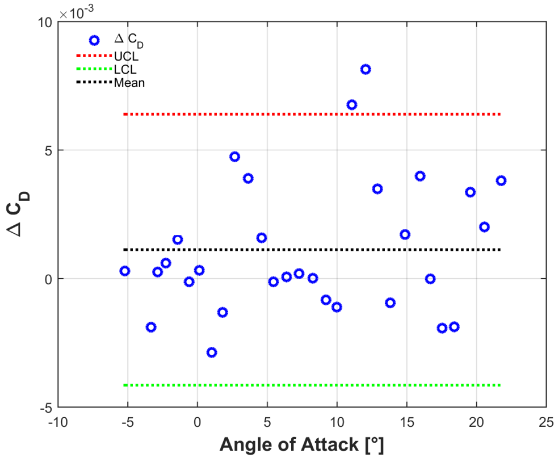

Figure 4.5: Undeflected Canard Repeat Runs

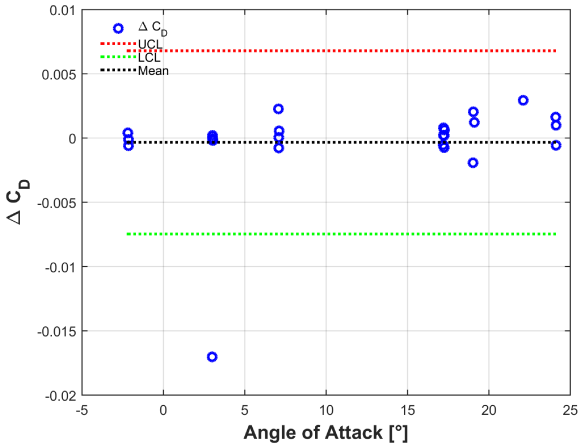

Figure 4.6: Deflected Canard Repeat Runs

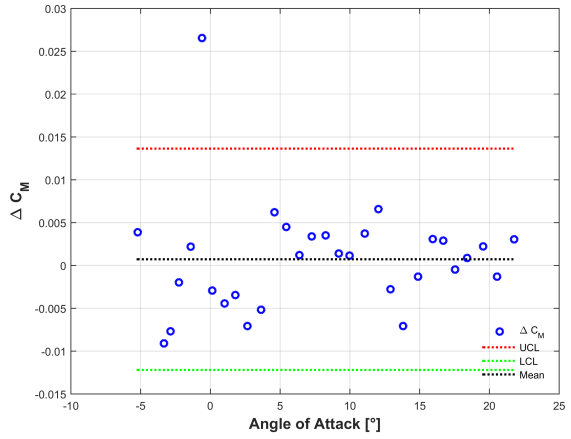

Figure 4.7: Undeflected Canard Repeat Runs

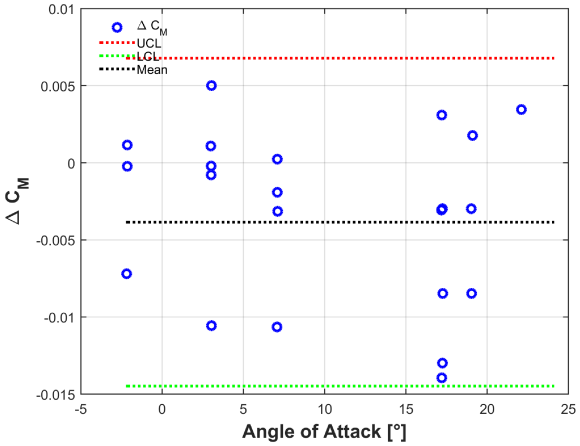

Figure 4.8: Deflected Canard Repeat Runs

Figure 4.9: Data Repeatability of Longitudinal coefficients

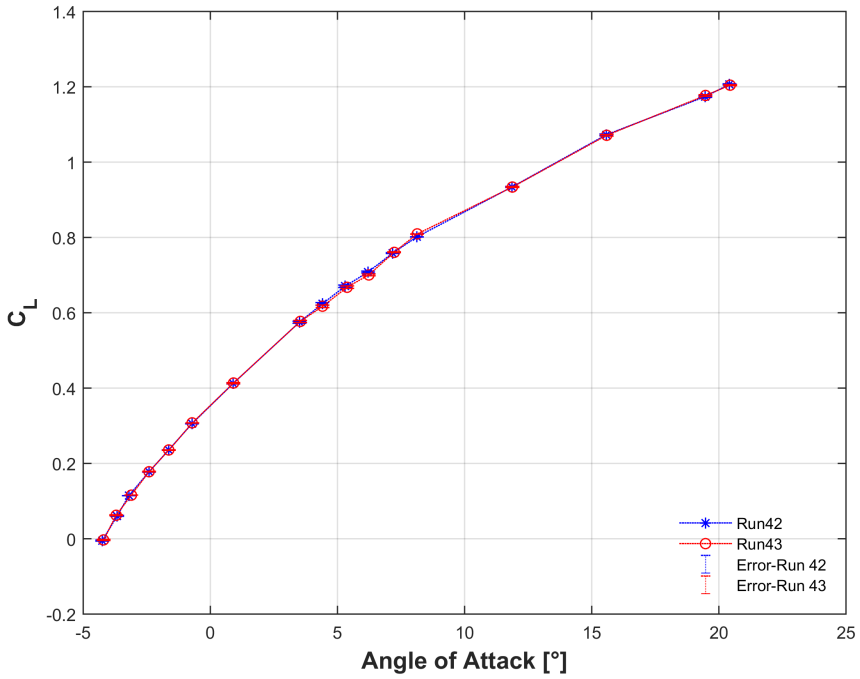

Figure 4.10: Lift coefficient repeatability of high canard 30 ° deflection

4.3.1. SHORT TERM REPEATABILITY

Short term repeatability of the low canard undeflected canard cases are presented in figs. 4.3, 4.5 and 4.7. Levels of repeatability show most of the data lie within the 2 sigma limits. The residual analysis of the group data for short term shows a shift in the drag coefficient of approximately 5 drag counts across the repeatable canard deflection tests. These deviations from the 2 sigma limits are observed at approximately 12-13 °, which coincides with the vortex breakdown on the undeflected low canard configuration, when the vortex trajectory shifts from the lower pressure side to the upper suction side of the wing. This sensitivity of the non-linear aerodynamic behavior is captured by the external balance system. For the Pitching moment coefficient at $\alpha = 0$ ° there is a deviation of 0.025 at the coefficient level and can be a spurious measurement data point.

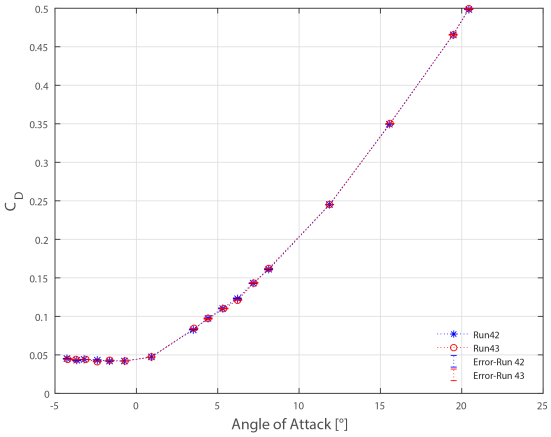

(a) Drag coefficient repeatability of high canard 30 ° deflection

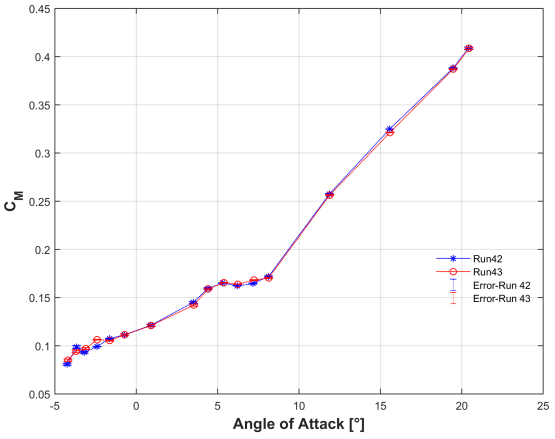

(b) Pitching moment coefficient repeatability of high canard 30 ° deflection

Figure 4.11: Longitudinal coefficients repeatability, short term repeatability

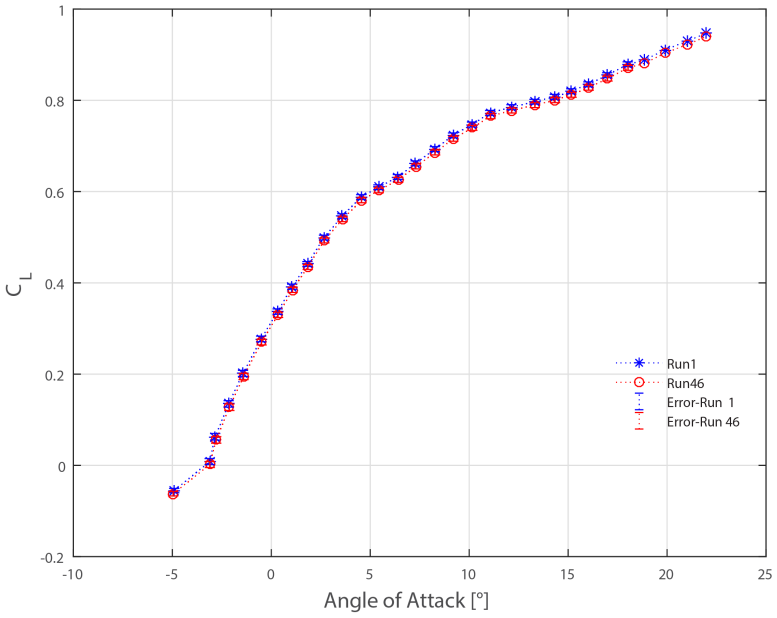

Figure 4.12: Lift coefficient repeatability of the baseline wing body configuration

Figures 4.10, 4.11a and 4.11b show the data repeatability of coefficients of the deflected high canard case. The experiment was designed such that the data points were tested in a random manner of different chosen incidences, with larger points concentrated at the start of the pitch up region(moderate angles of 4-9 °). It was seen that for short term wind tunnel data measurements, good repeatability was observed for all the longitudinal coefficients across the incidence range. This test was done with the aim to realize if the canard deflections would be able to hold position under wind loads.

4.3.2. LONG-NEAR TERM REPEATABILITY

Figures 4.4, 4.6 and 4.8 show the longitudinal axis coefficient residuals and the 95-percent confidence level bounds, for the high canard deflection case. Canard deflection case was chosen for long term repeatability studies to understand if the same setting angle could be repeated. As compared to the short-term, the long term results demonstrate levels of repeatability within the 2 sigma limits. Also, the

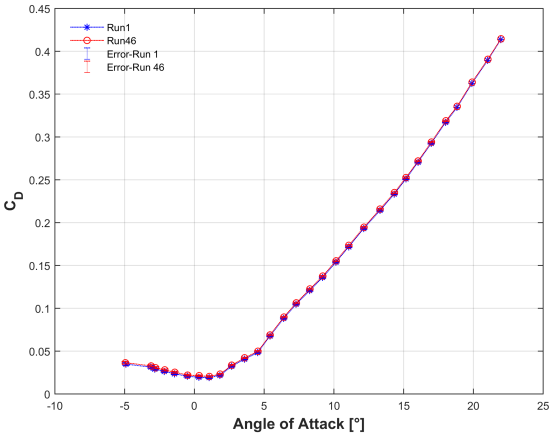

(a) Drag coefficient repeatability of the baseline wing body configuration

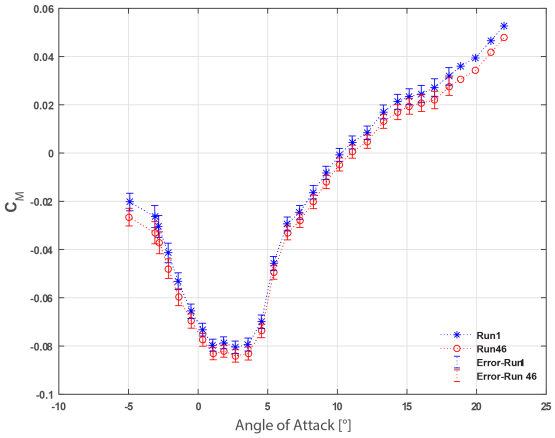

(b) Pitching moment coefficient repeatability of the baseline wing body configuration

Figure 4.13: Longitudinal coefficients repeatability, long term repeatability

residual analysis at moderate incidences shows a shift in the lift coefficient of approximately 0.04, and a drag coefficient of 0.015, which are out of bounds of the control limits. Comparatively larger deviations for the pitching moment of 0.012 are also observed at these moderate incidences, though within the bounds. These deviations were observed at the end of the linear lift region, and on initiation of region of re circulation with outboard separation across the repeatable canard deflection tests.

Long to near term repeatability were performed for different combinations. Baseline wing body close coupled configuration cases were repeated a couple of times post many configuration changes such as canard on, long coupled wing body configuration etc. and has good repeatability as seen in figs. 4.12, 4.21a and 4.21b. From the figures, it is observed the deviations are higher at moderate C_L of 0.6 when the pitch break tendency is observed. Deviations are also observed at higher angles of attack , due to pre-stall conditions which induces vibrations on the support structure.

4.3.3. ANGLE OF ATTACK, MEASUREMENT ACCURACY

Measurement and actual determination of the true angle of attack has a direct effect on repeatability of the longitudinal aerodynamic coefficients.

$$C_L = C_N cos\alpha - C_A sin\alpha \tag{4.1}$$

$$C_D = C_N sin\alpha + C_A cos\alpha \tag{4.2}$$

From eqs. (4.1) and (4.2) it is seen that the angle of attack determination and measurement has an important effect on meeting the repeatability targets. An error of 0.01 ° can lead to an increase in 1 drag count at moderate C_L of 0.6, thus making it critical to have an accurate angle of attack measurements. The determination of the true angle of attack can be affected by three factors. They are as follows :

- The first factor is the measurement from the sensor and its accuracy. The primary measurement is taken from an onboard accelerometer package, that as stated previously, has a quoted accuracy of 0.01°. This quoted accuracy is based on calibration performed in laboratory conditions at ambient temperature rather than in an actual dynamic wind tunnel test environment.
- The measurement of the sensor itself is affected by the stiffness of the model and support system at high angles of attack and high load conditions.
- The flow angularity in the test section is another important factor affecting the determination of the angle of attack.

4.3.4. BALANCE ACCURACY

A measurement may be accurate, however, factors such as system accuracy may hinder repeatability of data. Balance measurement accuracy measurements of the tare or wind off values with the stated repeatability goals are critical and need to be repeated to ascertain repeatability of the aerodynamic coefficient data. figs. 4.14, 4.15a and 4.15b illustrates the accuracy bands for the lift force, drag force, and pitching moment. It is observed from fig. 4.15a deviation in ΔF_x is higher as compared to the standard deviation from the calibrated value. This is because during the tare run the axial load component is loaded the least among the longitudinal components of the balance as no drag is produced. Non-linearity in the lower load range of axial load cell leads to higher standard deviation, implying a need for more calibration points. The measured standard deviations are tabulated in section 4.3.4 with the calibrated standard deviations.The data demonstrate good force and moment coefficient repeatability, particularly in relation to the new setup and flow environment in OJF. It can be said that the uncertainty error is acceptable for accuracy of the results.

	ΔFz[N]	ΔFx[N]	ΔMy[N-m]
Balance calibrated standard deviation	0.05	0.02	0.01
Baseline configuration standard deviation	0.028	0.034	0.013
Canard configuration standard deviation	0.05	0.024	0.023

Table 4.2: Standard deviation of balance measurements.

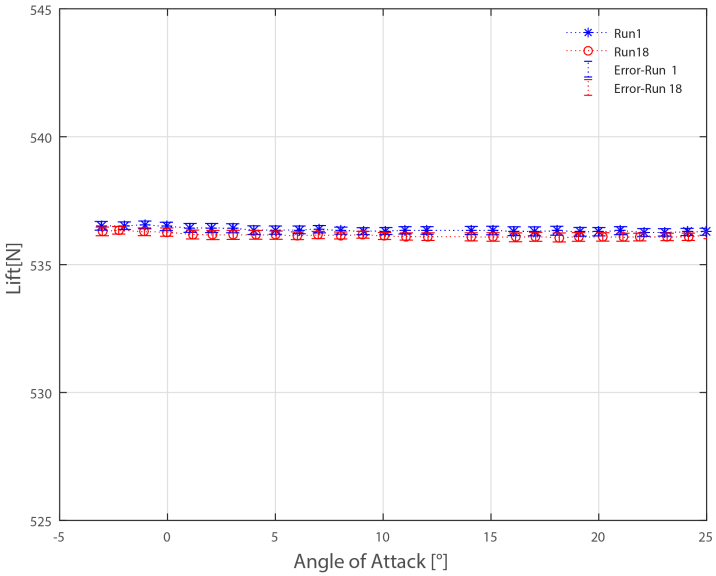

Figure 4.14: Lift force repeatability-Baseline configuration

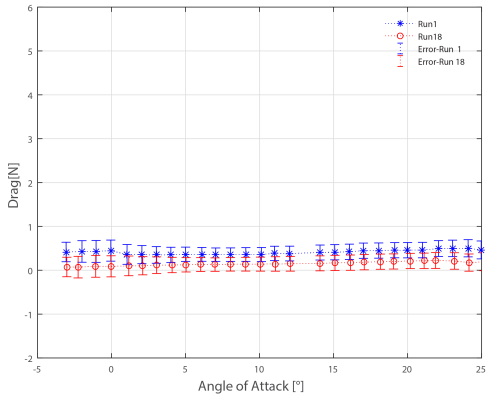

(a) Drag force repeatability-Baseline configuration

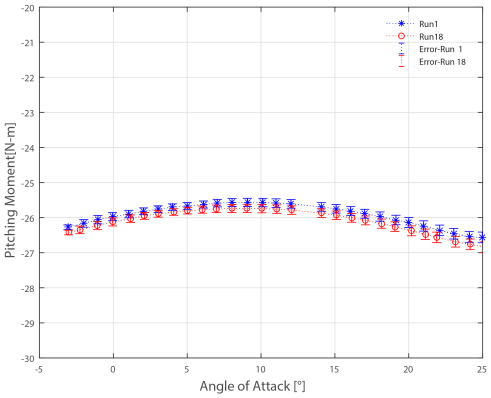

(b) Pitching moment repeatability -Baseline configuration

Figure 4.15: Longitudinal force repeatability, long term repeatability

4.3.5. EFFECT OF BOUNDARY LAYER TRANSITION TRIP STRIP

In order to simulate turbulent flow conditions, similar to the free flight conditions, the boundary layer was tripped using transition strips. Transition position was fixed using zig-zag transition strip, rather than the conventional carborundum grit, which is known to deteriorate with time. Considering that the experimental campaign was planned to be conducted in two schedules, the zig zag strips were preferred to ascertain good repeatability across the campaigns. It was applied on the nose cone, wing, and the canard installed at x/c= 0.05, on both the upper and lower sides. Transition strips of 0.394mm thickness were applied. The height and location of the transition strips were calculated based on reference given in Barlow,et.al. [5] and Braslow, et.al [58]. Small chord transition zig-zag trip was used to prevent large drag penalty.

$$h = 12K/Re_{ft} \tag{4.3}$$

where h, is the height of the transition strip in inches, Re_{ft}, is the effective Reynolds number per foot. K is the constant value based on effective Reynolds number and value of 600 is chosen for flow with Reynolds number exceeding 0.1 million. To have transition over the complete wing, lowest Reynolds number at the tip section is considered for calculation, which results in 0.365mm thickness of the transition strip.

The effectiveness of a boundary layer trip was validated by oil flow visualization and qualitatively measuring the turbulent boundary layer noise using a traversing microphone system, or so called stethoscope system. This was validated for flow Reynolds number of 0.5 million and at highest angle of attack corresponding to the vicinity of highest lift coefficient condition.

Results of the trip on and off tests for the wing body baseline configuration are presented in figs. 4.16, 4.17a and 4.17b. From fig. 4.16 It is observed that the lift curve slope in the linear region is lesser as compared to the clean or trip off configuration. This is possible due to the de-cambering effect on the application of the transition trip. For moderate angles of attack (10-12 °), a recirculation region is formed over the wing body which is observed in flow visualization, leading to further deterioration in the lift. At high angles of attack, there is an onset of stall that can be observed on the trip off configuration. However, with the trip on the configuration, the onset of the stall is delayed, due to probably presence of more resistant turbulent boundary layer preventing separation. Trip on run resulted in a slight increase in drag, with C_{Dmin} increasing by 4 drag counts, as seen in fig. 4.17a. With the fig. 4.17b, data indicates there is a slight increase in pitching moment instability at angles of attack of 4-5 °. This may be due to shifting in boundary layer from laminar to turbulent. This is similar to the observation made in Y. Lip et al [59].

In hindsight it could be noted that for this highly swept wing configuration, utilizing conventional tripping location at 5% of the chord of the wing, may result in deterioration of lift with formation of three dimensional separated regions. This phenomenon may be associated with the high sensitivity of the transition location with respect to the angle of attack, and thereby is difficult to ascertain a location for tripping the flow from laminar to turbulent. With the formation of leading edge vortex as a result of separation from the leading edge the re-attachment point on the wing may also vary with the trip strip on the upper surface. It is observed from [60], that when the transition trips are placed behind the separated region, it causes decreased performance in terms of lift and drag. Therefore, it would be recommended to trip only the pressure side of the wing to have a fixed transition location as a reference future numerical simulations or to have uniformity in testing across various wind tunnels, with different turbulence levels.

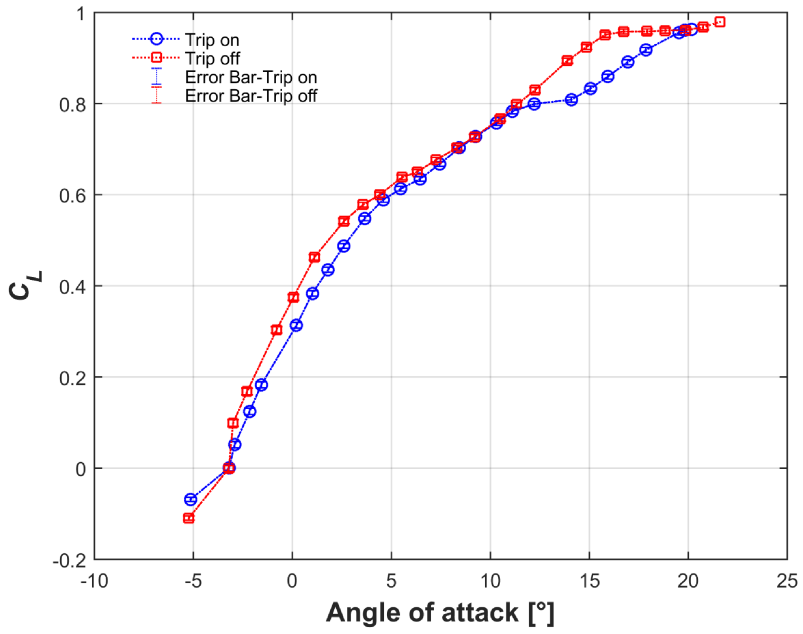

Figure 4.16: Lift coefficient - baseline wing body configuration

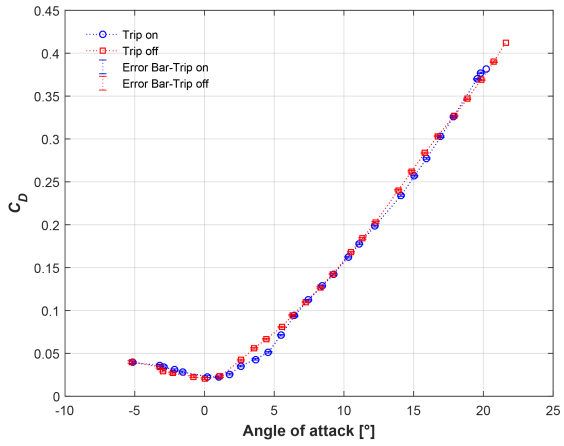

(a) Drag coefficient - baseline wing body configuration

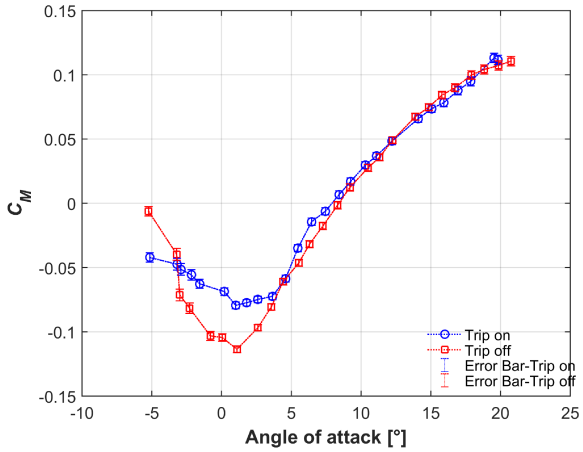

(b) Pitching moment coefficient - baseline wing body configuration

Figure 4.17: Longitudinal coefficients of baseline wing body configuration

Transition trip studies were conducted for the high canard configuration. The data of these run are presented in figs. 4.18, 4.19a and 4.19b. From fig. 4.18, it is seen that there is a slight decrease in the lift curve slope in the linear region with and without the trip. However, the deviation is mostly within the error band of the measurement. At moderate to high angles of attack the decrease in the slope of the lift curve is observed for the trip on run due to the de-cambering effect. The effect of transition trip on the drag is quite minimal as well and is associated with CD_{min} increase by 2 drag counts,which is within the error band of measurements. fig. 4.19a. With respect to the pitching moment, the data is presented in fig. 4.19b, the decrease in lift curve slope resulted in a significant nose-down pitching moment or increase in pitch stability in the region of 6-8 °. The trip on run of the canard helps in alleviating the pitch up as observed for the baseline configuration.

To critically analyse the effect of trip on the canard, it would be wise to study the pressure distributions over the canard, to understand the flow physics better and to draw a better conclusion.

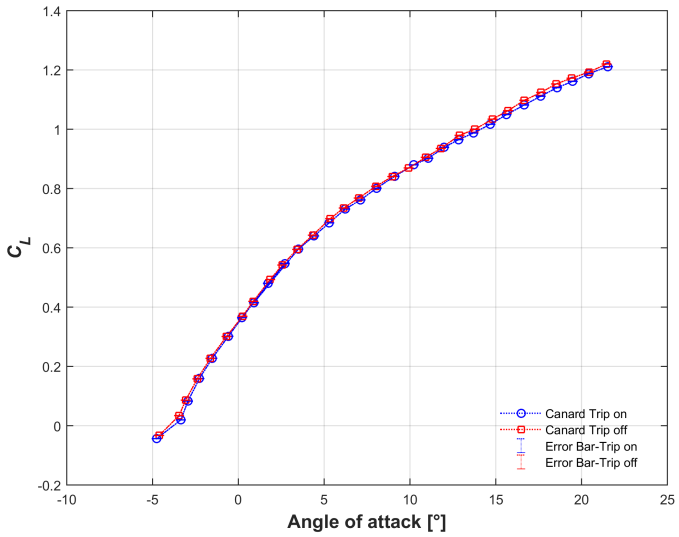

Figure 4.18: Lift coefficient -high canard trip configuration

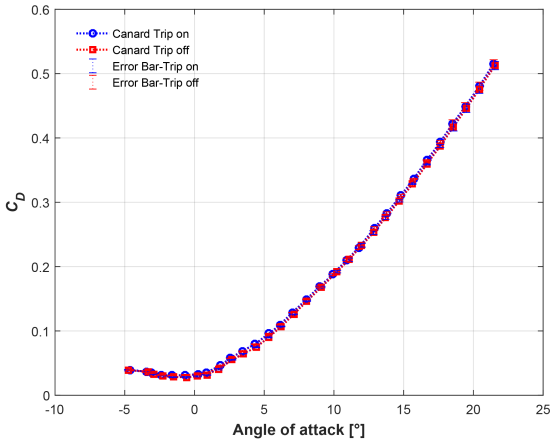

(a) Drag coefficient - high canard trip configuration

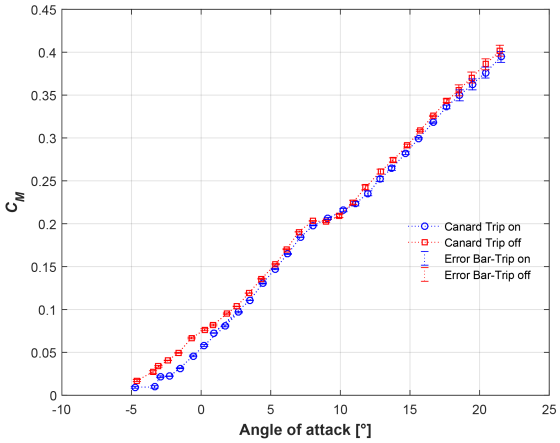

(b) Pitching moment coefficient - high canard trip configuration

Figure 4.19: Longitudinal coefficients of high canard trip configuration

4.4. BASELINE, WING BODY CONFIGURATION

4.4.1. EXPERIMENTAL RESULTS

From the lift characteristics fig. 4.20, it is observed that the lift curve can be categorized into 3 regions viz. linear lift region persists up until 6 ° and there is a region of slope change with a reduced $C_L - \alpha$ slope leading up until 15 ° and an increased $C_L - \alpha$ up until the measured range of 22 °.

To critically analyze and understand the results better, surface oil flow visualization is done in these regions. It is observed that potential flow largely exists over the upper surface of the wing until 4°. At 5-6 ° incidence there is a large outboard separation, with a region of re circulation zone leading to decreased $C_L - \alpha$ slope, and increased pressure drag. The increase in pitch up moment can be associated with the large outboard separation, leading vortex formation over the inboard wing and the center of lift moving inboard, this is synchronous with the literature studied in [16, 29].

The surface oil flow visulaization qualitative measurement is further corroborated with the wake rake analysis done for the wing body configuration at α=6° . Figure 4.28 shows that the there is an inboard leading edge vortex with an outboard wing vortex formed originating at the first kink on the wing. On the outboard wing there is a region of recirculation leading to traces of vorticity on the outboard kink as depicted in fig. 4.23b, with a large region of outboard separation, originating at around 70-75% of the wing semi span.The tip section of the wing is in the upwash field generated by the strake and forebody. With increase in angle of attack, the tip has an increase local incidence, resulting in it being heavily loaded. The induced velociy at the tips are high in this flow field and the thickened boundary layer cannot overcome the adverse pressure gradient. Thus, leading to large scale separation on the outboard panels. The occurrence of this outboard separation and re circulation region coincides with the marked increase in the pressure drag and the pitch up as observed from the balance force data measurements.

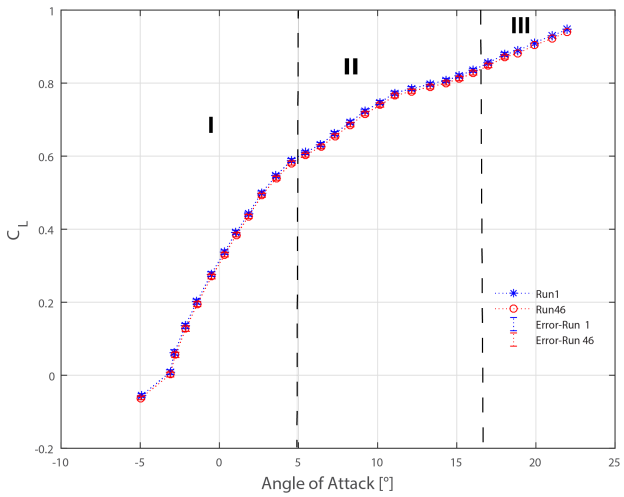

Figure 4.20: Lift coefficient - baseline wing body configuration

With an increase of incidence to α = 10.3 °, there is now a distinct suggestion of a wing vortex being formed at the first kink of the wing . There is a reduced recirculation region as seen in oil flow topology image of fig. 4.25a compared to fig. 4.24 with reduced outboard trailing edge separation.

At α=21 °, from the fig. 4.25b, the part-span wing vortex moves farther inboard, with increase in incidence and merges with the strake vortex. The separation line has reached about 25% of the gross wing semi-span, and all the flow outboard of the wing is benign in nature, which is largely attached except that there is trailing edge separation . The benign flow on the outboard wing is plausible due to the inboard strake vortex energizing the boundary over the outboard wing, thus making it stall resistant. Other than this there is an integral sign shaped separation line observed at 25% wing semi-span extending upto

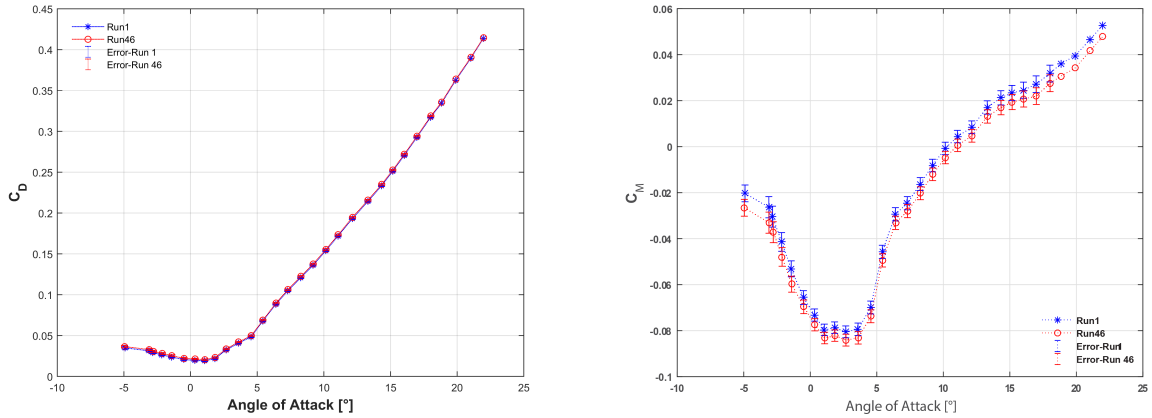

(a) Drag coefficient - baseline wing body configuration

(b) Pitching moment coefficient - baseline wing body configuration

Figure 4.21: Longitudinal coefficients of baseline wing body configuration

65% of the wing local chord. The vortices merge with a big turbulent core and such phenomenon has been observed previously from experiments conducted by Verhaagen et.al on a similarly swept double delta wing [61]. Another plausible reason for attached flow on the outboard wing at such high angles of attack, may be due to no adverse pressure gradient between the two vortices along the span wise direction to cause further separation on the outboard wing.

Generally it is observed that the vortex formation move inboard with increase in angle of attack, resulting in center of pressure to move inboard of the wing as a result of increased suction from the vortex. Further causing pitch up tendencies at high angles of attack as observed in conventional swept wings. Expected vortex flow trajectories derived from the surface oil flow topology are illustrated in figs. 4.26a, 4.26b and 4.27.

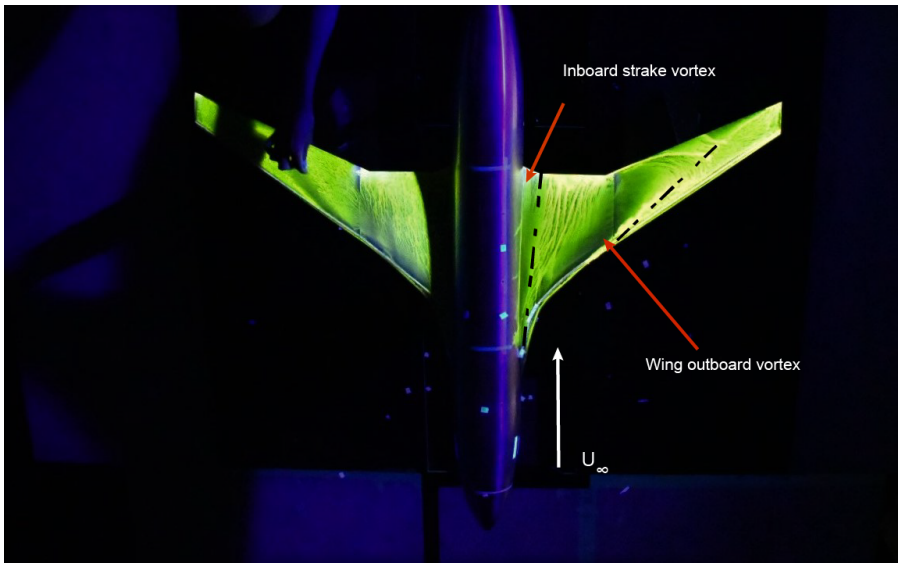

Figure 4.22: Surface oil flow visualization pattern of baseline wing body configuration, for α=6 °

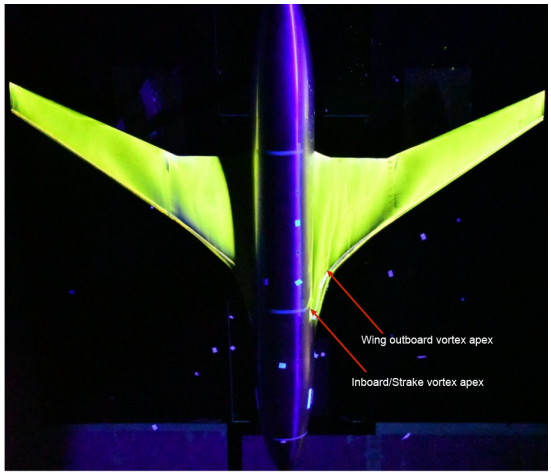

(a) Baseline configuration α=6 °, outling the apex of the vortex formation

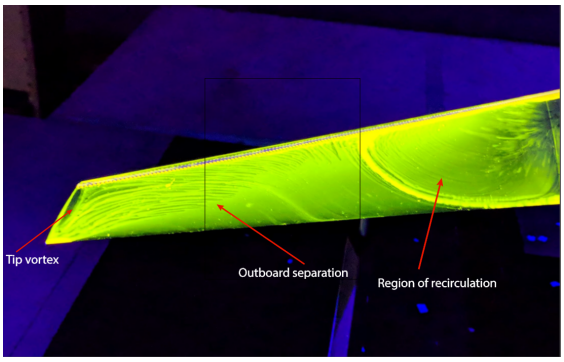

(b) Baseline configuration α=6°, illustrating the region of recirculation and outboard separation

Figure 4.23: Surface oil flow visualization pattern of baseline wing body configuration

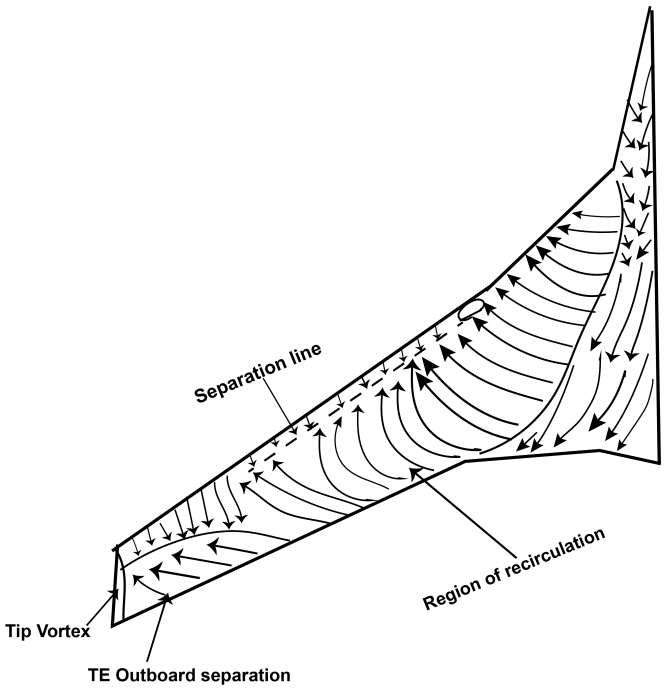

Figure 4.24: Surface oil flow visualization pattern of baseline wing body configuration, for α=6 °

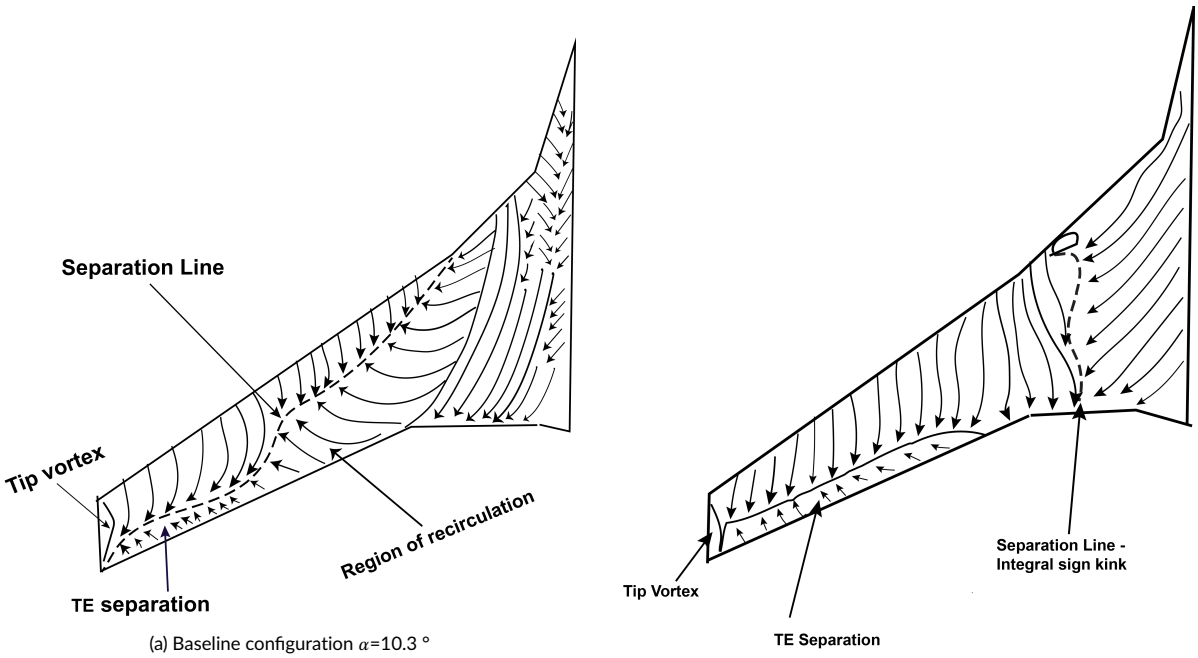

(a) Baseline configuration α=10.3 °

(b) Baseline configuration α=21°

Figure 4.25: Surface oil flow visualization pattern of baseline wing body configuration

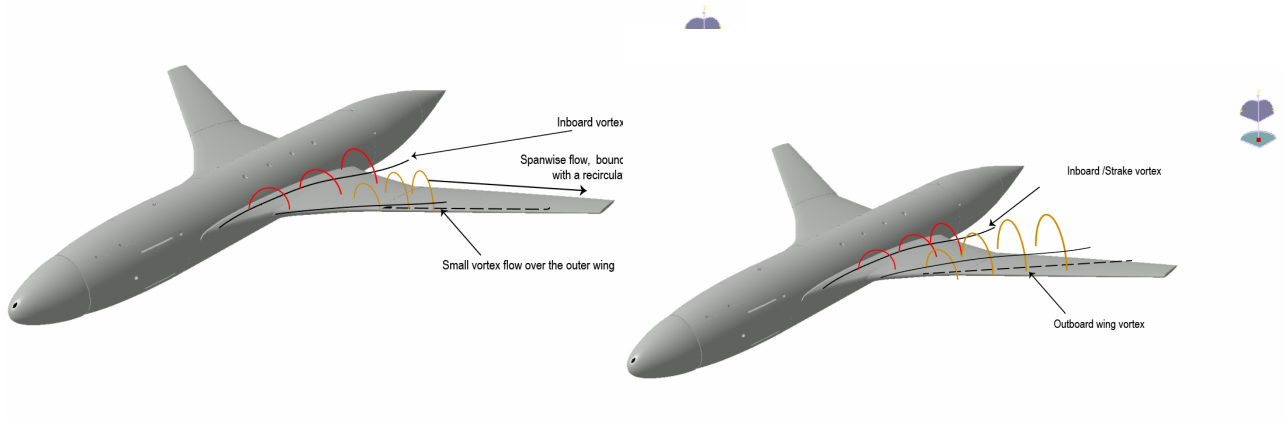

(a) Expected flow trajectory baseline configuration, α=6 °

(b) Expected flow trajectory baseline configuration, α=10.3 °

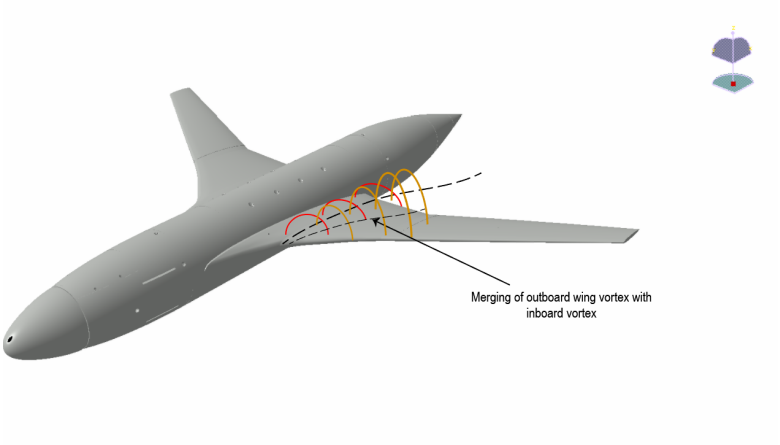

Figure 4.27: Expected flow trajectory baseline configuration, α=21 °

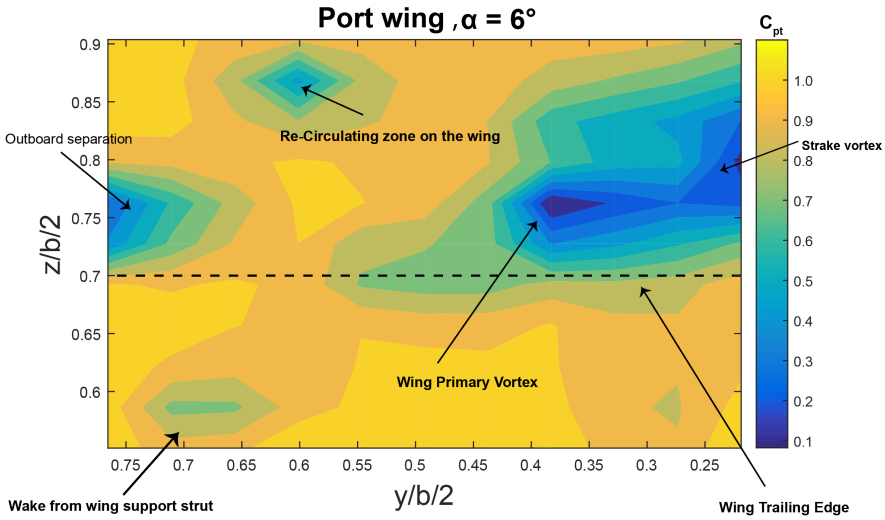

Figure 4.28: Cross flow plane visualization of total pressure loss contour plot for baseline configuration,α=6 °

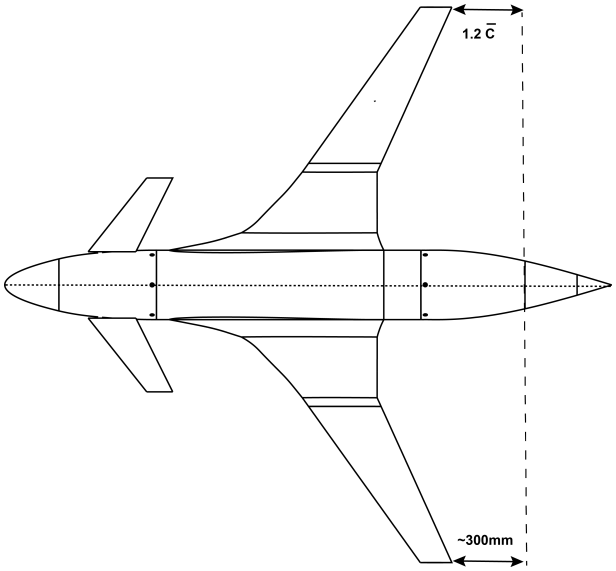

(a) Measurement plane for wake rake analysis for reference

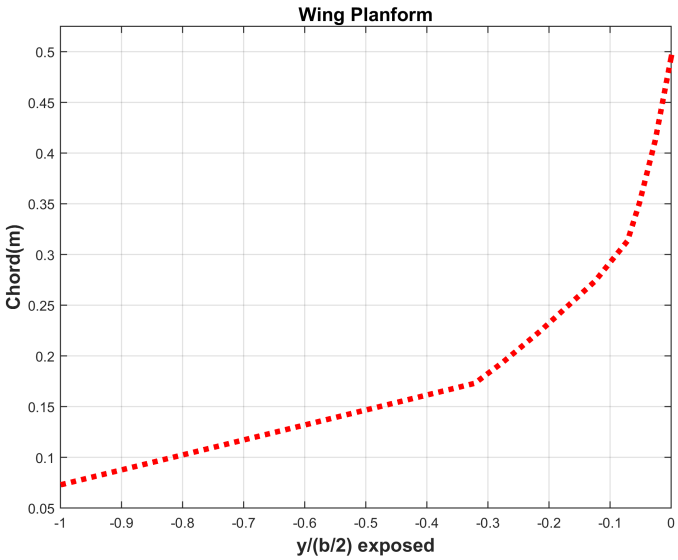

(b) Exposed port wing section distribution

Figure 4.29: Surface oil flow visualization pattern of baseline wing body configuration

4.4.2. APPLICATION OF LEADING EDGE SUCTION ANALOGY ON VORTEX FORMATION

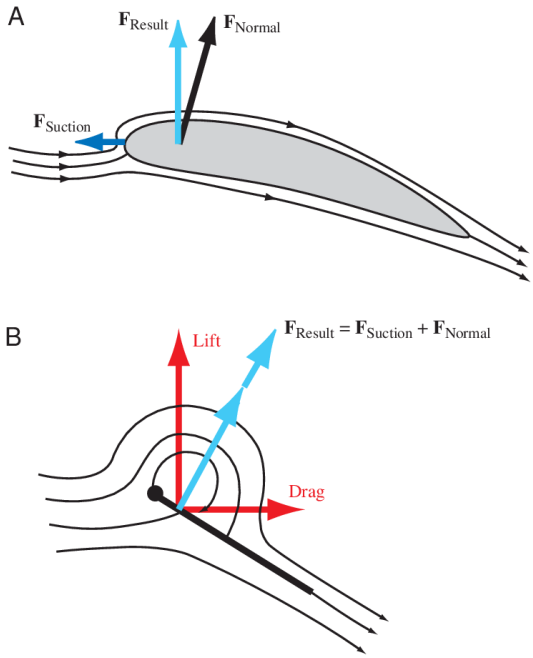

Figure 4.30: A .Flow around a blunt section, B. Flow around a thin section [8]

To understand the concept of leading vortex formed due to leading edge separation and the incidence at which vortex formation appears, Polhamus et.al [62–64] developed a theoretical approach called as leading edge suction analogy. This is important to understand as these vortices formation phenomenon have a significant impact on performance on the field performance of the configuration. The theoretical approach and its concept is explained subsequently.

Figure 4.30 illustrates the concept of leading edge suction and its contribution to drag reduction in an attached flow condition and increase in normal force when a leading edge separation occurs. This is an useful concept in determining the attached flow region and vortex flow region for highly swept wings, especially of low to moderate aspect ratios. For,an attached flow the sharp bending near the leading edge, creates a suction peak on the upper surface and results in increased suction at the leading edge in a forward direction. Thus, causing the normal force vector to tilt forward and be more perpendicular to the flow. The suction force as indicated acts opposite to the direction of axial force and indicates reduction of axial force or negative axial force or rather increase in thrust. With a leading edge separation and reattachment, the circumferential force generated by helical leading vortex is balanced by the extra suction force acting normal to the surface. The balancing suction force adds to the normal force generated by the lifting section causing the resultant to tilt backward, thereby increasing the induced drag.

Figure 4.31 shows that the maximum axial force coefficient is at around -2° corresponding to the C_{L0} and C_{Dmin} values. The axial force is highest at this point with only skin friction force acting on the wing body configuration.

With increase in incidence the axial force reduces indicating attached potential flow up until α=5° and there is an inflection point with increase in axial force indicating of leading edge vortex or and outboard separation at this low incidence.The increase in axial force reduces and becomes almost constant between 8-12°, indication of the recirculation region with increased turbulent flow and vorticity. After 12°, the slope of axial force coefficient increases for moderate to higher incidences showing the formation of sustained leading edge vortex system.

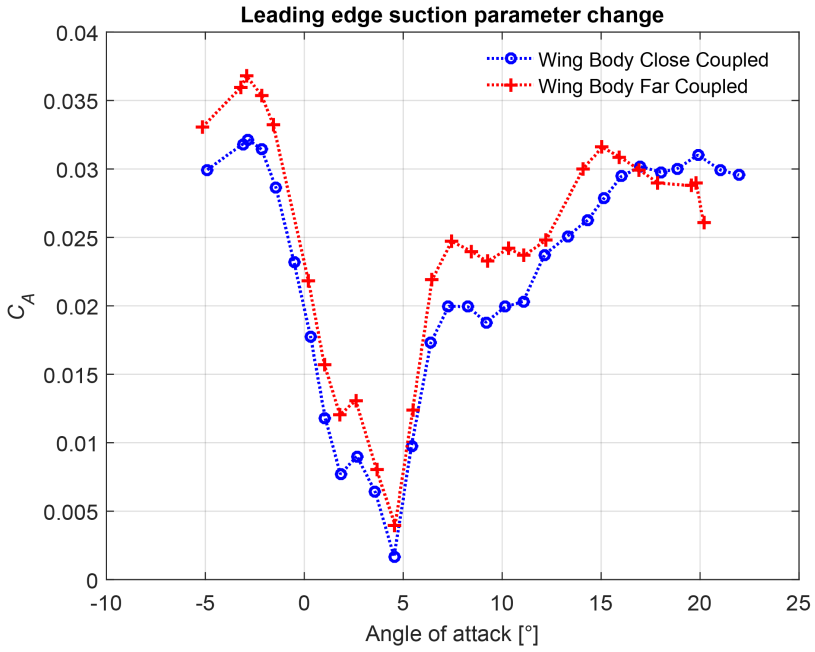

Figure 4.31: Axial force coefficient for wing body configuration

4.4.3. CFD DATA COMPARISION WITH WIND TUNNEL DATA OF BASELINE CONFIGURATION

As the experiments were carried out in a low-speed wind tunnel, for a 2% scaled model the Mach and Reynolds numbers of 0.1 and 0.5 million respectively were low when compared to those of full-scale take-off, landing conditions, where Reynolds number can vary in the range of 20-30 million . As discussed in section 1.0.2, the results obtained from the experiment will have been affected by relatively large boundary-layer thickness, and an absence of compressibility effects.The vortex interactions between the lifting surfaces are a direct result of viscous effects, the low Reynolds number may have led to offsets in a quantitative sense. However, the interactions are as a result of communication between the velocity and pressure fields in the vortical regions. Thus, the potential flow effect caused by the interactions will exist at these low Reynolds numbers and especially comparable in the potential flow region. Further, for the viscous interactions, the low Reynolds number condition is alleviated by the low Mach number condition, since the ratio of pressure and viscous forces scales with Re/M^2 as described by Sinnige et.al.[14]

From the fig. 4.32, the results of the experiment conducted at low speeds and CFD data at high speeds scale effectively with increased Reynolds number in the linear region. There is an increase in the quantitative value of the lift coefficient, which can be associated with the compressibility effect. The trend in both cases remain the same with the maximum usable lift at low sped and high speed is of the order 0.6. A nose down pitching moment trend is increased up to incidence of 3.5 ° and there after the pitch up tendencies are observed. This comparative study of force and moment data between CFD simulations and experiment, allows for the utilization of CFD flow field pressure measurements, which can be used to understand the force and moment trends from the wind tunnel. All the coefficient data are normalized with S_{ref} of the wind tunnel model as illustrated in fig. 3.26 and for calculation of the pitching moment moment reference point is shifted to corresponding value of the wind tunnel model.

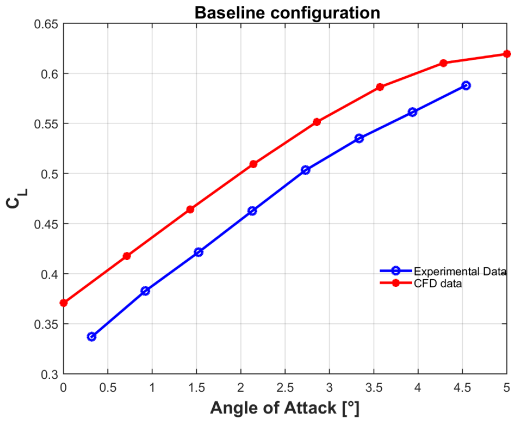

(a) Baseline configuration -Comparision of CFD Lift coefficient data with wind tunnel data

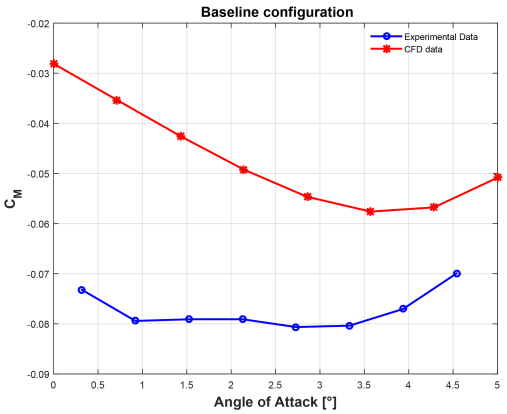

(b) Baseline configuration -Comparision of CFD Pitching moment coefficient data with wind tunnel data

Figure 4.32: Comparison of CFD and WT data for the baseline wing body configuration

4.5. EFFECT OF CANARD POSITION

In this section, results of effect of canard position both for axial proximity and vertical positions of the canard are discussed. In terms of axial proximity to the wing, as described in section 3.2, canards were tested as close coupled canard and far coupled canard configurations at 3 different vertical positions. Canard effect on lift with respect to the baseline configuration is illustrated in figs. 4.33 and 4.35. Individual canard force and moments weren't measured, due to non-availability of an internal balance and housing them within the scaled canard model, would have been rather difficult. Model component build up method was followed to determine the effects of canard. Interference effect of the canard on the wing was calculated as ΔC_L with respect to the baseline configuration and is depicted in fig. 4.33.

From fig. 4.33 it is observed that the close coupled canard configurations for all the three vertical locations have positive interference at all positive angles of attack. It is observed at low angles of attack, the wing contribution to total lift is reduced, due to the canard downwash on the inboard wing. Yet, the total lift of the configuration is almost equal to the wing alone configuration, due to positive contribution from the canard. For the high and mid-close coupled canard configurations, the mutual interference increases linearly with incidence. With the low close coupled canard configurations there is a marked increase in interference values with respect to the baseline configuration at low incidences or in the linear region of lift. This effect can be associated with the plausible wake from the low canard moving the stagnation point on the leading edge to a lower position, thereby creating an upwash,by means of increasing the curvature on the main wing. This causes an increase in the effective angle of attack, resulting in a higher lift for the potential region. The effect is corroborated from CFD surface pressure plots of the inboard section of the wing (i.e. 23% and 30% of the wing semi-span,fig. 3.24) as seen in fig. 4.34, where 'U' represents the upper side and 'L' represents the lower side of the wing. There is an increase in suction peak on the inboard sections of the wing for the low coupled canard as compared to the high or mid close coupled canard.

At high incidences, mutual interference effect of canard on the wing is high due to the inward movement of the canard vortex which creates a downwash flow field on the main wing alleviating the vortex breakdown to a higher angle of attack as compared to the canard off case. The canard vortex also allows the flow to remain attached along the wing chord.

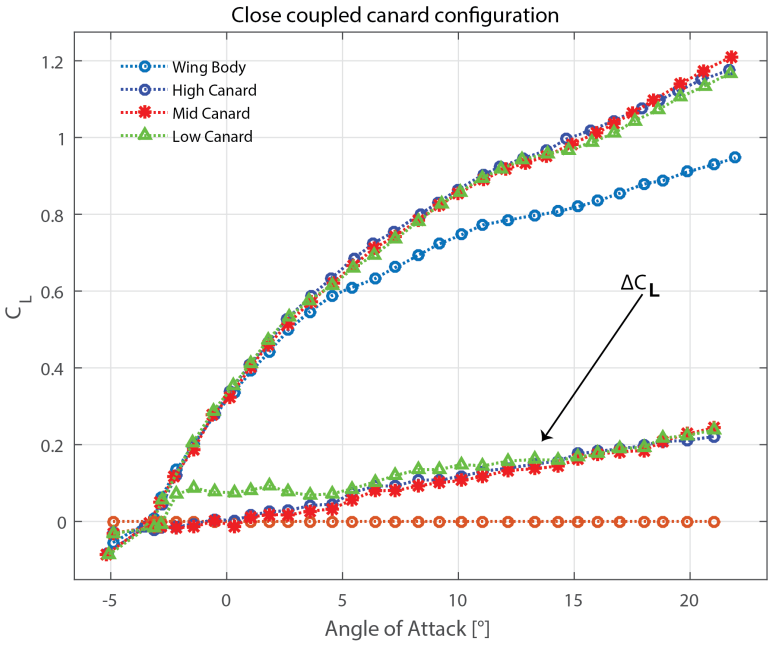

Figure 4.33: Lift coefficient data, effect of close coupled canard configuration

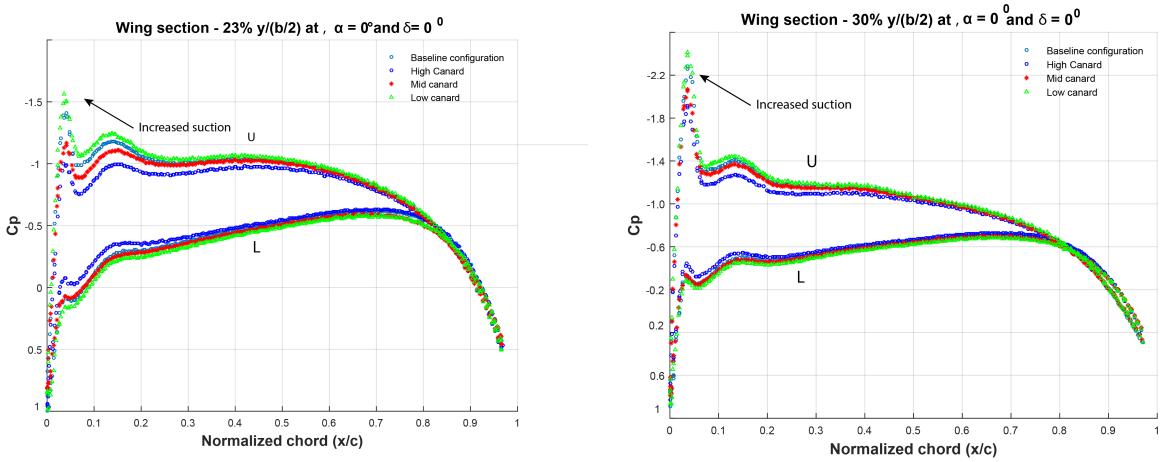

Figure 4.34: Surface pressure coeffiecients for close coupled canard configuration [4]

From fig. 4.35 it is observed that the far coupled canard configurations for all the three vertical locations have unfavorable/negative mutual interference at low incidences. However, for the high incidences, the favorable mutual interference increases linearly with incidence, with mid canard configuration providing the largest mutual interference. The low close coupled canard configurations has the least favorable mutual interference. As reported from literature, the interference effect are diminished with the increase in distance from the parent wing. The pressure and velocity field interactions are reduced, with each lifting surface acting as an independent wing.

Figure 4.36 illustrates the pitching moment variation based on the canard position. From the chosen moment reference point the canard adds instability to the configuration and it is observed that in both cases based on axial proximity there is a linear increase of instability, up until 15 ° incidence. With respect to the vertical locations of the canard, it can be seen that with an increase in canard's height there is a corresponding increase in the nose up pitching moment, with not much of difference in high

and mid canard configurations. The high canard pitching moment largely remains linear upto 22 °, with mid canard showing a reduction in slope (i.e a nose down pitching moment). In the case of low canard configuration, there is a increase in nose down pitching moment contribution at 15 °. This phenomenon can be due to either extra suction over the wing, leading to higher lift contribution from the wing which results in shifting of the center of lift rearwards, resulting in a nose down moment. The other possible reason could be if the canard vortex breakdown, which results in lower lift contribution from the canard.

The cause of canard vortex breakdown in the vicinity of 15° for the low canard configuration, can be associated with its relative vertical position to the wing, where it impinges on the leading edge of the wing, splitting into canard upper and lower vortex. The canard lower vortex trajectory passes below the wing resulting in it encountering the increased pressure from the wing pressure side, leading to higher adverse pressure gradient on the canard vortex. Canard vortex at this incidence is unable to overcome this adverse pressure gradient, resulting in a canard vortex breakdown at its outboard sectuib. Other than this the canard low vortex results in creating an unfavorable increase of suction on the wing lower surface, which is seen in the fig. 4.34. A schematic of the flow trajectories for the wing and the canard vortex system, for the low close coupled canard is illustrated in the fig. 4.41 and further corroborated with the stream traces in the fig. 4.42. Similar observations were made from the total pressure contour plots illustrated in the reference [1]

One of the plausible explanations of reduced wing suction at high angles of attack is explained in Bergmann et al. [40] for a highly swept delta wing and canard configuration. The low canard's vortex trajectory passes on the lower side of the wing, however, at high angles of attack the vortex trajectory shifts from below the wing to the upper side. At this incidence in which there is a shift in vortex trajectory from the lower surface to the upper surface, the canard and wing vortices merge, due to strong mutual interference. This results in loss in suction on the wing. Thus, the destabilizing nose up pitching moment contribution of the canard is increased and nose down contribution from the wing is reduced. Other than this, with increase in incidence the canard leading edge vortex moves further inboard with canard contribution to lift increases as seen from fig. 4.33. At the same time the wing vortex system moving inboard resulting in the center of lift of the configuration moving further forward and thus increased pitch up the moment at higher incidences. However, this theory has to be ascertained with extensive flow field measurements using pressure measurements along the span and to understand the flow trajectories using wake rake analysis with particle image velocimetry (PIV).

To understand the non linear aerodynamic behavior better, formation and breakdown of vortex system on the wing and canard configuration, it was necessary to plot the movement of the neutral point for the configuration. To understand the incremental lift or reduced lift from one of the lifting surfaces, rather than plotting center of pressure, neutral point for the whole configuration provides better insight. Neutral point aids in understanding the contribution of the lifting surfaces to total lift, in comparison to the center of pressure is a point where the total resultant lift of the system acts. Thus, making it difficult to identify lift contributions on the lifting surfaces. Neutral point by definition is the moment center for an airplane, for which change in incidence results in no change in total moment of the configuration [65]. Expressing neutral point mathematically yields the following M_α=0. By convention it is represented as % of mean aerodynamic chord (MAC) of the wing, with the 0% located at the leading edge of the wing and 100% located at the trailing edge of the wing. However, for canard configurations the neutral point is located ahead of the main/parent wing and aft of the canard. The conventions are reversed for the chosen reference system and is depicted in the section 4.5.

To compute the neutral point, the pitching moment coefficient for moment reference point ranging from 0% to 100% of the mean aerodynamic chord of the wing were plotted as contour plot as shown in fig. 4.37. Local slope of the pitching moment coefficient as function of angle of attack is computed for neutral stability ,i.e,dcm/dα= 0. In other words the trim point is computed for the given canard and wing system at a particular incidence. As the wing contribution of lift decreases, the neutral point tends to move further forward towards the canard, and with reduced canard lift the neutral point tends to move backward towards the wing leading edge. This is indicative of requirement of larger moment arms to trim the aircraft on reduction of contribution of lift from one of the lifting surface.

The neutral point shift based on canard vertical position for close couple canard are plotted in the figs. 4.39, 4.40a and 4.40b. For the mid and high close coupled canard configurations, it is observed for incidences 6-8°, the neutral point shifts forward, this corresponds to outboard separation on the parent wing in conjunction with downwash from the mid and high canard reducing wing lift contribution. In case of low canard configuration, reduction in wing contribution to lift takes place for incidences 4-6°. For incidences 10-12°, nonlinearity in pitching moment is observed. This phenomenon is reflected with the neutral point shifting rearwards towards the wing. Thus, indicating a reduction in canard lift due to plausible vortex breakdown on the canard. This effect is pronounced for low canard at these incidences, with pronounced change in slope of the pitching moment, resulting in a larger nose down contribution from the wing. At higher incidences from 16-22°, with both the wing and canard vortex system moving inboard and increase in strength of vortex, instability increases with neutral point shifting forward towards the canard.

In conclusion, canard and wing vortex system interactions are evaluated from the pitching moment curve as compared to the lift coefficient curve. Lift coefficient curve is slightly non-linear and details of the interactions between the two vortex system are difficult to evaluate. On the other hand pitching moment is sensitive to changes in the vortex system, especially the canard, as it at a large distance from the chosen moment reference point. A slight change in the lift contribution of canard is amplified and observed in the pitching moment curve. For the chosen moment reference point, wing contributes a neutral pitching moment slope for low to moderate angles of attack, where as canard ahead of the reference point provides destabilizing nose up pitching moment contribution. In presence of the canard, with the wing vortex breakdown delayed, the non-linear characteristics of the pitching moment curve is dominated by the contribution of the canard.

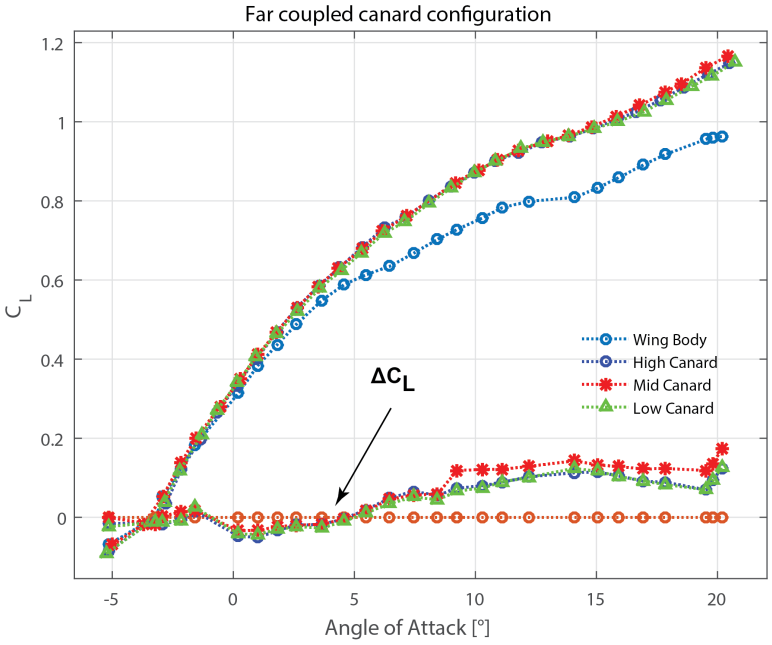

Figure 4.35: Lift coefficient data, effect of far coupled configuration

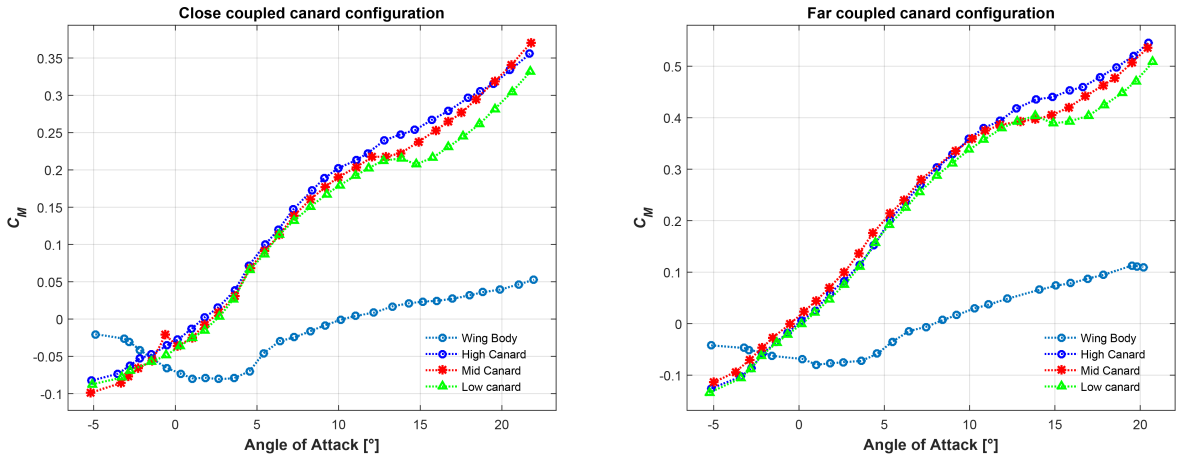

Figure 4.36: Pitching moment variation based on canard position

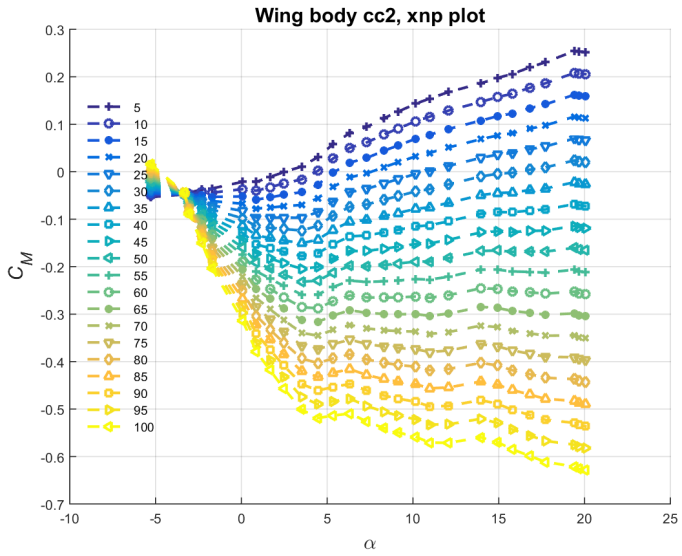

Figure 4.37: Pitching moment coefficient contour plot as a function of anlge of attack, for different % MAC reference points

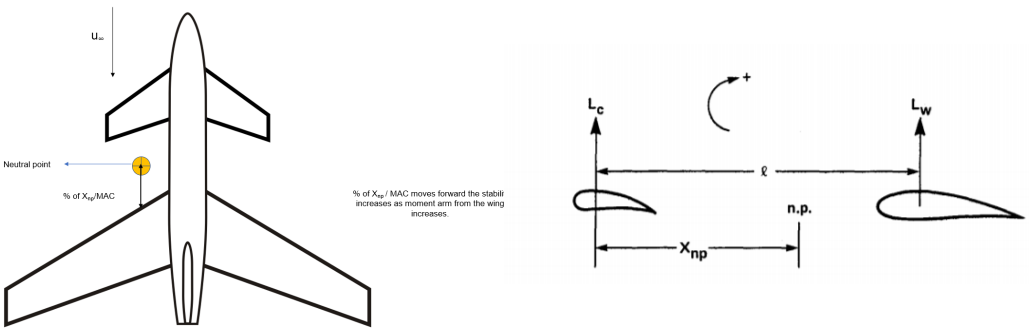

Figure 4.38: Schematic of neutral point for canard and wing configuration

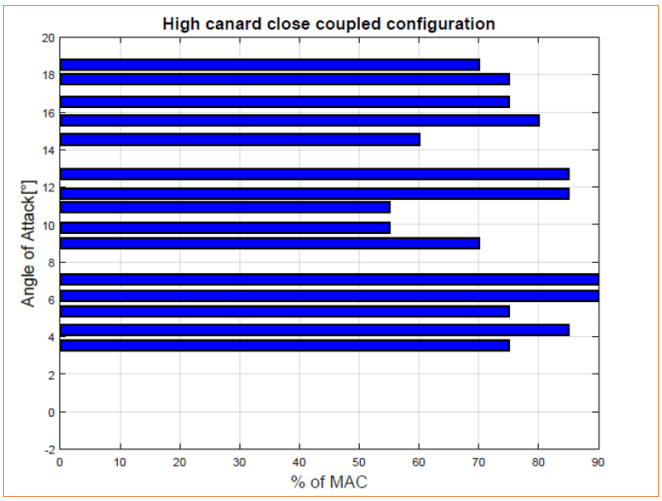

Figure 4.39: Neutral point variation for high close coupled canard configuration

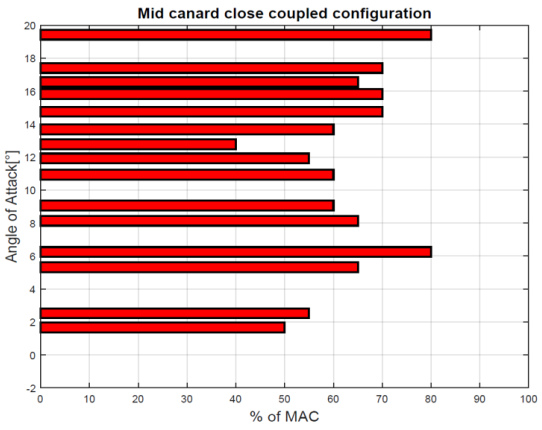

(a) Neutral point variation for mid close coupled canard configuration

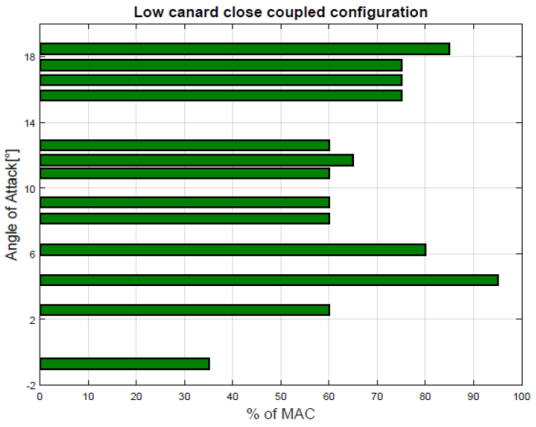

(b) Neutral point variation for mid close coupled canard configuration

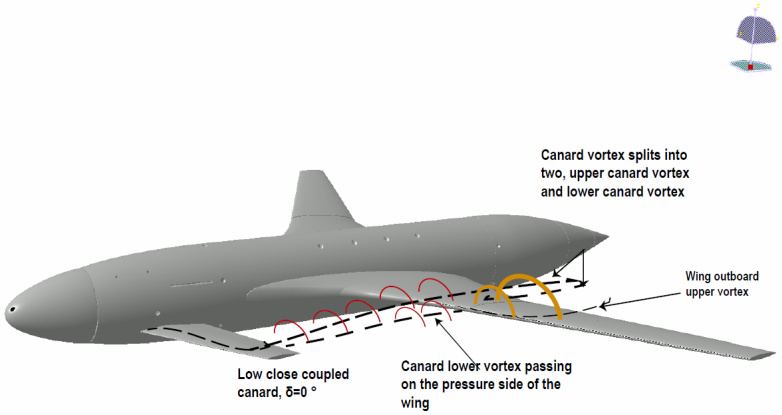

Figure 4.41: Flow trajectory schematic for canard and wing vortex systems, for the low close coupled canard configuration

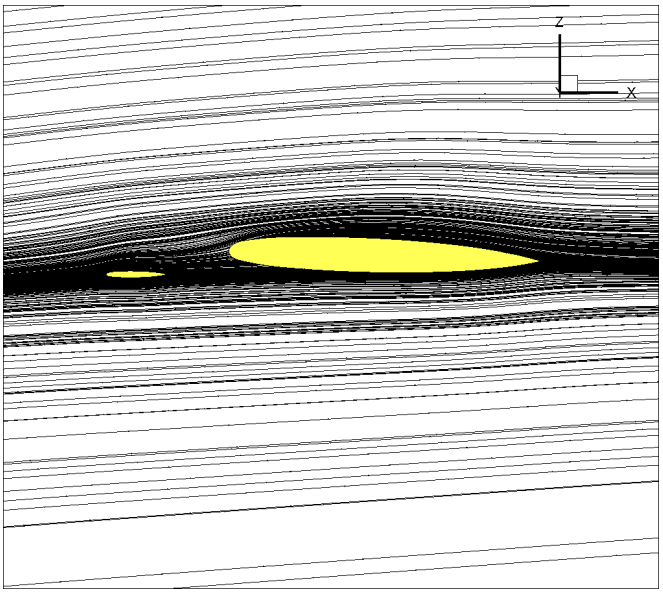

Figure 4.42: Simulated particle traces for the low close coupled canard configurations

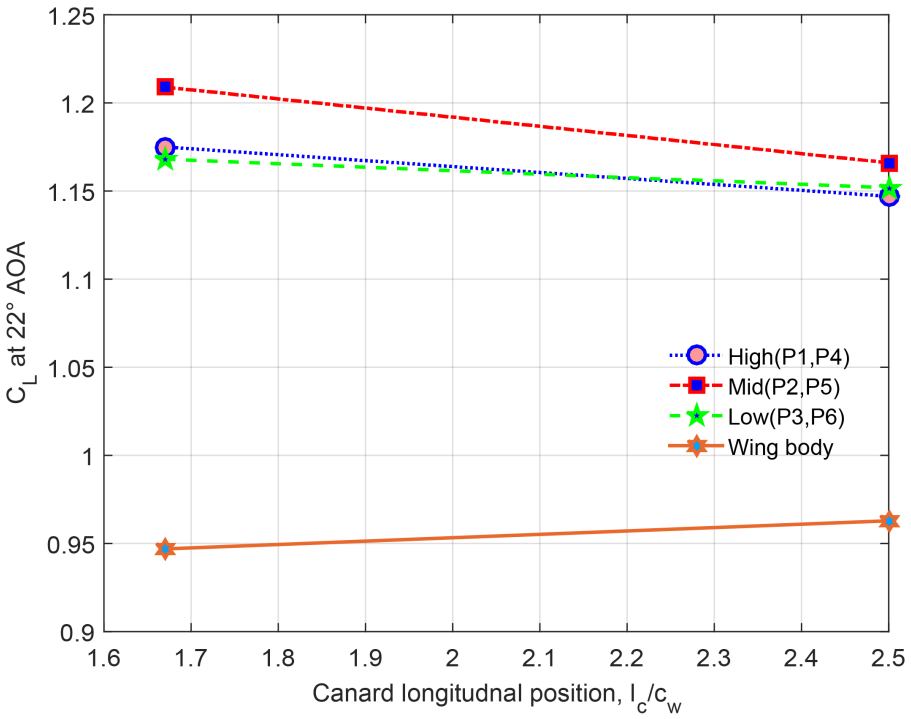

Figure 4.43: Lift coefficient at 22 ° and its variation with canard position

To understand the favorable/positive interference of the canard on the main wing, relative to their position with main wing at high incidences, fig. 4.43 is plotted. This figure details the variation of the C_L at the highest measured angle of attack for various canard configurations. It is observed that the mid canard configuration provides the highest lift for both close and far coupled canard configuration. The high and low canard have almost the same C_L values at these high incidences. It is observed that the far coupled canard configurations have a reduction in 4-5% C_L at these high angles of attack , with the exception of low canard configuration, where it tends to remain the same. Reduced mutual interference effects for the far coupled configuration is the cause of this decrease. There is an increase in C_L at 22 °, for the wing body far coupled configuration due to the larger upwash or cambering effect induced by the additional fuselage plug or extension, which was added to simulate the far coupled canard configurations. These results indicated reduced interfernce effects with the low canard configuration at high angles of attack as compared to the mid and high canard configuration, irrespective of the axial location or proximity of the canard to the main wing.

4.5.1. INDUCED DRAG FACTOR VARIATION-CANARD POSTION

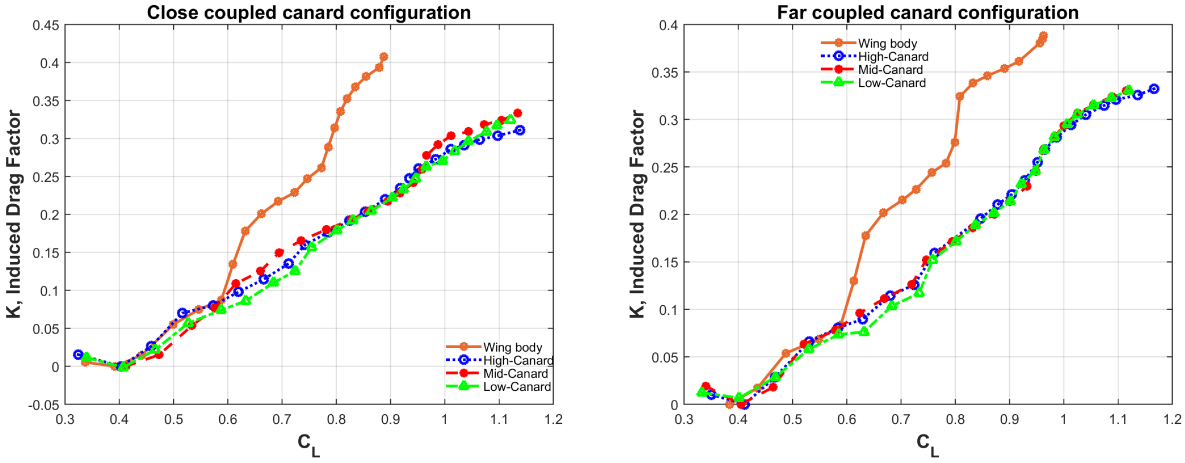

(a) Induced drag factor variation for close coupled canard configuration

(b) Induced drag factor variation for far coupled canard configuration

Figure 4.44: Induced drag factor variation based on canard position

One of the main criticism and thereby reluctance to utilize canard configurations in commercial aircrafts has been its tendency to increase the induced or vortex drag. For a lift producing canard results in canard contributing to increase in vortex drag in level flight or low angles of attack. Presence of canard alters the wing lift distribution by creating a downwash field (based on its vertical position) on the inner wing and creating an upwash on the outboard wing due to the canard tip vortex, thus resulting in deviance from the elliptical lift distribution. This further causes an increase in induced drag of the total configuration. However, due to mutual interference at high angles of attack, especially for close coupled canard configurations, results in lower induced drag. Thus, it is important to understand which configuration causes the highest induced drag and thus variation in the wing flow field.

$$K = \frac{C_D - C_{Dmin}}{(C_L - C_{L0})^2} \tag{4.4}$$

The induced drag factor is calculated from the eq. (4.4) to compare different canard configurations. It is observed from the data plotted in fig. 4.44a, that the high canard configuration has the highest induced drag factor at low angles of attack due to it having the highest downwash on the wing inboard, largely altering the spanwise lift distribution. Low canard has the least increase in induced drag at low incidences or moderate C_L values, this suggests that the low canard doesn't alter the spanwise lift distribution significantly. The wake and tip vortex trajectory from the low canard passes down on the pressure side or lower side of the wing, rather than inducing downwash like the mid or high canard configuration. From 0.6 C_L onwards, with the end of the potential region, there is a decrease in induced drag in comparison to the main wing for all the canard configurations. This is because of the mutual positive influence of canard and parent wing, which causes the free-rolling vortices to be stabilized and delaying the vortex bursting on the main wing, especially at high angles of attack. At high angles of attack or high lift coefficients, there is not much difference in the induced drag factor for all canard positions. However, high canard showing a slight deviation, by being a bit lower. This suggests reduced vortex bursting on the wing and alleviating it to a higher incidence.

Similar trends are observed for the far coupled canard configurations in the fig. 4.44b, however, the magnitudes of induced drag factor are slightly reduced due to longer moment arm and lack of mutual interference which alters the wing flow field. At high angles of attack and high C_L all the vertical positions of the canard have the same increase in induced drag factor with little change, showing loss in interference at high angles of attack.

4.6. EFFECT OF CANARD DEFLECTION

In this section the effect of canard deflection on the lift and pitching moment characteristics of the configuration are evaluated.

4.6.1. LIFT CHARACTERISTICS

Close coupled canard deflection configuration has a pronounced impact on wing performance and vortex interactions. For the far coupled canard deflection, this interaction has less significance and majorly depends on the lift of the canard configuration to provide trim and pitch control.

Figures 4.45 to 4.47 shows the lift and moment curves for the close coupled canard deflection configuration. The canard deflection δ_c ranging from -10 to+10 ° is presented for all the three vertical positions of the canard. From figs. 4.45a, 4.46a and 4.47a it is observed that during the negative deflection or the unloading cases there is no non-linearity being observed, with the reduced lift of the overall configuration as compared to the undeflected canard condition. The reduction in the lift is due to the decrease in the canard lift contribution.

For the positive deflection canard case, the canard is highly loaded and generates greater lift, which results in a greater downwash in the canard wake. This downwash reduces the effective wing angle of attack, and thereby reducing the wing contribution to the total lift. It is seen that the overall lift of the configuration remains the same as the undeflected case, with a marginal increase at high incidences for the high and mid canard cases. For the low canard case, the lift further falls as compared to the undeflected case for the region between 5 and 10 °. This is explained further in section section 4.6.2

4.6.2. PITCHING MOMENT CHARACTERISTICS

Canard pitching moment changes are more sensitive as compared to the wing pitching moment changes from the moment reference point chosen, which is the wing body aerodynamic center. Thus, any changes or non linear phenomenon on canard is reflected in the pitching moment graphs plotted in figs. 4.45b, 4.46b and 4.47b. From these figures it is seen that for $\delta = 10$ ° deflection cases there is a significant drop in pitching moment or nose down pitching moment . This is observed between the incidences of 5-10 °, and it being pronounced for mid and low close coupled canard configurations. This nonlinear behavior of a sudden drop in pitching moment could be either associated with reduced lift in the canard or the extra suction on the main wing, both of these conditions shifting the wing body canard aerodynamic center backward and thereby causing a dip in the pitching moment slope.

This pitching moment changes are primarily associated with the canard and wing interaction of the two leading-edge vortex systems on the highly swept leading edge lifting surface configurations. This canard and wing vortex trajectory and its interactions are specific to a given angle of attack range. To understand this vortex interaction, especially in the nonlinear behavior of the pitching moment curve, a wake rake analysis of total pressure contours was done for a high canard configuration. The result of the contour plot is shown in fig. 4.48. From this contour plot it is observed that the canard vortex system convects inboard on the upper side of the wing due to the accelerated velocity flow created by the suction or upper side of the wing. This canard vortex inturn diminshes the formation of the inboard or strake vortex on the wing, thereby delaying the vortex breakdown and causing attached flow over the wing inboard up to high angles of attack. However, the wing sections outboard of the canard span, is in an upwash field and the wing outboard vortex strength increased. This phenomenon observed leads to high suction on the wing upper surface, resulting in higher lift contribution from the wing, and inturn the nose down pitching moment contribution. However, for the mid and low close coupled canard deflection configurations it is plausible that the canard vortex passes on the lower side of the wing, due to its relatively low position with the wing.

This statement is further corroborated by the surface pressure plots on the inboard wing sections measured from CFD section 4.6.2. It is observed for the lower canard configuration there is an increase in the suction on the lower/pressure side of the wing, which indicates formation of a wing vortex on the lower side of the wing. The canard vortices, encounter a increased pressure on the lower side of the wing leading to canard vortex breakdown along its outboard section. This leads to a reduction in canard

lift leading to a change in the slope of the pitching moment curve. Pitching moment at these incidences has an increased pitch down tendency,thereby indicating the center of pressure of the configuration shifting rearwards. The decrease in the suction peak for canard 87.5% semi-span station is observed for both mid and low canard configuration as seen in fig. 4.50.

At α =10 ° range and above the two vortex systems unmerge and the canard portion of lift increases, with vortex moving indboard causing the center of lift for the configuration to move forward .Thus, leading to further increase in pitching moment or pitch up with change in incidences.

It is observed in conclusion that deflection of the canard results in altering the flow trajectory and vortex strength of the main wing and is dependent largely on the canard trailing vertical location with respect to wing chord line or axis.

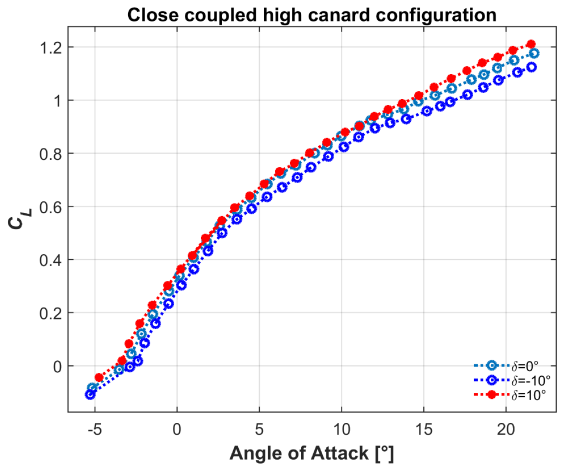

(a) Lift coefficient -high canard deflection

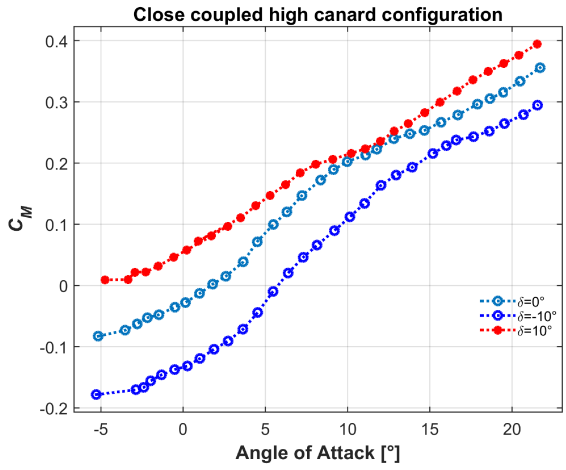

(b) Pitching moment coefficient - high canard deflection

Figure 4.45: Longitudinal coefficients of high canard deflection configuration

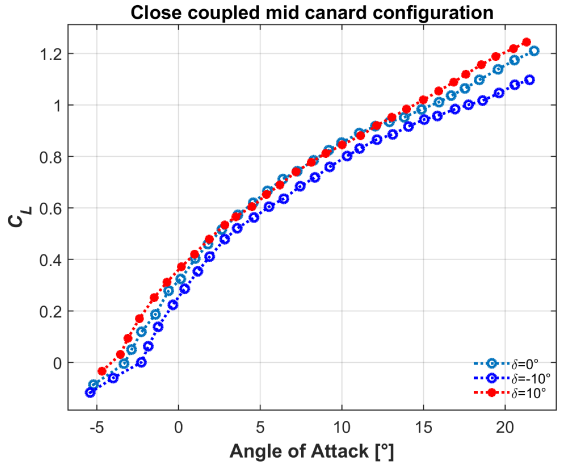

(a) Lift coefficient -mid canard deflection

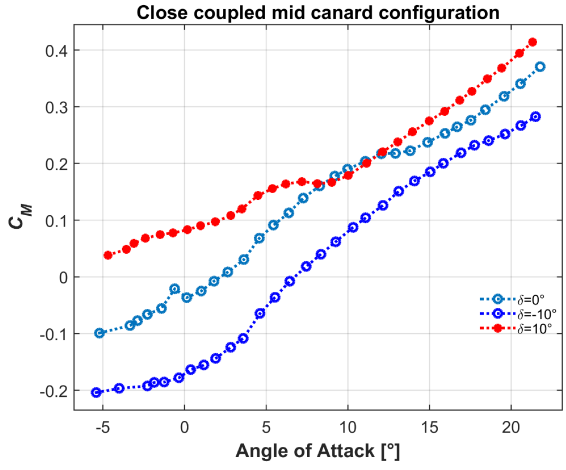

(b) Pitching moment coefficient - mid canard deflection

Figure 4.46: Longitudinal coefficients of mid canard deflection configuration

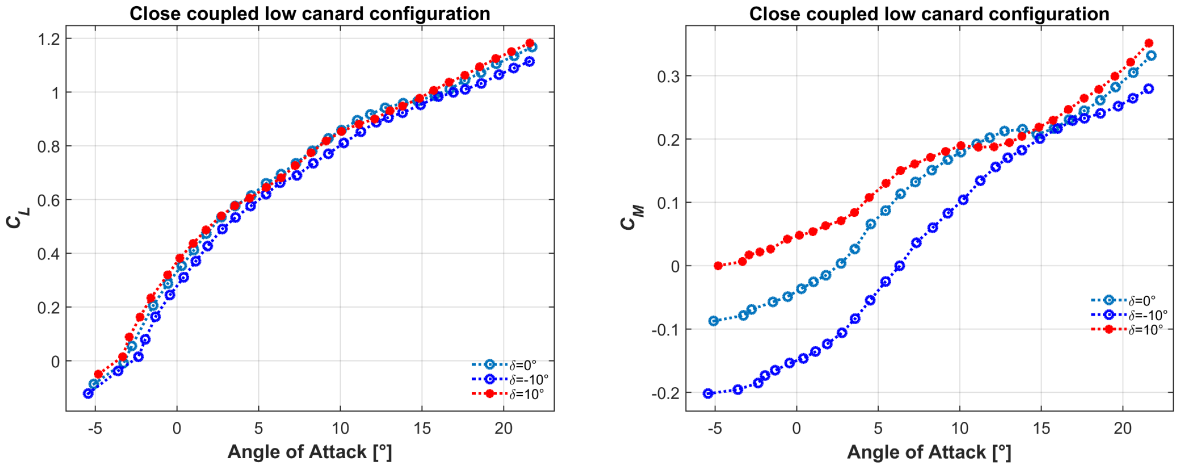

(a) Lift coefficient -low canard deflection

(b) Pitching moment coefficient - high canard deflection

Figure 4.47: Longitudinal coefficients of low canard deflection configuration

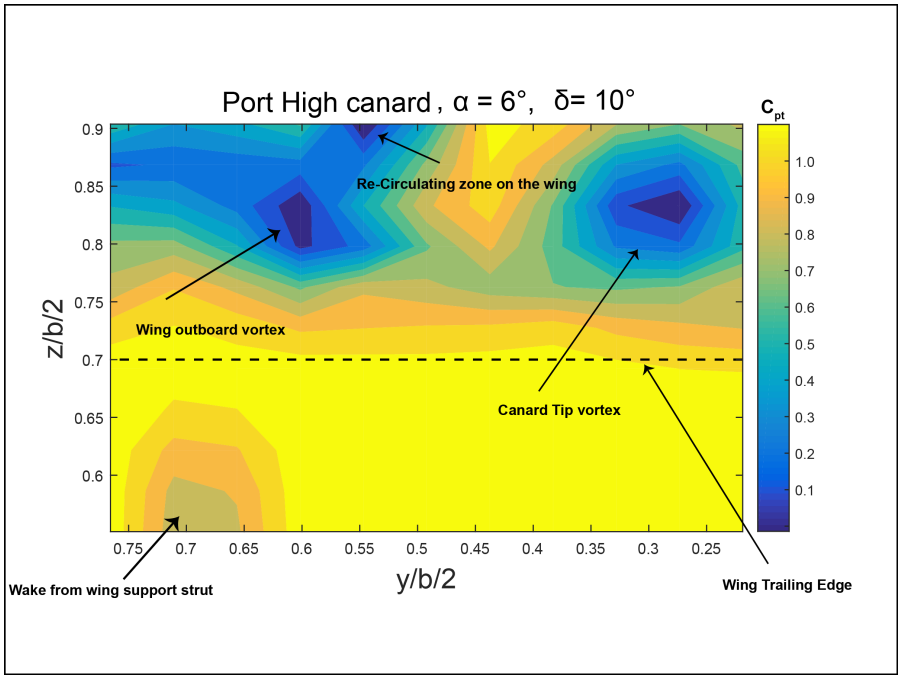

Figure 4.48: Cross flow plane visualization of total pressure contour plot for high canard deflection, α=6 °, δ=10 °

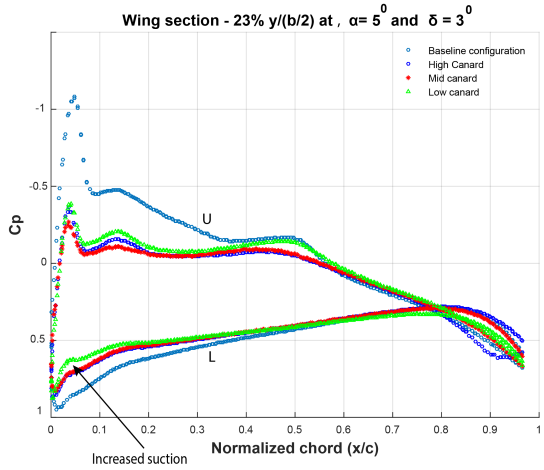

(a) Surface pressure coefficient for the deflected close coupled canard configuration, y/(b/2)=23%, M=0.8,α=5 °, Re=10 million, [4]

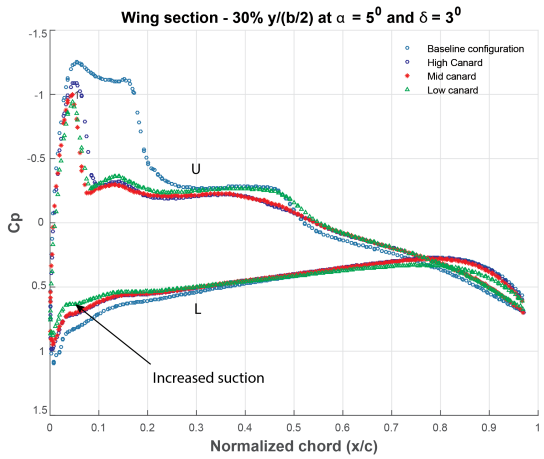

(b) Surface pressure coefficient for the deflected close coupled canard configuration, y/(b/2)=30%, M=0.8,α=5 °, Re=10 million, [4]

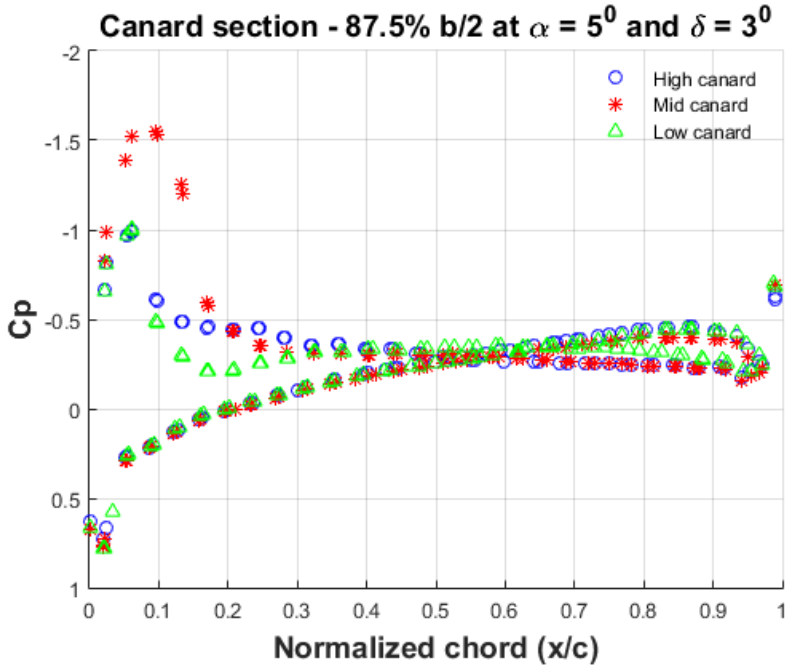

Figure 4.50: Surface pressure coefficient on the canard for the deflected close coupled canard configurations, y/(b/2)=87.5%, M=0.8,α=5 °, Re=10 million, [4]

4.6.3. SURFACE OIL FLOW VISUALIZATION TOPOLOGY- CANARD DEFLECTION

The differences in surface oil flow patterns for $\delta = 5$ and 10 °are illustrated in figs. 4.51a and 4.51b. The separation line on both the canard and wing are indicated. With increase in canard deflection it is observed that the separation line on the canard moves inboard indicating the vertically upward in conjuction with and inward shift of the canard vortex trajectory. This inward shift in the canard vortex trajectory leads to delaying the formation of wing strake vortex inboard, and tends to push the vortex formation on the wing further outboard. The suppression of the strake vortex can be observed by comparing the total pressure contours of fig. 4.28 and fig. 4.48.

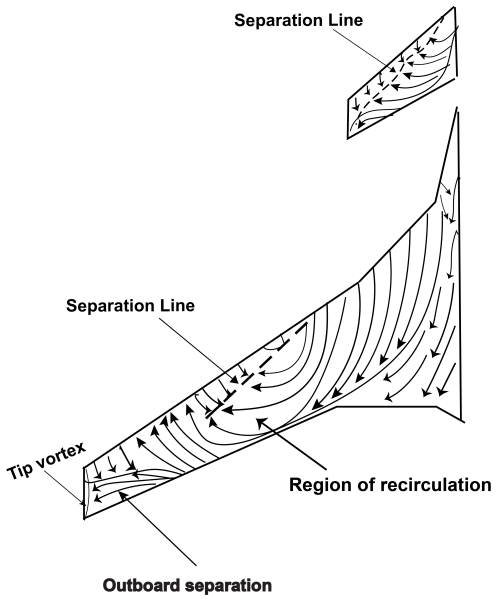

(a) High canard delfection,α=6°,δ=5°

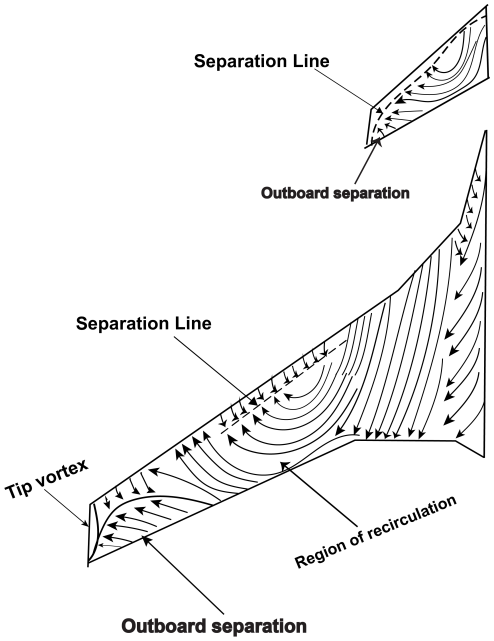

(b) High canard delfection,α=6°,δ=10°

Figure 4.51: Surface oil flow visualization pattern of canard deflection configuration

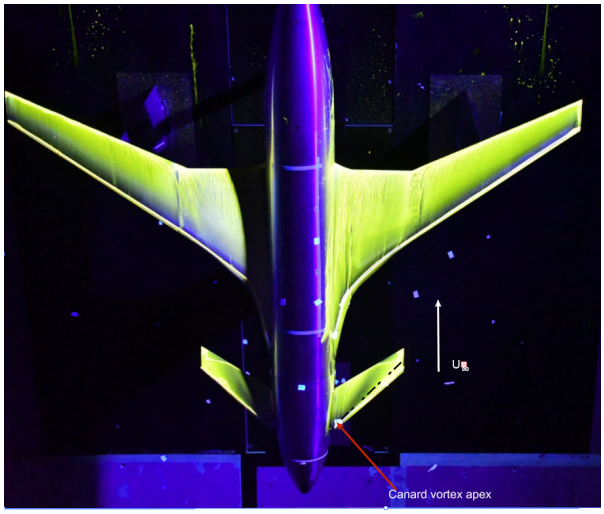

Figure 4.52: Surface pressure coefficient for the deflected close coupled canard configuration, y/(b/2)=23%, M=0.8,α=5 °, Re=10 million, [4]

4.7. INDUCED DRAG FACTOR VARIATION-WITH CANARD DEFLECTION

The effect of canard deflection on the induced drag factor (k) are presented in figs. 4.53, 4.54a and 4.54b. From the figures, it can be seen that for a positive deflection of 10 °, there is an increase in induced drag as compared to the reference wing body baseline configuration, especially at low lift coefficients. One of the reasons is that the canard with positive deflections is highly loaded and results in a higher induced drag contribution to the configuration. At these low lift coefficients, it is observed that the canard with its downwash modifies the lift distribution on the wing in an unfavorable manner. The downwash from the canard deflection reduces the effective angle of attack of the inboard wing, resulting in reduced lift over the inboard wing and thereby creating a load distribution on the wing which deviates from the ideal elliptical lift distribution, resulting in higher induced drag. As the incidence is increased further the favorable effects of the canard and wing interaction are observed leading to a decrease in induced drag factor which is lesser than that of the wing body baseline configuration.

Negative deflection -10 ° of the canard reduced the induced drag factor to values below the basic wing body configuration at both low and high coefficients of lift. This trend is due to the off loading of the canard, which reduces the induced drag contribution for the total configuration. Also, at low incidences and low lift coefficients the canard downwash does not create a downwash on the inboard of the parent wing, thereby not altering the designed lift distribution on the wing. However, at high lift coefficients, the deviation in induced drag factor is minimal between the positive, negative and undeflected canard cases.

For the far coupled canard configuration similar trends are observed, the magnitude of the induced drag factor is slightly reduced due to reduced interference between the wing and the canard.

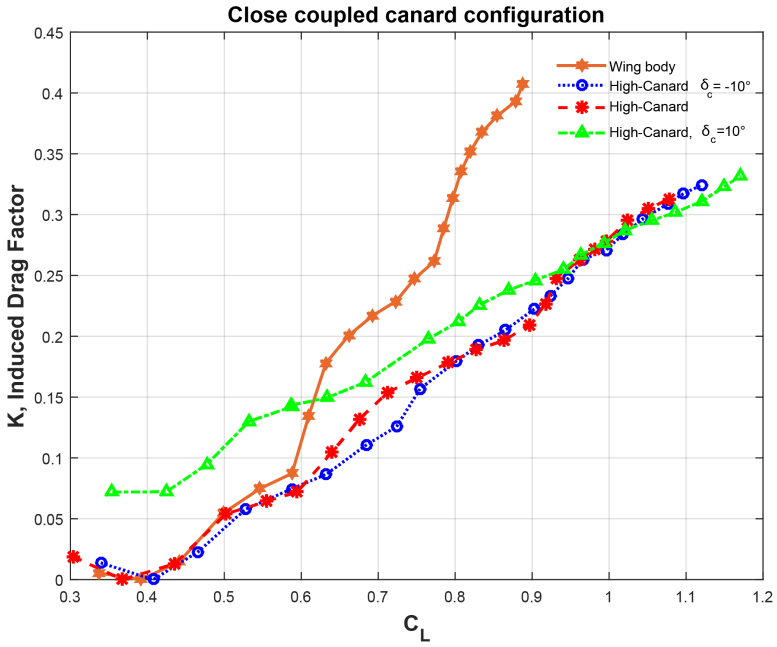

Figure 4.53: Induced drag factor variation for high canard deflection configuration

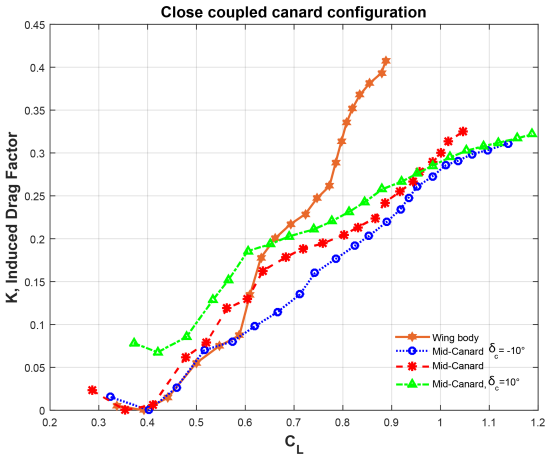

(a) Induced drag factor variation for mid canard deflection configuration

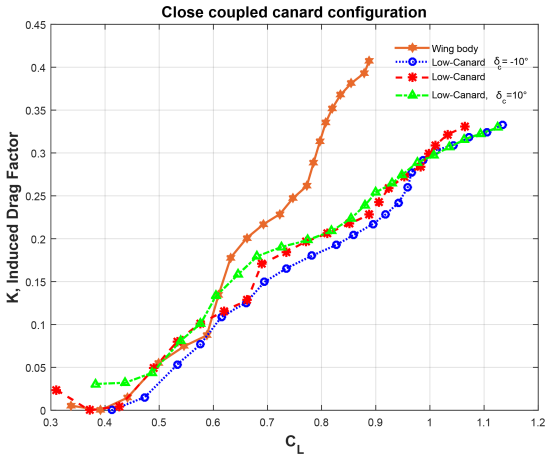

(b) Induced drag factor variation for low canard deflection configuration

Figure 4.54: Induced drag factor variation based on close coupled canard deflection

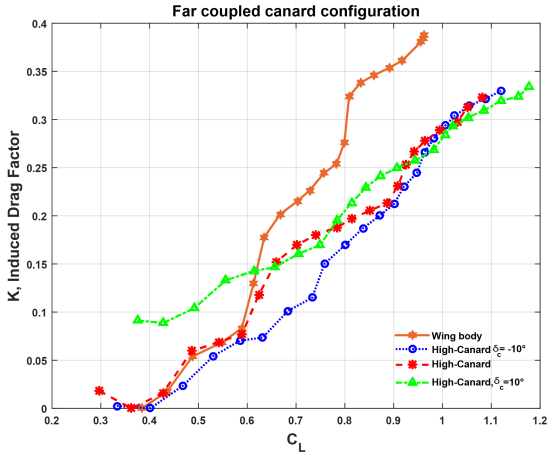

(a) Induced drag factor variation for high canard deflection configuration

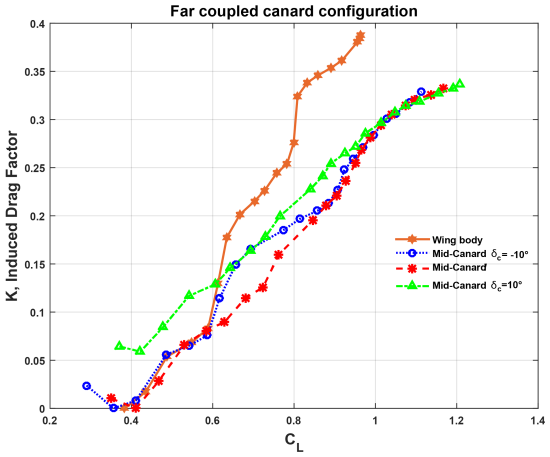

(b) Induced drag factor variation for mid canard deflection configuration

Figure 4.55: Induced drag factor variation based on far coupled canard deflection

4.8. TRIM CALCULATION

In order to assess the aerodynamic performance of a practical aircraft design configuration, calculating and analyzing trimmed lift and drag is essential. Though these calculations are not part of this study, however, this data would be useful in understanding the trimmed aerodynamic performance, usable C_L limits for the canard-wing body configurations. Thus, assiting in especially identifying the effect various canard positions and deflection on achieving trim for the configuration for a chosen moment reference point location.

Utilization of wing trailing edge flap deflection in tandem with the canard to trim the additional nose down pitching down moment would serve as a more realistic condition for assessment of trimmed performance at low speeds.

Contour plot of pitching moment about the chosen reference point are depicted in figs. 4.56, 4.57a and 4.57b for high,mid and low close coupled canard and its deflected configurations. The trimmed (C_M=0) pitching moment curve is highlighted and the from the figure it is understood that positive deflections could trim the said configuration at low lift coefficients and negative canard deflections would be required to trim the configuration at moderate lift coefficients of 0.4-0.6. It is also observed that the low canard configuration has the largest C_L range of trim.

From fig. 4.58, for the close coupled canard configurations it is understood that the high canard configuration provides the best trim lift to drag ratio for moderate lift coefficients. However, low canard provides a better range of trim across the usable C_L range. The mid canard provides the least trim lift to drag ratio across its trimmable range.

Similarly, from fig. 4.59, for the far coupled canard configurations, owing to larger moment arm, the trim range for both the deflected high and mid canard configurations is increased. However, there is a reduction in the trimmed lift to drag ratio as compared to the close-coupled canard configuration, which may be due to :

- The additional skin friction drag resulting from the extension of the center fuselage to simulate the far coupled configuration.
- Overall reduction in lift of the configuration, as the interference effects are lost, thereby leading to lesser lift to drag ratio
- Based on the moment reference point chosen, higher instability results with the aerodynamic center of the configuration shifting further forward than the close coupled canard configuration, leading to higher unloading of the canard. Thus, resulting in a drop of lift to drag ratio.

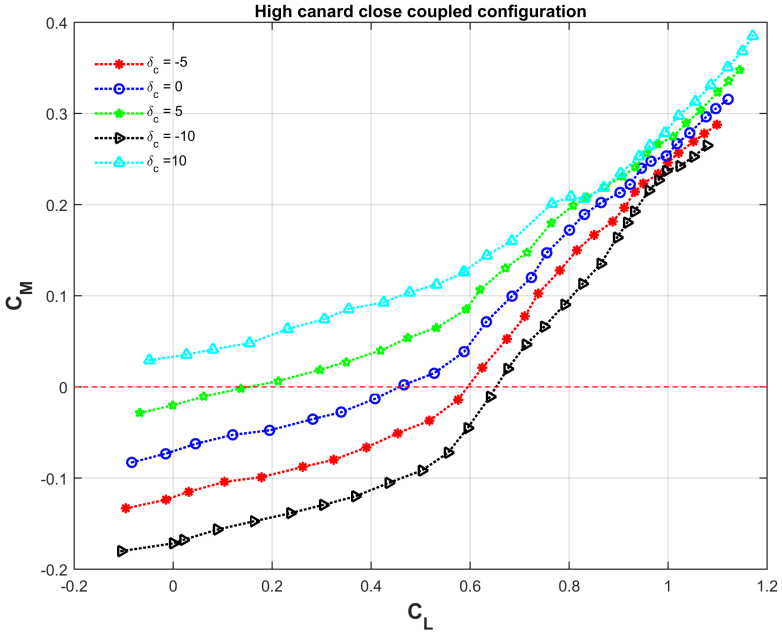

Figure 4.56: Pitching moment coefficient vs Lift coefficient- High canard deflection

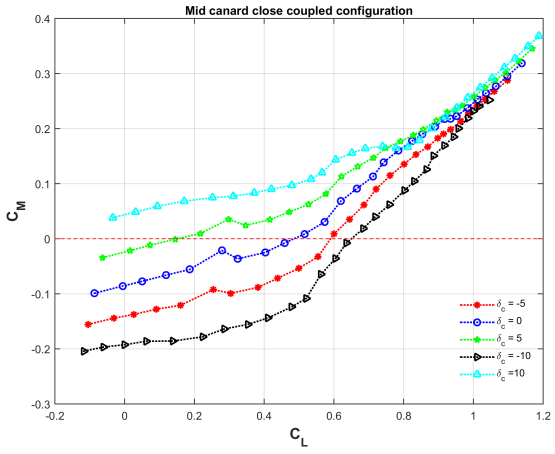

(a) Pitching moment coefficient vs Lift coefficient-mid canard deflection

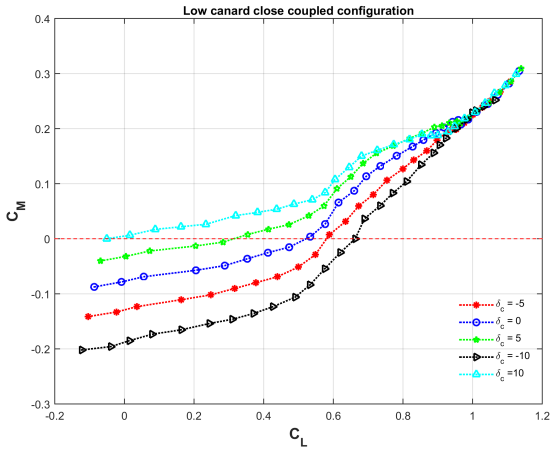

(b) Pitching moment coefficient vs Lift coefficient- low canard deflection

Figure 4.57: Longitudinal coefficients of low canard deflection configuration

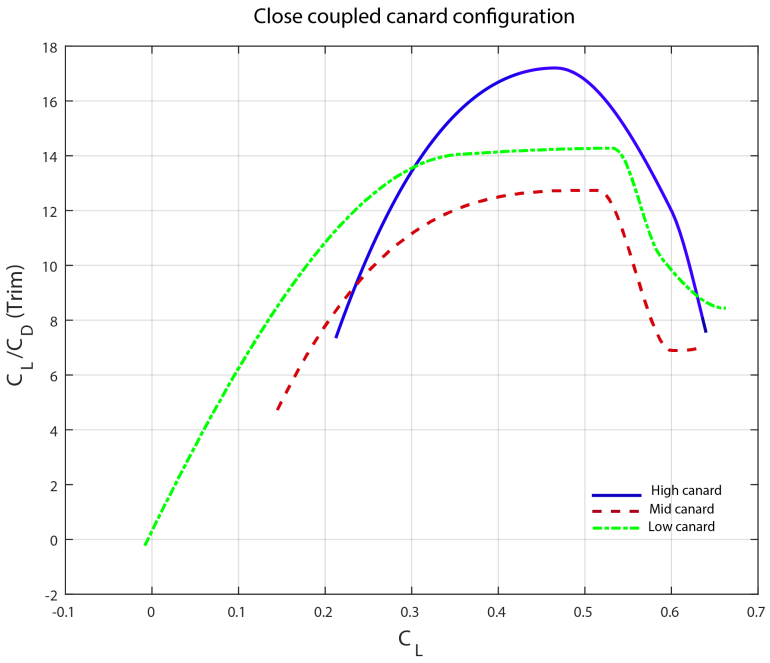

Figure 4.58: Lift to drag ratio for close coupled canard configuration trim

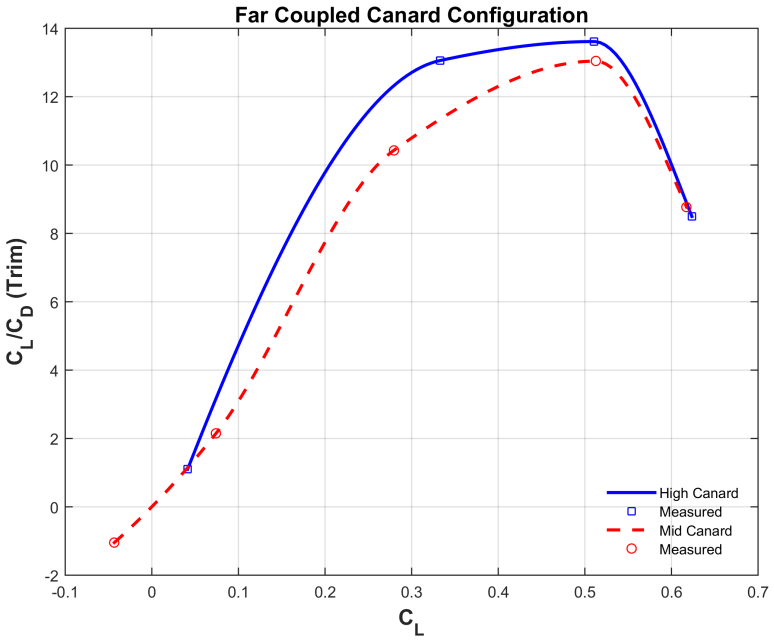

Figure 4.59: Lift to drag ratio for far coupled canard confiugration trim

5

CONCLUSIONS AND RECOMMENDATION

5.1. CONCLUSION

Wind tunnel experiments were conducted on a close and far coupled canard and multi cranked wing combination for an angle of attack range of -5 to+22 °, in symmetric flow conditions. The generic wind tunnel model consisted of a multi-cranked wing, a 45° swept canard and an axis symmetric body of revolution as a fuselage. Two axial positions along with three vertical positions of the canard and its deflections were varied, and analyzed. A low speed force and moment database was compiled with surface oil flow visualization and wake rake analysis was carried out at Reynolds number of 0.5 million.

5.1.1. MULTI-CRANKED WING BODY AERODYNAMICS

It is understood from the test results that the multi cranked wing body configuration has an outboard tip stall problem. Thus, leading to longitudinal instability with a large pitch up observed at low-moderate angles of around α =5 °. Pitch up thus limits the range of usable lift, this results in decreased low-speed performance. This is contrary to objective of achieving a higher Lift to drag ratio, with a reduced outboard sweep.

The flow discontinuity is first observed at the leading edge extension kink. This separation can be traced to the sudden discontinuity along the leading edge of the cranked wing, and the spanwise flow, causing it to occur first at this point. With the increase in incidence the strength of the vortex increases with the formation of part span vortex from the re-circulation region.

At high incidences the strake vortex merges with the wing vortex, creating a streamwise vortex along the separation line. This vortex system keeps the flow on the outboard wing more benign and reduces the region of the outboard stall, with only trailing edge stall being observed from the surface oil flow visualization. Owing to the concentration of large suction peaks associated with vortex generation on the inboard wing and plausible vortex breakdown at the rear of the wing chord, the center of pressure tends to move inboard resulting in increased pitch up at these high angles of attack.

The wing design from the layout point of view seems attractive, meeting the volumetric requirements of housing unconventional fuels or leading edge device systems, with a strong structural layout. However, the pitch up at moderate C_L is a problem and limits the usable C_L. This has to be alleviated to increase the range of usable C_L, by changes in the wing planform. From these baseline tests the region of outboard stall, regions of vortical flow on the wing were observed and analyzed. The wing design can be further fine tuned to improve these characteritistics.

Some recommendations for improved performance of the outboard wing are as follows:

- Providing a notch at the leading edge or a pylon vortex generator which creates a counter rotating vortex as compared to the leading vortex from the main wing, reducing the magnitude of pitch up.

- Utilizing leading edge slats to reduce the outboard wing effective angle of attack to alleviate the pitch up to high angles of attack. Other than this outboard stall devices such as wing fence, vortex generators can be utilized to re-energize the boundary layer and preventing the outboard stall.

5.1.2. EFFECT OF CANARD POSITION

With the canard on configuration, the interactions between the canard and wing vortex systems dominate the flow characteristics of this configuration. For the close coupled canard configurations the interactions between the main wing and the canard result in favorable interference for lift at all positive angles of attack. The interference increases at higher angles of attack, resulting in substantial increase of lift as compared to the canard off case for all the three canard vertical positions.

With increasing incidences both the canard and wing vortex tends to move inboard, resulting in center of pressure shifting inboard of the lifting surfaces, causing pitch up tendencies.

Mid and low close coupled canard configurations owing to their vertical location with respect to the wing, there is a tendency of the canard vortex system to flow over the lower side of the wing at moderate angles of attack. This results in vortex breakdown at the canard, as it encounters increased pressure (adverse pressure) from the lower/ pressure side of the wing and causes a sudden drop in pitching moment. This effect reduces with increasing angle of attack as the canard vortex systems switches sides by passing over the suction side of the wing, where the accelerating flow field of the main wing alleviates the vortex breakdown effect in the canard.

For the high close coupled canard configuration the canard vortex does not pass over the wing lower surface at these incidences and there is no sudden drop in pitching moment observed. From these results it is quite clear that for occurrence of vortex breakdown over the canard is largely dependent on the vertical position of the canard with respect to the wing.

In previous paragraphs the effect of wing on the canard was studied. In these subsequent paragraphs the effect of canard on the main wing is tried to be understood. For the mid or high canard flowfield, the canard-induced downwash was found to weaken or delay formation of the wing leading-edge vortex. Formation of the wing leading-edge vortex shifts outboard to wing secton outboard of the canard span.

These results confirm and provide an explanation for the canard's potential for delaying wing vortex breakdown which has been noted from the literature study.

The interaction effect of the low close coupled canard and the wing is dominant and interesting to understand. Due to the interaction between the low-canard vortex and the wing lower surface, unfavorable lift and drag characteristics for the low-canard configuration are evident as angle of attack is increased.

At low angles of attack, the low-canard wake causes the stagnation point to shift downwards on the wing, causing an increase in effective angle of attack. For certain higher angles of attack, the canard vortex strikes the wing and the vortex is split into upper and lower vortices.

For the far coupled canard configurations the interaction effects are minimal with larger deflections required to trim the configuration. However, the range of C_L for which trim can be achieved is increased. Considering the minimized interactions between the canard and the wing, the lift distribution on the main wing is not affected, leading to lower values of induced drag. Favorable interactions between the canard and the main wing are observed only at moderate to high angles of attack. The effect of vertical position of the canard with the main wing is similar to that of the close coupled canard configuration.

Based on these observations, the designer has been provided host of design choices to evaluate and apply for utilization in novel configurations using such wing planform layout. Mid and high close coupled canard provide acceptable performance as lifting canard. Low canard configuration limits the favorable interference effect and may lead to control problems with sudden vortex breakdown at moderate to high angles of attack. Canard and wing vortex interactions prevent main wing from undergoing large

pitch up as compared to the canard off case. Though an explicit canard stall does not occur, the vortex breakdown on the canard at moderate angles of attack provides indication of allowable incidence range in which the aircraft can operate. Thereby, complying to the requirement of airplane stall resistance.

5.1.3. EFFECT OF CANARD DEFLECTIONS

On canard positively being deflected, a pronounced effect on aerodynamic interactions are observed, particularly for wing lift and configuration pitching moment. Visualization of the canard-wing-body flow-field shows a complex flow structure consisting of several interacting canard and wing vortices. Specifically at significantly large canard deflection angles, inboard of the wing is in the downwash of the canard, leading to effective decrease in angle of attack. However, outboard of the canard tip span the effective angle of attack transitions to increase in angle of attack on the main wing. Thus, resulting in large variation of spanwise lift distribution and thus leading to increased induced drag .

Based on the observations made in the previous section on the criticality of the trailing edge of the height of the canard with respect to the wing. Mid and low canard with positive deflection result in lowering the trailing edge to the main wing. Thus, resulting in canard vortices passing on the lower side of the wing. This results in vortex breakdown and loss in control power at moderate to high angles of attack. Also, the high loading on the canard results in a region of separation on the outboard of the canard causing a further drop in the C_L-α and C_M-α slope as compared to the undeflected canard case.

Negative canard deflections or unloading of the canard results in reduced interference on the parent wing, with reduced induced drag and inturn higher lift to drag ratios. For all the three canard vertical positions there is no drop in the C_M-α indicating no vortex breakdown or stall on the canard. To minimize the induced drag in level flight, canard can be unloaded. However, to trim the excess nose down pitching moment from the wing trailing edge devices utilizing positive deflections would be favorable for take off and landing performance. At these conditions maximizing lift would be important. Also, the downwash and upward inward movement of the canard vortices will keep the flow attached over the inboard wing. Thus, increasing the effectiveness of the trailing edge flap.

These findings both correlate with, and provide an explanation for, much of the experimental results presented in the literature. Precise understanding of such aerodynamic effects were needed to be understood in the design and optimization of future canard aircraft configurations with a compound swept cranked wing.

Some of the key findings from the experimental campaign are as follows:

Baseline configuration

- 'Pitch up' tendencies of the multi-cranked wing are observed at moderate lift coefficient of 0.6.
- Region of re-circulation is reduced and formation of part span vortex is observed from 10-15 ° Angle of Attack.
- Post 15 ° Angle of Attack, the strake vortex and the wing vortex system merge inboard of the wing span, leading to strong inboard vortex lift with a large turbulent core as observed in [61] shifting the wing lift vector further inboard and resulting in continued pitch up at high angles of attack.

Effect of Canard Position

- All close coupled canard configurations lead to favorable mutual interference at positive incidences with a linear increase of the incidence.
- High close coupled canard configuration is the least loaded and doesn't undergo a vortex breakdown and reduction in C_M-α slope at moderate angles of attack, i.e. in the C_{Lmax} range of 0.8-1
- Mid close coupled canard has the best mutual interference effects at moderate to high angles of attack (10- 22), with highest maximum lift coefficient.

- Low close coupled canard has the least mutual interference effects at moderate angles of attack, with least maximum lift coefficient. However, it has the best mutual interference at low angles of attack, creating a upwash over the wing from its wake.
- In the far coupled canard configuration (lc/ $\overline{c}$ = 2.5), the positive mutual interference is largely reduced. hence C_{Lmax} is reduced by ~8-10%.

Effect of Canard deflection

- Inhibits the formation of wing leading edge vortex system on the wing inboard, with suppression of suction peak observed from the deflected and undeflected cases. Lift measured at highest incidence is for the high canard configuration, indicating it producing the largest downwash on the wing alleviating the wing vortex breakdown to higher incidences.
- Origin of the Wing vortex system is shifted outboard, occuring at station of the wing which is outboard of the canard span. This results in increased induced drag due to alteration of the wing lift distribution from the elliptical lift distribution.
- Control power reduction is observed for all the positive deflected canard positions. Canard is highly loaded and is susceptible to stall/wing vortex break down on the outboard section of the canard.

Trim

- High close coupled canard configurations provide the best trimmed lift to drag ratio for low to moderate lift coefficient (0.3 - 0.6).
- Low close coupled canard has the highest trimmable points.

5.2. RECOMMENDATIONS FOR FUTURE WORK

This section provides some recommendations for future directions of work that can be carried out using the experimental test bed. The recommendations can be broadly classified on the basis of the experimental setup and research direction.

5.2.1. EXPERIMENTAL SETUP

- Leading edge of the boundary splitter plate can be further rounded to avoid any doubts on LE separation, current one had a relatively sharp LE, which was sanded to an extent.
- Altering bell crank position of the linear actuator to extend the range of the model to a higher range of attack.
- Angle of attack sensor to be made closed loop in tandem with the linear actuator design.
- Oil flow measurements- Utilization of Titanium dioxide or China clay method would help better to understand the surface streamlines better. Considering the vorticial flow associated with the configuration, the oil is highly swept away, and it is difficult to interpret the topologies of the flow.
- Requirement of stronger UV light on both starboard and port side of the wing to avoid shadow regions. This would aid in understanding any asymmetry in the flow.
- Pressure measurements on the wing and canard to better understand the local flow field in coherence with the global force and moment measurements.
- Canard-alone strain gauge force measurements will help quantize the effect of canard on the wing, and also characterize canard alone performance.
- Wake rake measurements with an automated traverse, to increase the number of measured points and identify the vortex flow trajectories. Measurement in planes ahead of the wing to understand the vortex evolution of the canard and its effect on the wing vortex aerodynamics.

5.2.2. RESEARCH DIRECTION

- Experimental campaign to measure and characterize the open jet facility tunnel flow parameters, especially the flow angularity in pitch and yaw planes and the turbulence levels. This would help set up the boundary conditions for the simulations and critically analyzing the results both from the experiment and simulations, in turn help in critically compare the experimental simulations with the numerical simulations.
- Extensive flow field measurements with aid of Particle Image Velocimetry (PIV), wake rake measurements to understand better the vortex breakdown process, vortex trajectories of canard on the wing.
- Wing outboard stall devices to be incorporated to prevent outboard separation at low angles of attack. Wing droop or wing leading edge slat would alleviate the outboard stall and in turn reduce the pitch up effect.
- For tip stall alleviation, highly swept back wing tip extension similar to küchemann tips could be added to generate vortex over the tip of the wing to keep the flow outboard attached for pre and post stall conditions. Also, the vortex flow over the tip would alleviate pitch up tendencies with higher lift generated and prevention of outboard separation due to vortex lift.
- Active flow control technique of spanwise blowing over the outboard wing could prevent flow separation on the outboard wing, thereby, alleviating to pitch up to higher angles of attack.
- Trim calculations with trailing edges flap deployed will be a representative case to determine the low speed trim.
- Different canard planforms and airfoil sections can be tested for maximizing the mutual interference and also to achieve airplane stall.
- Canard flaps can be utilized to trim the aircraft, rather than an all moving canard, control power determination can be studied this way.
- CFD/numerical model, validating the experimental database, including the wing body effects.
- Unsteady experimental and numerical studies can be carried out to characterize the dynamic response of such configurations.
- Experiments at the low-speed facility of Delft university (i.e. low turbulence tunnel), where the effect of Reynolds number can be characterized better.
- To conduct tests in asymmetrical conditions. To characterize the lateral and directional parameters. Especially, determining the aileron power at low speeds based on interaction of canard tip vortices with ailerons.

BIBLIOGRAPHY

[1] E. L. Tu, *Numerical Study of Steady and Unsteady Canard-Wing-Body Aerodynamics*, Tech. Rep. NASA TM 110394 (1996).

[2] K. TOYODA, *Aerodynamic interference caused by the inboard leading-edge flap on the outboard area of the cranked arrow wing*, Procedia Engineering **99**, 1642 (2015).

[3] H. Heyson, *Linearized theory of wind-tunnel jet-boundary corrections and ground effect for v/STOL aircraft.* (1963).

[4] B. Aswathanarayana Gowda, *Aerodynamic effect of canard on a blended wing body aircraft in transonic regime: A numerical study using SU2*, Master's thesis, TU Delft (2017).

[5] A. BARLOW, Jewel B.; RAE JR.William H.;POPE, *Low speed wind tunnel testing, 3rd edition* (John Wiley and Sons, 1999).

[6] J. M. Delery, *Physics of vortical flows*, Journal of Aircraft **29**, 856 (1992).

[7] N. Lambourne, *The bursting of leading-edge vortices-some observations and discussion of the phenomenon.* ARCR & M. **3282**, 1 (1962).

[8] S. Sane, *The aerodynamics of insect flight. journal of experimental biology.* Journal of experimental biology **4191-208** (2003).

[9] *http://www.acare4europe.org/sria/flightpath-2050-goals* (2018) accessed.

[10] D. KUCHEMANN, *The aerodynamic design of aircraft. Progress in aeronautical sciences* (Pergamon, London, 1978).

[11] C. P. VANDAM, *High angle-of-attack aerodynamic characteristics of crescent and elliptic wings*, Tech. Rep. NASA CR 184992 (NASA, 1989).

[12] D. Küchemann, *KÜCHEMANN, D. On the Possibility of Designing Wings That Combine Vortex Flows with Classical Aerofoil Flows*, Tech. Rep. RAE TM AERO 1363 (RAE, 1971).

[13] G.H.Lee, *Aerodynamics of the crescent wing,* (2018), accessed.

[14] T. Sinnige, *Aerodynamic and Aeroacoustic Interaction Effects for Tip-Mounted Propellers*, Master's thesis, TU Delft (2018).

[15] B. F. R. EWALD, *Wind tunnel wall correction, Canada* (AGARD, 1998).

[16] A. Benoliel and W. Mason, *Pitch-up characteristics for hsct class planforms - survey and estimation*, 12th Applied Aerodynamics Conference, Fluid Dynamics and Co-located Conferences .

[17] R. Whitford, *Design for air combat*, Whitford,Jones Publishing (1989).

[18] D. L. Antani and J. M. Morgenstern, *Hsct high-lift aerodynamic technology requirements*, AIAA-92-4228,Aircraft Design Systems Meeting (1992).

[19] W. Swan, *Design evolution of the boeing 2707-300 supersonic transport. part 1: Configuration development, aerodynamics, propulsion, and structures*, AGARD Aircraft Design Integration and Optimization **1** (1974).

[20] C. P. Nelson, *Effects of Wing Planform on HSCT Off-design Aerodynamics* (Washington).

[21] G. B. B. and K. E. Washburn, *A study of canard-wing interference using experimental pressure data at transonic speeds.*, Tech. Rep. NASA TP-1355 (1979).

[22] S. F. Roelof Vos, *Introduction to transonic aerodynamics„* ISBN 97817-9747-94-0-4 .

[23] J. Rom, *"high angle of attack aerodynamics"*, Springer Nature America,Inc. **Print ISBN 1-4612-7686-9** (1992).

[24] a. G. J. Coe Jr, P. L.Kjelgaard, *Low-speed aerodynamic characteristics of a highly swept untwisted uncambered arrow wing*, Tech. Rep. (1983).

[25] a. R. P. COE JR, Paul L, *Effects of wing leading-edge deflection on low-speed aerodynamic characteristics of a low-aspect-ratio highly swept arrow-wing configuration. [wind tunnel tests]*, Tech. Rep. NASA TP 1434 (1978).

[26] P. L. Coe, J. Huffman, J. K., and J. W. Fenbert, *Leading-edge deflection optimization for a highly swept arrow wing configuration*, Tech. Rep. NASA TP 1777 (1980).

[27] J. E. Lamar and C. J. Obara, *Review of cranked-arrow wing aerodynamics project: Its international aeronautical community role*, 45th AIAA Aerospace Sciences Meeting and Exhibit (2007).

[28] S. B. Anderson and T. W. Feistel, *Historic review of canard configurations*, (1985), nASA Ames Research Center, California.

[29] M. GHOREYSHI, *Simulation validation of static and forced motion flow physics of a canard configured transcruiser„* 22nd AIAA Computational Fluid Dynamics Conference, AIAA AVIATION Forum, (AIAA 2015-3426) (2015).

[30] H. Behrbohm, *Basic low speed aerodynamics of the short-coupled canard configuration of small aspect ratio*, SAAB TN-60 (1965).

[31] S. U. Ilan M. Kroo, *Minimum induce drag of canard configurations*, Journal of Aircraft **19**, 792 (1982).

[32] D. R. SATRAN, *Wind-tunnel investigation of the flight characteristics of a canard general-aviation airplane* (1986).

[33] J.Roskam, *Airplane design, darcorporation,* (1985).

[34] J. Er-el and A. Seginer., *Vortex trajectories and breakdown on wing-canard configurations*, Journal of Aircraft **22** (1985).

[35] L. B.B.Gloss, *Canard wing lift interference related to maneuvering aircraft at subsonic speeds*, (1973), nASA Technical Report,NASA TM X-2897.

[36] P. Hummel and H.-C. Oelker, *Vortex interference effects on close-coupled canard configurations in incompressible flow*, in *Proceedings of the Symposium on the International Vortex Flow Experiment on Euler Code Validation* (Stockholm, Flygtekniska Forsoksanstalten, Bromma, Schweden 47-61, 1986).

[37] H.-C. Oelker and P. Hummel, *Experimentelle untersuchungen an entenkonfigurationen*, Flows with separation , 172 (1986).

[38] P. Hummel, *Documentation of separated flows for computational fluid dynamics validation*, AGARD-CP-437 **2**, 15 (1988).

[39] H.-C. Oelker and P. Hummel, *Investigations on the vorticity sheets of a close-coupled delta canard configuration*, ICAS-Proceedings **1**, 657 (1989).

[40] A. Bergmann and D. Hummel, *Aerodynamic effects of canard position on a wing body configuration in symmetrical flow* (Institute of Fluid Mechanics,Technical University Braunschweig, Germany, 2001) 39th Aerospace Sciences Meeting and Exhibit.

[41] B.B.Gloss, *Effect of canard location and size on canard wing interference and aerodynamic center shift related to maneuvering aircraft at transonic speeds*, (1974), nASA TND-7505.

[42] J. F. HOWARD, Richard M.; O'LEARY, *Flowfield study of a close-coupled canard configuration*, Journal of aircraft , 908 (1994).

[43] D. W. Lacey and S. a. Chorney, *Subsonic Aerodynamic Characteristics of Close-Coupled Canards with Varying Area and Position Relative to a 50 deg Swept Wing*, Tech. Rep. TN-AL-199 (Naval Ship Research and Development Center, 1971).

[44] D. W. Lacey, *Aerodynamic Characteristics of the Close-Coupled Canard as Applied to Low-to Moderate Swept Wings, vols. 1–4.*, Tech. Rep. AERO-1257-VOL-1-4 (NAVAL SHIP RESEARCH AND DEVELOPMENT CENTER BETHESDA MD AVIATION AND SURFACE EFFECTS DEPT, 1979).

[45] K. M. Lee and E. M. A. Murman, *comparison of experimental and preliminary numerical results for close-coupled canard-wing*, MIT CFPL-TR-88-8 (1988).

[46] J. M. A. Longo and A. Pas, *Numerical simulation of vortical flows over close-coupled canard-wing configuration*, AIAA-Paper No90-3003 (1990).

[47] E. L. Tu, *Navier-stokes simulation of a closecoupled canard-wing-body configuration*, J. Aircraft **29**, 830 (1992).

[48] R. J. Margason and J. E. Lamar, *Vortex-lattice fortran program for estimating subsonic aerodynamic characteristics of complex planforms*, NASA TN D-6142 (1971).

[49] I. Kroo, *Applied Aerodynamics: a digital textbook* (Desktop, Aeronautics, 1997).

[50] E. Torenbeek, *Synthesis of subsonic airplane design* (Springer, Dordrecht, 1982).

[51] D. Myring, *A theoretical study of the effects of body shape and Mach number on the drag of bodies of revolution in subcritical axisymmetric flow*, Tech. Rep. (ROYAL AIRCRAFT ESTABLISHMENT FARNBOROUGH (UNITED KINGDOM), 1981).

[52] L. Lignarolo, D. Ragni, C. Krishnaswami, Q. Chen, C. S. Ferreira, and G. Van Bussel, *Experimental analysis of the wake of a horizontal-axis wind-turbine model*, Renewable Energy **70**, 31 (2014).

[53] L. L. M. VELDHUIS, *Support Interference Effects of a Ventral Sting on a Body of Revolution.*, Tech. Rep. LSW 89-2 (Delft University of Technology, 1988).

[54] M. CIOBACA.V.; MELBER-WILKENDING.S.;POTT-POLLENSKE, *A CFD PROCESS CHAIN FOR SIMULATING OPEN WINDTUNNEL TEST SECTIONS.*, Tech. Rep. ISBN 978-3-00-027782-5 (DLR,Braunschweig, 2009).

[55] H. H. Heyson, *"Nomographic solution of the momentum equation for VTOL-STOL aircraft."* (NASA, 1961).

[56] H. H. Heyson, *Equations for the application of wind-tunnel wall corrections to pitching moments caused by the tail of an aircraft model* (NASA, 1966).

[57] C. HALL and B. PRIOR, *Crescent-winged aircraft, including tests leading-edge droop designs and several tailplane heights*, .

[58] A. L. Braslow and E. C. Knox, *Simplified method for determination of critical height of distributed roughness particles for boundary-layer transition at mach numbers from 0 to 5*, (1958).

[59] L. P. Yip, *Wind-tunnel investigation of a full-scale canard-configured general aviation airplane*, (1985).

[60] S. Mack, C. Brehm, B. Heine, A. Kurz, and H. Fasel, *Experimental investigation of separation and separation control on a laminar airfoil*, in *4th Flow Control Conference* (2008) p. 3766.

[61] N. Verhaagen, *An experimental investigation of the vortex flow over delta and double-delta wings at low speed*, Tech. Rep. (TECHNICAL HIGH SCHOOL DELFT (NETHERLANDS) DEPT OF AEROSPACE ENGINEERING, 1983).

[62] E. C. Polhamus, *A concept of the vortex lift of sharp-edge delta wings based on a leading-edge-suction analogy*, (1966).

[63] E. C. Polhamus, *Application of the leading-edge-suction analogy of vortex lift to the drag due to lift of sharp-edge delta wings*, (1968).

[64] E. C. Polhamus, *Predictions of vortex-lift characteristics by a leading-edge suctionanalogy*, Journal of aircraft **8**, 193 (1971).

[65] J. D. Phillips, *Approximate neutral point of a subsonic canard aircraft*, (1985).

6

APPENDIX A :WIND TUNNEL MODEL GEOMETRIC PARAMETERS

6.1. MODEL GEOMETRY

The models consist of Al-6061 alloy wings and central core for its attachment with the fuselage. The modular fuselage is made of 6061 alloy as well. The canards with the aluminum fairings built up around a 6mm mild steel spar. Attachment of the canards is done via the spar to the central machined aluminum block in the nose block. flush with the fuselage. Six canard mounting positions are provided. To achieve the far coupled configuration the cylindrical part of the fuselage is extended. Each canard can be rotated through a deflection range from -35 to +35 degrees in 1-degree increments. Rotation point for canards is 25 % of the exposed surface root chord. The moment reference point for the generic modular research model is 0.10$\overline{c}$.

Detailed dimensions of the wings are given in Table A1, A4, A5 and A6. Table A2 presents geometric parameters of the canard. Table A3 details the dimensions of the fuselage. Figure A2 to Figure A12 provide the detailed manufacturing drawing of the different components making up the modular wind tunnel model.

Quantity	Value	Unit
Span,b	1.28	m^2
Reference planform area, S_{refw},	0.2512	m
Reference chord,$\overline{c_w}$	0.2452	m
Taper ratio,Λ_w	0.165	–
Aspect ratio, AR_w	6.52	–
Dihedral root of the wing	0	deg
Dihedral tip of the wing	2.85	deg
Root Incidence, with respect to fuselage reference line line	2	deg
Inner wing twist, ϵ_{in}	0.046	deg
Outer wing twist, ϵ_{out}	-2	deg
wing pivot point x	0.0845	m
wing pivot point z	0.149	m
Maximum thickness,% chord	11	
	–	
Moment reference point, MRP_x	0	
Moment reference point, MRP_z	0	

*n0011sc-il-naca-langley-symmetrical-airfoil

Table 6.1: Wing model parameters

Quantity	Value	Unit
Span,b	0.54	m
Reference planform area, S_{refc},	0.0459	m^2
Reference chord, $\overline{c_c}$	0.085	m
Taper ratio, Λ_c	0.545	–
Aspect ratio, AR_c	6.35	–
Dihedral root of the canard	0	deg
Dihedral tip of the canard	0	deg
Root Incidence, with respect to fuselage reference line line	0	deg
Inner wing twist, ϵ_{in}	0.0	deg
Outer wing twist, ϵ_{out}	0	deg
Leading edge sweep angle,λ	45	deg
Maximum thickness,% chord	10	
	–	

*64A010 airfoil

Table 6.2: Canard model parameters

Quantity	Value	Unit
Total fuselage length	1.4	m
Nose Block length	0.35	m
Constant cross-section center fuselage length	0.65	m
Aft Block length	0.40	m
Center fuselage diameter	0.16	m

Table 6.3: Fuselage model parameters

Station	y/(b/2)(mm)	Twist(deg)
1	94.804	0.046
2	109.551	0.088
3	120.5	0.201
4	150.312	0.529
5	200.401	1.079
6	235.503	1.446
7	280.614	1.554
8	291.465	1.432
9	301.149	0.813
10	327.337	0.547
11	379.672	0.288
12	405.846	0.03
13	432	-0.236
14	458.169	-0.501
15	484.331	-0.759
16	510.15	-1.109
17	536.656	-1.285
18	563.015	-1.55
19	589.581	-1.806
20	615.1	-2.064
21	641.224	-2.1

Table 6.4: Wing twist distribution

Section Number	Chord(mm)
section 1	494.373
section 2	412.725
section 3	350.735
section 4	313.406
section 5	273.688
section 6	224.558
section 7	193.186
section 8	173.002
section 9	171.583
section 10	169.698
section 11	164.849
section 12	162.314
section 13	155.411
section 14	148.53
section 15	141.652
section 16	134.756
section 17	127.876
section 19	114.1
section 20	107.222
section 21	100.34
section 22	93.442
section 23	86.571
section 24	79.678
section 25	72.8

Table 6.5: Wing Chord distribution

$y/(b/2)_{exposed}$	Λ_{le}(deg)
0.03	79.908
0.05	76.792
0.07	73.717
0.12	53.109
0.21	44.45
0.28	41.816
0.32	38.881
0.33	36.25

Table 6.6: Wing Leading sweep distribution

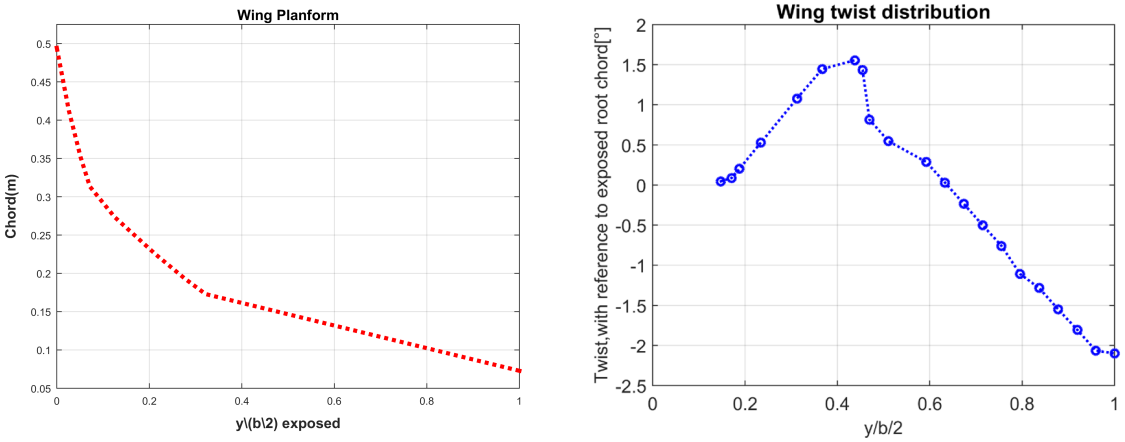

(a) Wing planform view

(b) Wing twist distribution

Figure 6.1: Wing chord and twist distribution

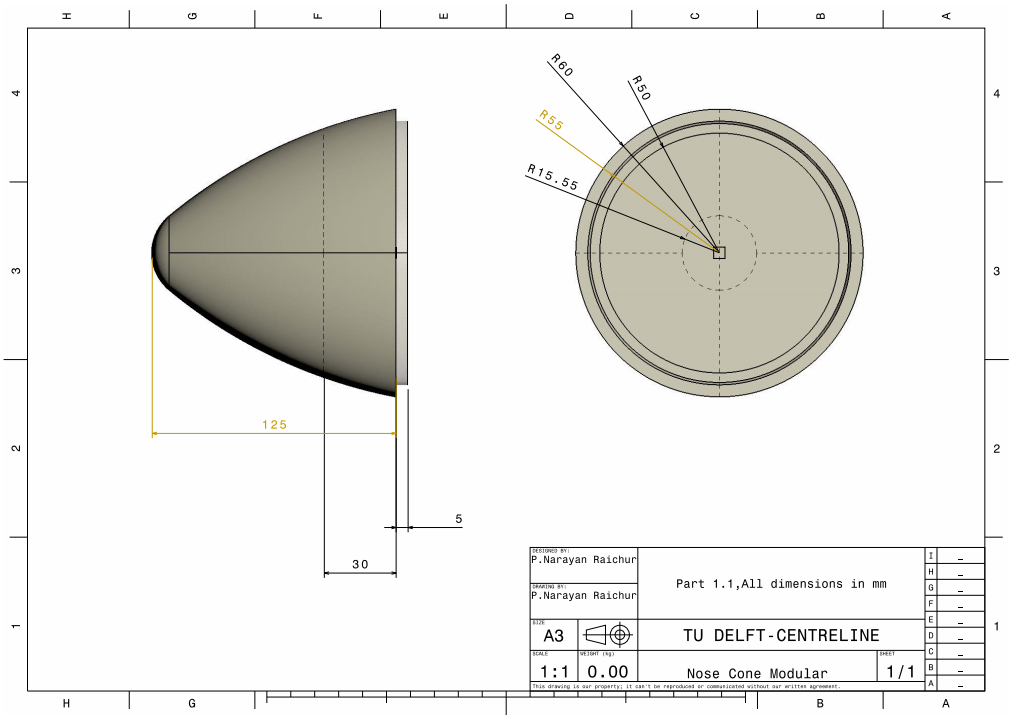

Figure 6.2: Manufacturing drawing of the Nose Cone

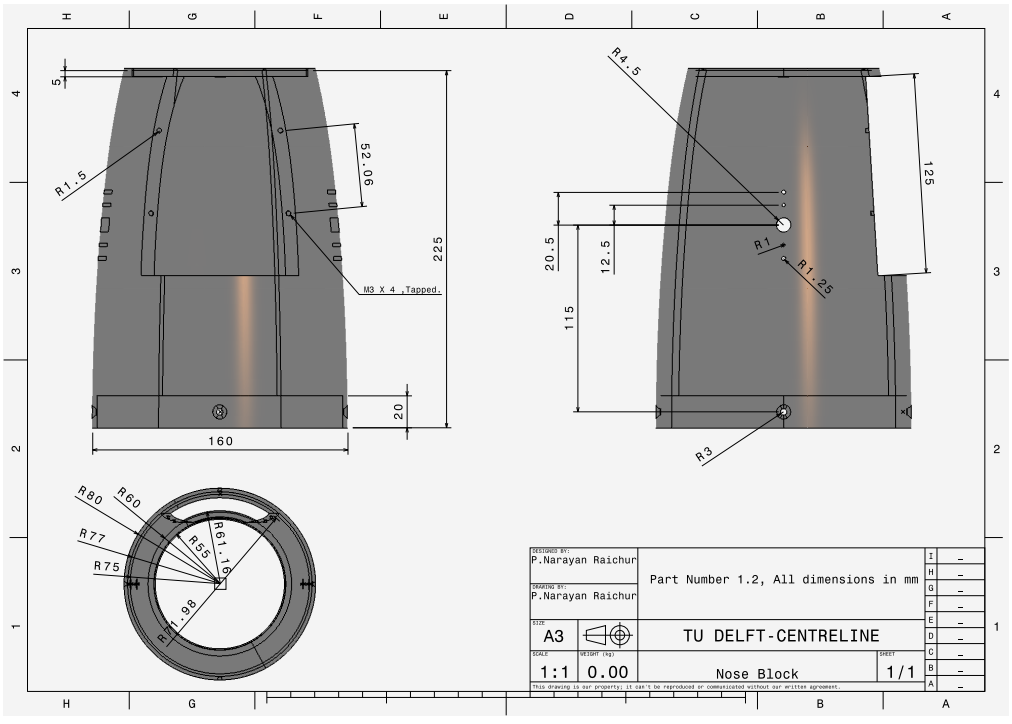

Figure 6.3: Manufacturing drawing of the Nose block

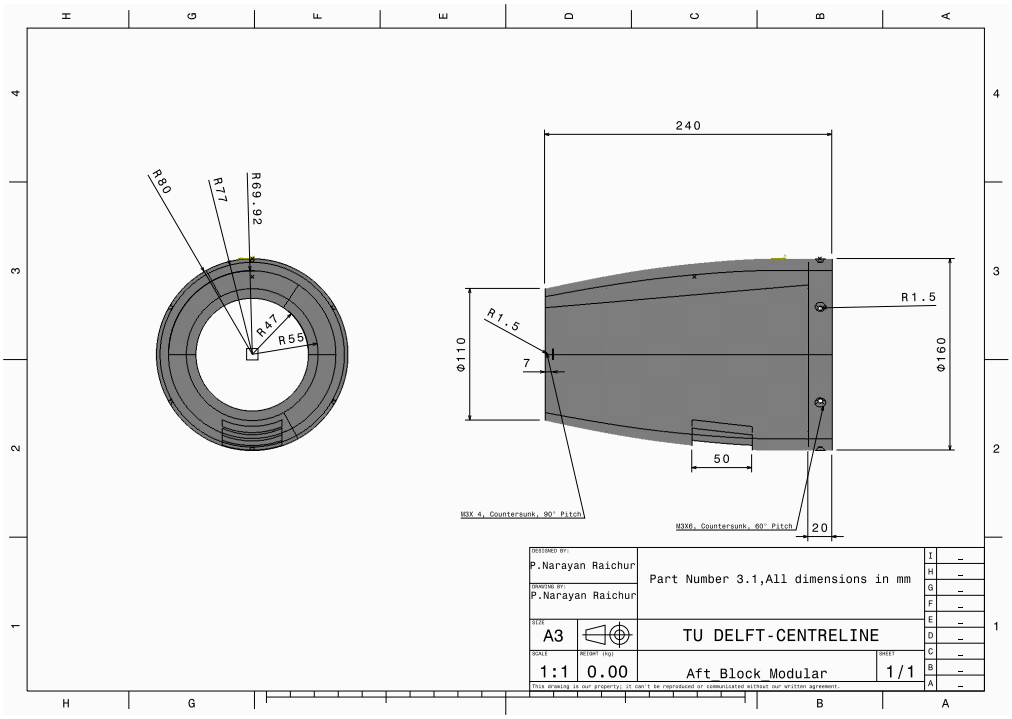

Figure 6.4: Manufacturing drawing of the Modular aft block

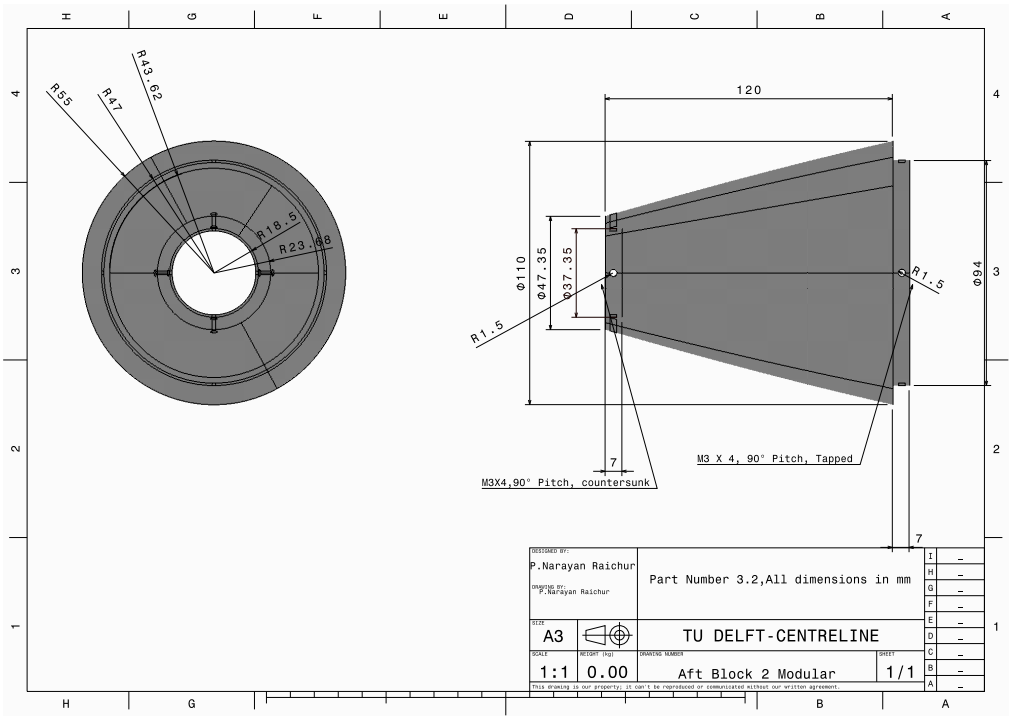

Figure 6.5: Manufacturing drawing of the Modular aft block 2

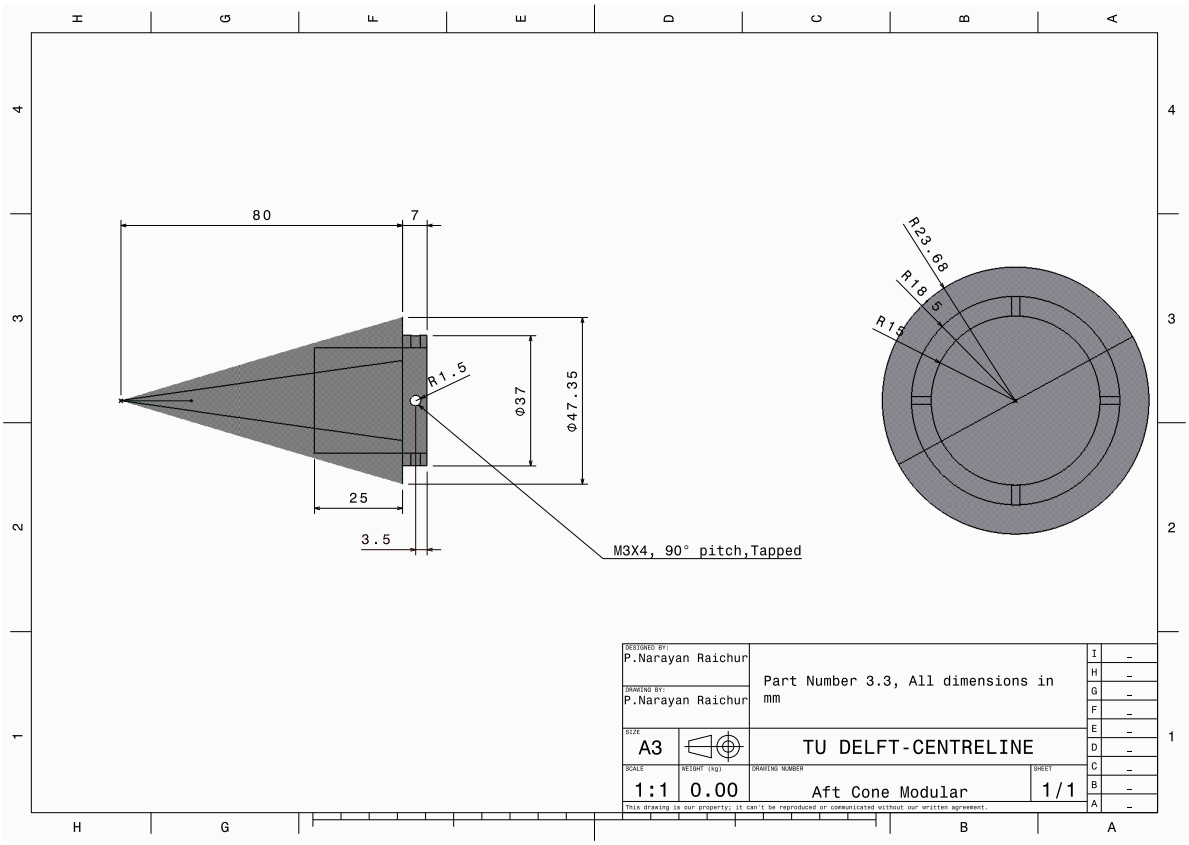

Figure 6.6: Manufacturing drawing of the aft cone

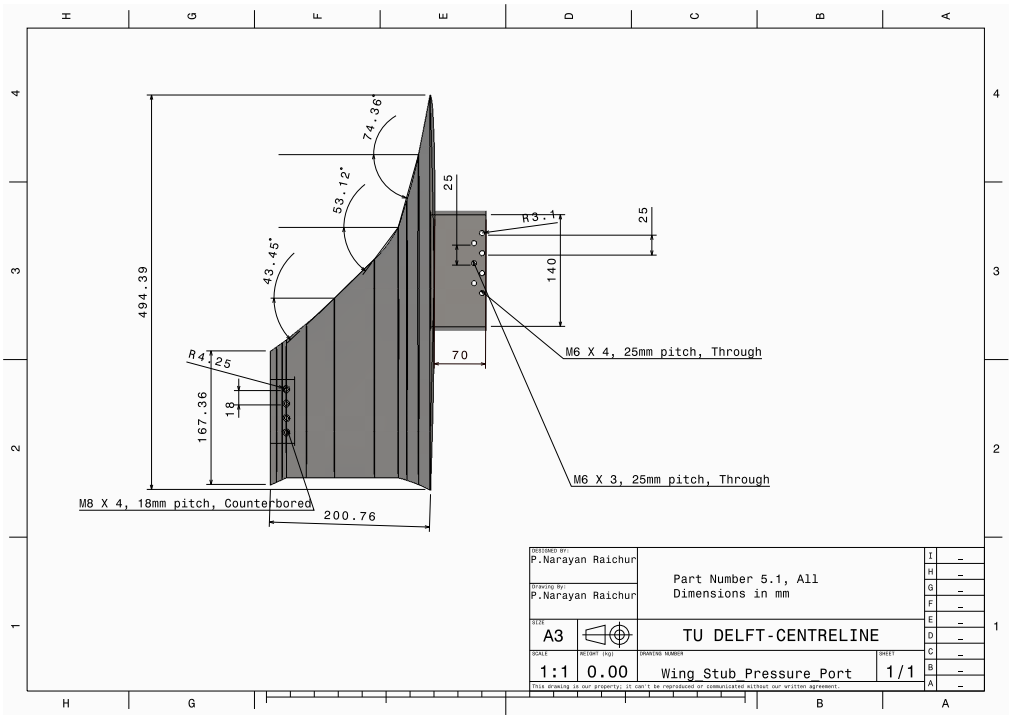

Figure 6.7: Manufacturing drawing of the inboard wing

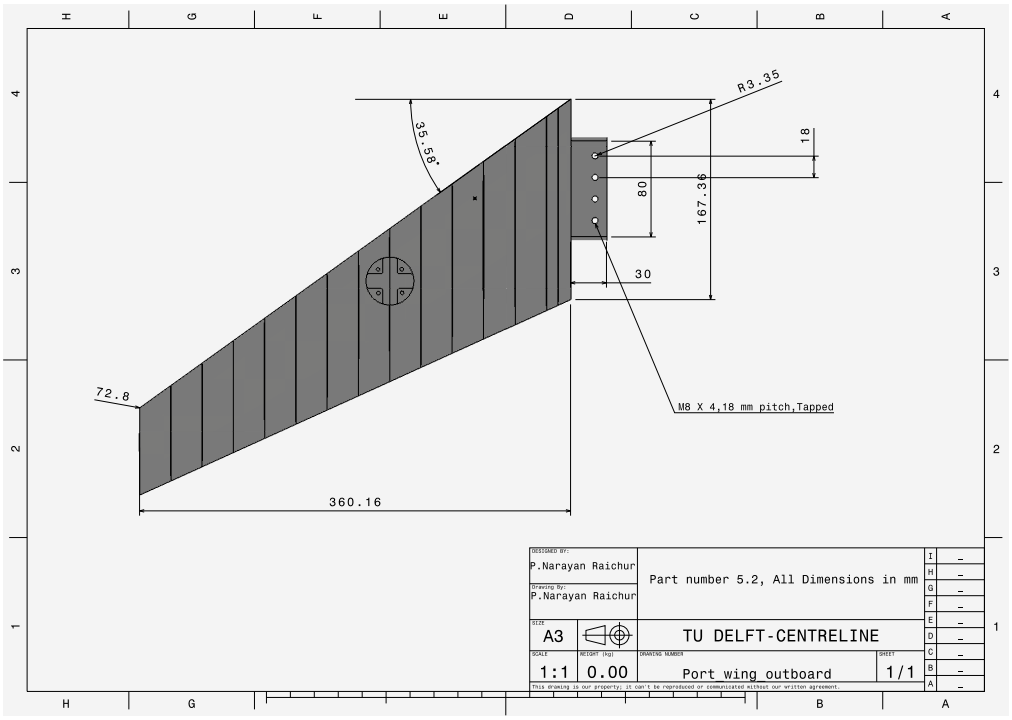

Figure 6.8: Manufacturing drawing of the outboard wing

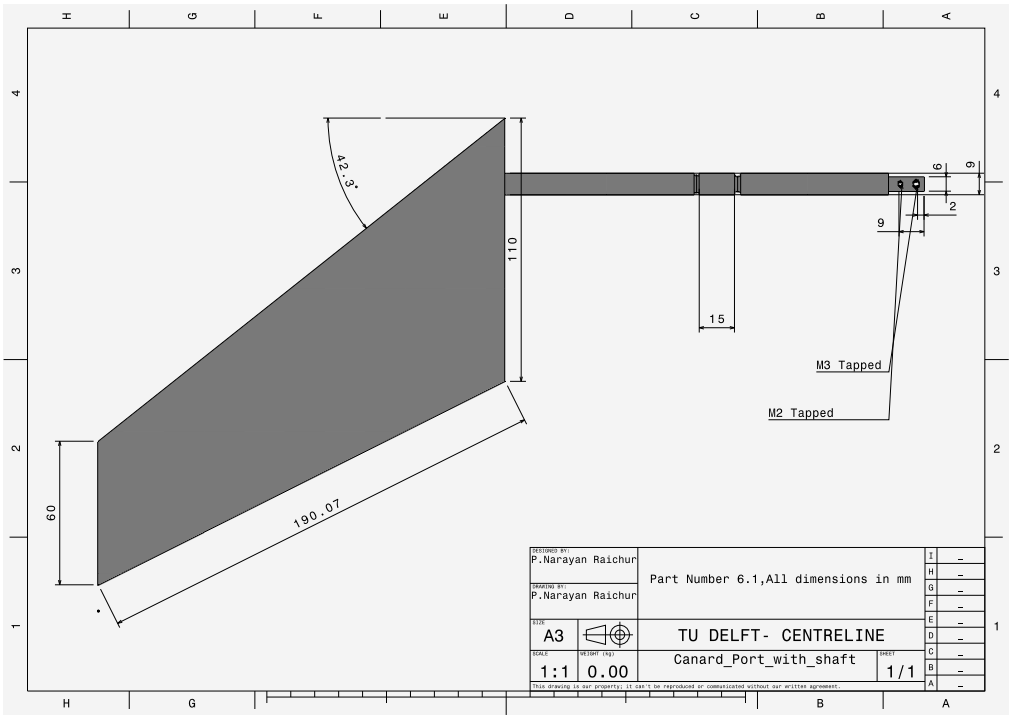

Figure 6.9: Manufacturing drawing of the port canard with the pivot mechanism

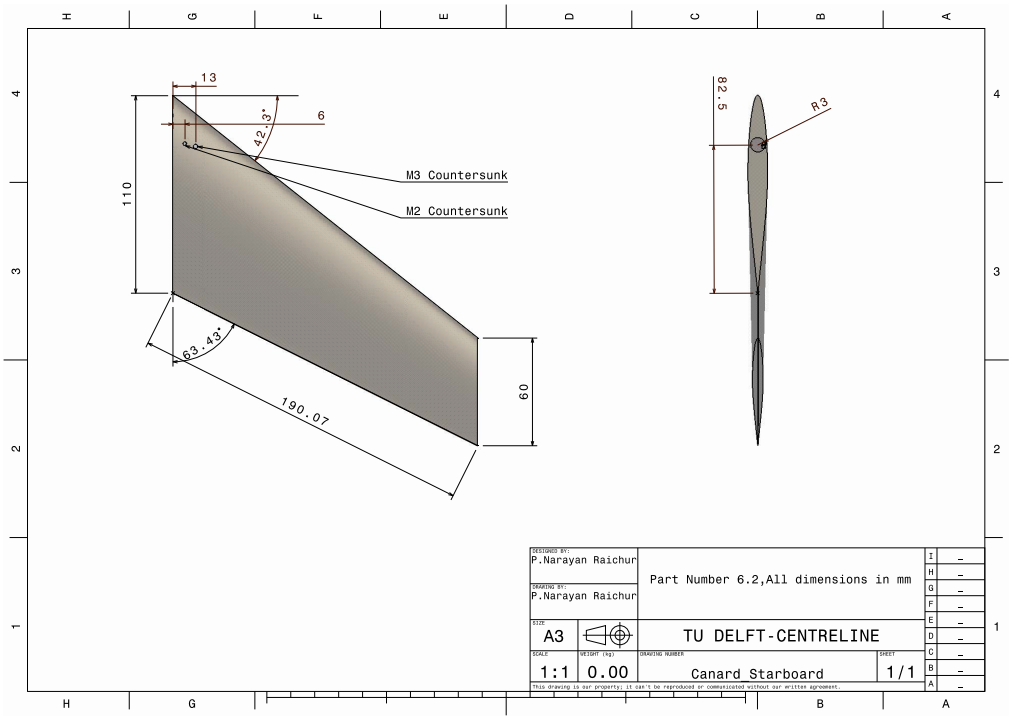

Figure 6.10: Manufacturing drawing of the starboard canard

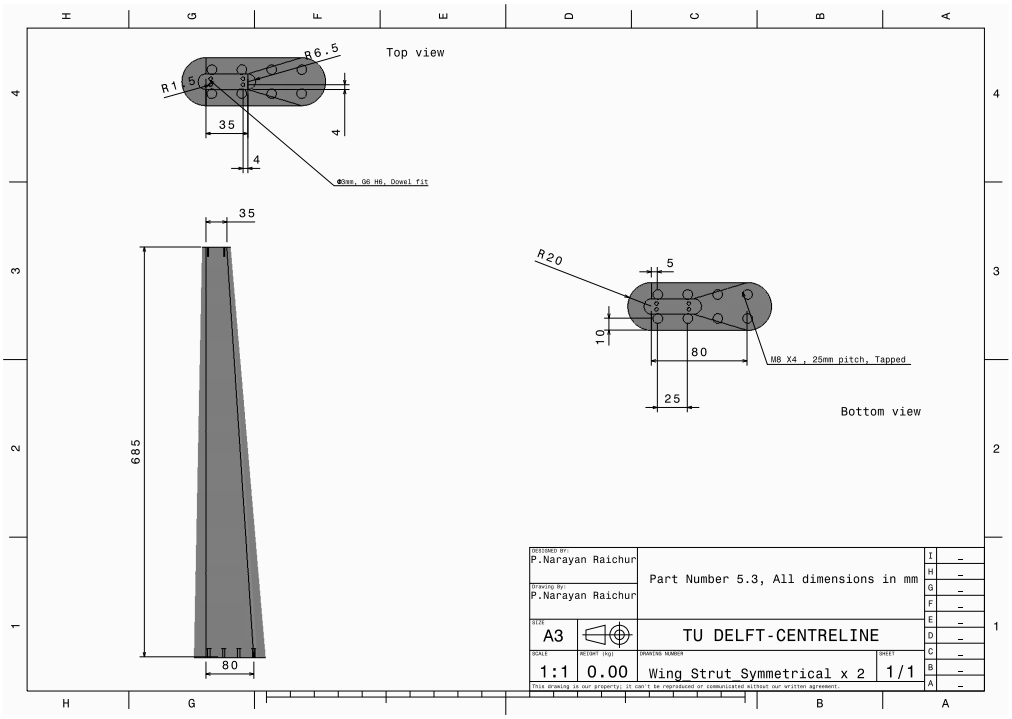

Figure 6.11: Manufacturing drawing of the wing support strut

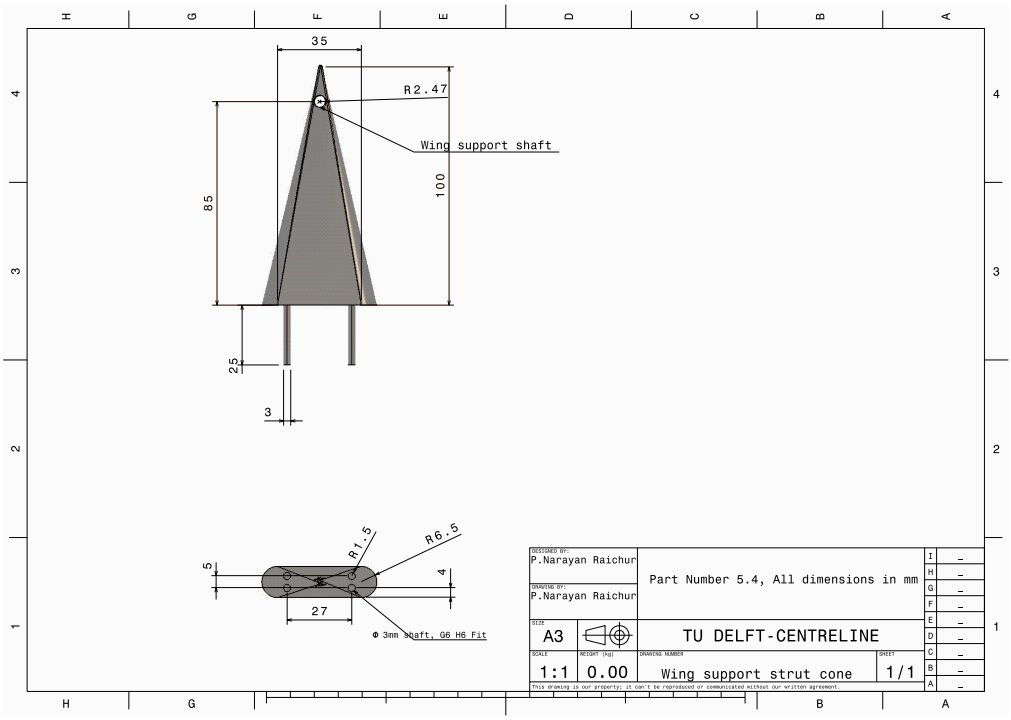

Figure 6.12: Manufacturing drawing of the wing attachment pivot

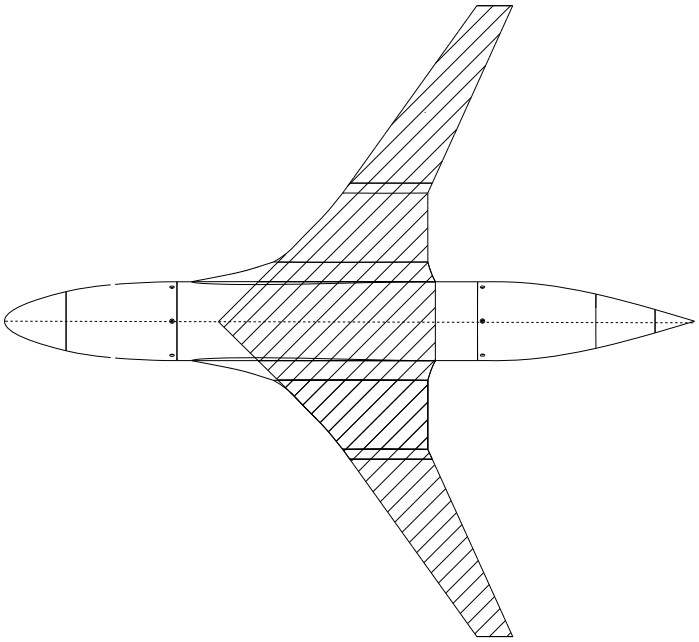

Figure 6.13: Wing reference area